

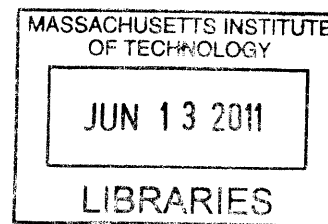
# Functional and Responsive Surfaces via Initiated Chemical Vapor Deposition (iCVD)

By

Mahriah E. Alf

B.S. Chemical Engineering, B.S. Spanish  
University of Wisconsin – Madison, 2006

M.S. Chemical Engineering Practice  
Massachusetts Institute of Technology, 2008



**ARCHIVES**

SUBMITTED TO THE DEPARTMENT OF CHEMICAL ENGINEERING IN PARTIAL  
FULFILLMENT OF THE REQUIREMENTS FOR THE DEGREE OF

DOCTOR OF PHILOSOPHY IN CHEMICAL ENGINEERING  
AT THE  
MASSACHUSETTS INSTITUTE OF TECHNOLOGY

JUNE 2011

© 2011 Massachusetts Institute of Technology. All rights reserved.

The author hereby grants to MIT permission to reproduce and to distribute publicly  
paper and electronic copies of this thesis document in whole or in part  
in any medium now known or hereafter created.

Signature of Author: \_\_\_\_\_

\_\_\_\_\_  
Department of Chemical Engineering  
May 24, 2011

Certified by: \_\_\_\_\_

\_\_\_\_\_  
Karen K. Gleason  
Professor of Chemical Engineering  
Thesis Supervisor

Certified by: \_\_\_\_\_

\_\_\_\_\_  
I. Alan Hatton  
Professor of Chemical Engineering  
Thesis Supervisor

Accepted by: \_\_\_\_\_

\_\_\_\_\_  
William M. Deen  
Professor of Chemical Engineering  
Chairman, Committee for Graduate Students

# Functional and Responsive Surfaces via Initiated Chemical Vapor Deposition (iCVD)

By

Mahriah E. Alf

Submitted to the Department of Chemical Engineering  
on May 24, 2011 in Partial Fulfillment of the  
Requirements for the Degree of  
Doctor of Philosophy in Chemical Engineering

## ABSTRACT

Stimuli-responsive polymers provide a method to control system behavior through the use of an external stimulus, such as temperature, pH, or electric fields among others. Temperature-responsive polymers, especially those based on *N*-isopropylacrylamide (NIPAAm), are of particular research interest due to the ease of implementation of temperature changes to systems as well as the large accessible range of hydrophilic / hydrophobic switching. Initiated chemical vapor deposition (iCVD) is shown to be a useful technique for surface modification with NIPAAm-based polymers due to its ability to provide complete functional retention and applicability to “real world” substrates, which many times have varying compositions and / or micro- or nano-structured surfaces. The novel copolymer thin film of iCVD poly(NIPAAm-co-di(ethylene glycol) divinyl ether) (p(NIPAAm-co-DEGDVE)) is shown to exhibit a sharp lower critical solution temperature (LCST) transition, better-than or equivalent to other surface-modification techniques, while also being able to achieve a wider range of thicknesses from the nano- to micro-scale, which is especially useful for flow control, actuator or sensor applications. The bottom-up film growth of iCVD allows for compositional gradients throughout the thickness of a polymer film. A novel NIPAAm-based copolymer with a NIPAAm-rich surface layer is developed which exhibits both fast swelling and deswelling kinetics. Quartz crystal microbalance with dissipation monitoring (QCM-D) is used to study the transition behavior of these films. These data provide valuable information relating to the polymer conformational changes throughout the transition region and help elucidate thermodynamic and mesh characteristics of the films. Finally, an application is developed which utilizes both iCVD and a complementary technique, oxidative CVD (oCVD), to create self-heating membranes with responsive permeability characteristics.

Thesis Supervisor: Karen K. Gleason  
Title: Professor of Chemical Engineering

Thesis Supervisor: T. Alan Hatton  
Title: Professor of Chemical Engineering

## Acknowledgments

Although sometimes I feel like it was just yesterday that I walked into my first class at MIT, it is truly amazing all that I have learned and accomplished throughout my five years here. I don't think much of it would be possible without the influence of the people that have been a part of my life for these past five years and beyond.

First and foremost I would like to thank my parents. My mom has been a constant source of support and has instilled in me a work ethic and desire to succeed, showing me that I am capable of whatever I put my mind to. Although my father is no longer with us, he has taught me to look for the fun and joy in life and to not stress and miss out on the life experiences that are all around me. Without this attitude, I don't know if I could have made it through the highs and lows of thesis work, or found the activities I have participated in that have made my graduate studies so well-rounded and fulfilling.

My time at MIT has also given me the opportunity to work with many great people academically. At the top of that list would be my advisors, Professors Karen Gleason and T. Alan Hatton. Karen, your mentorship has been invaluable in both technical research and in learning effective communication skills for writing and presentations. Alan, I have enjoyed our discussions your motivation to look at problems from new and interesting perspectives, effectively providing breadth to my thesis work. Thank you to my committee members, Professors Gregory Rutledge and Chris Love. Your discussions have been useful in helping me to focus my project and providing suggestions to better understand the systems that I have studied.

I have appreciated the support of the Gleason Group members, especially my classmates Miles Barr, Jingjing Xu and Nathan Trujillo. But, thanks to everyone for making the group such a positive place to work in and keeping up the spirit of camaraderie that helps to make our group run smoothly.

My friends from both MIT and beyond have also helped me greatly both from their support as well as by keeping my life exciting. Dr. Earl Solis, you don't know how much you improved my MIT experience, we have had more good times than I could possibly count. To my friends from college Katie Liss, Erica Hong and Mairin Reed, I don't think there is another group of people that I spend time with that can make me laugh and enjoy myself as much as you guys do. To my classmates, thank you for helping me through the trials and tribulations of first year and beyond.

I also want to thank the Practice School Program. I enjoyed and appreciated the work experiences we were given. It was through this program I was able to make some important connections with BP. On that note, a big thank you to BP Alternative Energy Division for providing me the opportunity to go to Antarctica. This was not only one of the greatest experiences of my graduate career, but possibly also of my life.

Finally, I think it's important to thank those people who have been integral in allowing me to participate in activities outside of school, which has kept me sane through the past five years...remember variety is the spice of life! Thank you to MIT Masters Swimming, and especially coach Bill Paine, for allowing me to coach on and off during my time here and providing such a constructive environment. Thanks to the Thirsty Ear for providing a social outlet and many fun times bartending.

## Table of Contents

<b>1. CHAPTER ONE: <i>INTRODUCTION</i></b>	<b>15</b>
1.1 MOTIVATION	16
1.2 INITIATED CHEMICAL VAPOR DEPOSITION	19
1.3 <i>N-ISOPROPYLACRYLAMIDE</i>	21
1.4 SCOPE OF THESIS	23
1.5 REFERENCES	25
<b>2. CHAPTER TWO: <i>SHARP HYDROPHILICITY SWITCHING AND CONFORMALITY ON NANOSTRUCTURED SURFACES PREPARED VIA INITIATED CHEMICAL VAPOR DEPOSITION (ICVD) OF A NOVEL THERMALLY RESPONSIVE COPOLYMER</i></b>	<b>28</b>
2.1 ABSTRACT	29
2.2 INTRODUCTION	30
2.3 RESULTS AND DISCUSSION	33
2.4 CONCLUSIONS	42
2.5 EXPERIMENTAL	42
2.6 ACKNOWLEDGEMENTS	45
2.7 REFERENCES	45
<b>3. CHAPTER THREE: <i>NOVEL N-ISOPROPYLACRYLAMIDE BASED POLYMER FILM ARCHITECTURE FOR FASTER LCST TRANSITION KINETICS</i></b>	<b>48</b>
3.1 ABSTRACT	49
3.2 INTRODUCTION	50
3.3 EXPERIMENTAL	55
3.4 RESULTS AND DISCUSSION	57
3.5 CONCLUSIONS	74
3.6 ACKNOWLEDGMENTS	75
3.7 REFERENCES	75

<b><u>4. CHAPTER FOUR: INSIGHTS INTO THIN, THERMALLY-RESPONSIVE POLYMER LAYERS THROUGH QUARTZ CRYSTAL MICROBALANCE WITH DISSIPATION MONITORING (QCM-D)</u></b>	<b>79</b>
<b>4.1 ABSTRACT</b>	<b>80</b>
<b>4.2 INTRODUCTION</b>	<b>81</b>
<b>4.3 EXPERIMENTAL</b>	<b>85</b>
<b>4.4 RESULTS AND DISCUSSION</b>	<b>87</b>
<b>4.5 CONCLUSIONS</b>	<b>103</b>
<b>4.6 ACKNOWLEDGMENTS</b>	<b>104</b>
<b>4.7 REFERENCES</b>	<b>104</b>
<b><u>5. CHAPTER FIVE: FACILE VAPOR PHASE METHOD TO PREPARE DYNAMICALLY SWITCHABLE MEMBRANES</u></b>	<b>107</b>
<b>5.1 ABSTRACT</b>	<b>108</b>
<b>5.2 INTRODUCTION</b>	<b>109</b>
<b>5.3 EXPERIMENTAL</b>	<b>113</b>
<b>5.4 RESULTS AND DISCUSSION</b>	<b>116</b>
<b>5.5 CONCLUSIONS</b>	<b>126</b>
<b>5.6 ACKNOWLEDGMENTS</b>	<b>126</b>
<b>5.7 REFERENCES</b>	<b>127</b>
<b><u>6. CHAPTER SIX: CONCLUSIONS</u></b>	<b>130</b>

## List of Figures

Figure 1-1. The reaction mechanisms of (a) PECVD and (b) iCVD. Panel (a) reproduced from <sup>21</sup> , copyright 2005 Taylor & Francis Group, LLC. Panel (b) reproduced from <sup>22</sup> , copyright 2009 the Owner Societies.....	20
Figure 1-2. Schematic of cross-section of an iCVD reactor showing the initiation and surface-polymerization steps of the deposition process. This is not drawn to scale.....	20
Figure 1-3. (a) structure of NIPAAm monomer and pNIPAAm. (b) schematic for understanding polymer conformational changes involved in the LCST transition from <sup>25</sup> .....	22
Figure 2-1. QCM-D LCST analysis a) i. schematic representation of achievable thickness range and LCST transition sharpness for pNIPAAm-based films from iCVD as compared to low density grafted layers, <sup>[8, 9]</sup> high density grafted layers, <sup>[9, 11]</sup> and plasma enhanced CVD <sup>[7]</sup> based on QCM-D data. a) ii. table comparing important characteristics of the same surface polymerization techniques. b) QCM-D data of the 7 <sup>th</sup> harmonic from iCVD p(NIPAAm-co-DEGDVE) film at temperatures around the LCST. The solid lines correspond to data obtained ramping up temperature, while the dashed lines correspond to ramping down temperature. ....	32
Figure 2-2. FTIR spectra of a) NIPAAm monomer, b) commercial pNIPAAm reference sample, and c) iCVD pNIPAAm homopolymer. Peaks associated with the vinyl bonds of the monomer are marked (*) and are absent in the polymer spectra. Additionally, no differences between the conventionally synthesized and iCVD-polymerized materials can be resolved by FTIR. ....	34
Figure 2-3. a) Correlation between pNIPAAm film thickness and area under the FTIR spectra C=O stretching peak centered at 1645 cm <sup>-1</sup> . Solid line represents linear fit to this data. b) Composition of three representative p(NIPAAm-co-DEGDVE) films deposited under the same conditions (as given in methods). The small compositional differences seen here are due to slight NIPAAm flow rate variations during the deposition. Compositions were calculated from area under the C=O stretching peak compared to the pNIPAAm calibration.....	35

Figure 2-4. QCM-D frequency data with the fitted s-curve of the form given in Equation 1. The fitted parameters of the curve shown here are  $490 \pm 30$  Hz,  $1.2 \pm 0.3$  °C<sup>-1</sup>,  $20 \pm 3$  Hz and  $28.5 \pm 0.3$  °C for A, B, C and T<sub>LCST</sub> respectively. .... 36

Figure 2-5. SEM images of a cross-section of iCVD p(NIPAAm-co-DEGDVE) coated trenches cut into a silicon wafer with aspect ratios of a) i. and b) i. 7:1, and a) ii. and b) ii. 14:1. a) represents poor conditions for conformality, where b) represents improved conditions for conformality on a complex geometry. The black lines are guides to highlight film thickness. SEM images of c) i. uncoated and ii. 200 nm coated electrospun nanofiber mats, and d) i. uncoated and ii. coated carbon nanotube forests. The scale bar on each image represents 1 μm. The black lines in image d) ii. highlight polymer film thickness of approximately 150 nm. .... 38

Figure 2-6. a) Static contact angles both below and above the LCST on various coated substrates including i. flat Si wafer, ii. electrospun nanofiber mat and iii. MWCNT forest. b) Fluorescence images at 40x magnification of p(NIPAAm-co-DEGDVE) coated nanofiber mats after soaking for 30 minutes in tetramethylrhodamine-labeled BSA in PBS at i. 25 °C and ii. 40°C. The mat at 40 °C was rinsed at 25 °C resulting in image iii. The white lines represent the edge of the mat. c) QCM-D data depicting frequency vs. time as BSA was introduced to the system at time 0 at two different temperatures..... 40

Figure 3-1. Schematic of the process used to synthesize graded polymer films with a NIPAAm-rich surface. Preparation of (a) the copolymer base layer of homogeneous composition, (b) the as-deposited graded film, and (c) the graded film after rinsing..... 52

Figure 3-2. The QCM-D transient (a) frequency and (b) dissipation curves of the 3<sup>rd</sup>, 5<sup>th</sup> and 7<sup>th</sup> order harmonics for an iCVD film of p(NIPAAm-co-EGDMA) having a uniform composition. These data show the kinetic response of the system to each temperature step given on the second y-axis. Panels (a) and (b) are then used to form the (c) frequency and (d) dissipation curves after 20 minutes of equilibration time at each temperature step. Solid lines correspond to data points taken as the temperature was stepped up, while the dashed lines correspond to decreasing temperature. .... 58

Figure 3-3. The QCM-D transient (a) frequency and (b) dissipation curves of the 3<sup>rd</sup>, 5<sup>th</sup> and 7<sup>th</sup> order harmonics for graded iCVD film having a p(NIPAAm-co-EGDMA) base beneath a NIPAAm-rich surface layer. These data show the kinetic response of the system to each

temperature step given on the second y-axis. Panels (a) and (b) were used to prepare the curves for the (c) frequency and (d) dissipation after 20 minutes of equilibration time at each temperature step. Solid lines correspond to data taken as the temperature was stepped up, while the dashed lines correspond to decreasing temperature steps..... 61

Figure 3-4. Schematic depicting qualitatively the physical area of QCM-D sampling for the 3<sup>rd</sup>, 5<sup>th</sup> and 7<sup>th</sup> order harmonics of the graded p(NIPAAm-co-EGDMA) film along a cross-section of a coated quartz crystal both (a) below and (b) above the film's LCST. Note that the vertical axis is not drawn to scale but is merely a schematic to illustrate the differences in the harmonic order sampling within the film. The gray horizontal line represents the threshold below which the film is sufficiently attached to the crystal to be considered part of the crystal's mass and the labeled 3<sup>rd</sup>, 5<sup>th</sup>, and 7<sup>th</sup> order harmonic curves represent how far past this threshold each of the harmonic orders penetrate. The penetration depth varies from harmonic to harmonic as well as depending on radial distance from the edge of the crystal as depicted qualitatively by the shapes of the curves. Each of the harmonic orders samples the amount of film and fluid below each of their respective curves, thus illustrating the difference in sample size for the different harmonic orders, especially for the swollen polymer below its LCST. .... 64

Figure 3-5. (a) The QCM-D transient responses of the 3<sup>rd</sup> order harmonic of a blank crystal to stepping the temperature up (dark grey, solid lines) and down (light grey, dashed lines). Each response is well described by Eq. 2, allowing extraction of a single first-order time constant. (b) Time constants obtained using Eq. 2 to fit the transient responses for the 3<sup>rd</sup>, 5<sup>th</sup> and 7<sup>th</sup> order harmonics of the blank QCM-D crystal. Solid lines correspond to stepping the temperature up, while dotted lines indicate that the temperature is being stepped down..... 67

Figure 3-6. (a) The QCM-D transient responses of the 3<sup>rd</sup> order harmonic of a quartz crystal coated with 80 nm of homogeneous p(NIPAAm-co-EGDMA) to stepping the temperature up (dark grey) and down (light grey). Each response is well described by Eq. 3, allowing extraction of two first-order time constants. (b) Time constants obtained using Eq. 3 to fit the transient responses for the 3<sup>rd</sup>, 5<sup>th</sup> and 7<sup>th</sup> harmonics of the coated QCM-D crystal. Arrows on the figure indicate those data points corresponding to  $\tau_1$  (QCM-D system) and  $\tau_2$  (polymer film). Solid lines correspond to stepping the temperature up, while dotted lines indicate that the temperature



is being stepped down. The error bars represent 95% confidence intervals for the fits. .... 69

Figure 3-7. (a) The QCM-D transient responses of the 3<sup>rd</sup> order harmonic of a quartz crystal coated with 65 nm of a p(NIPAAm-co-EGDMA) film with a NIPAAm-rich surface to stepping the temperature up (dark grey) and down (light grey). Each response is well described by Eq. 2, allowing extraction of a single first-order time constant. (b) Time constants obtained using Eq. 2 to fit the transient responses for the 3<sup>rd</sup>, 5<sup>th</sup> and 7<sup>th</sup> order harmonics of the coated QCM-D crystal. Solid lines connecting points correspond to stepping the temperature up, while dashed lines indicate that the temperature is being stepped down. The error bars represent 95% confidence intervals for the fits. .... 71

Figure 3-8. (a) FTIR spectra for iCVD films of (i) pNIPAAm, (ii) graded p(NIPAAm-co-EGDMA) with NIPAAm-rich surface, (iii) p(NIPAAm-co-EGDMA) homogeneously crosslinked film, and (iv) pEGDMA. The asterisks correspond to peaks uniquely associated with NIPAAm, while the dashed line corresponds to the C=O stretching peak uniquely associated with EGDMA. These ..... 73

Figure 4-1. (a) UV-vis transmission at 500 nm for pNIPAAm standard solution polymerized and iCVD chains around their LCST's. (b) The van't Hoff form (Eq. 2) of data from (a). The solid and dashed lines depict the regression lines used to calculate the enthalpy change associated with the LCST transition for the pNIPAAm standard and iCVD sample respectively. Data points taken below the LCST transition region are excluded because variations seen at such a low fractional conversion are not significant because they are within the experimental error of the instrument. Only those points taken through the transition region provide the slope proportional to the enthalpy of the transition. .... 90

Figure 4-2. (a) QCM-D data for 50 nm iCVD p(NIPAAm-co-DEGVE) films around the LCST. Data from the 3<sup>rd</sup>, 5<sup>th</sup> and 7<sup>th</sup> order harmonics are included for comparison. (b) van't Hoff form of data from (a) used to calculate the enthalpy change associated with the LCST transition. The solid, dashed and dotted lines correspond to the linear fits for the 3<sup>rd</sup>, 5<sup>th</sup> and 7<sup>th</sup> harmonics respectively..... 94

Figure 4-3. DSC thermograms for (a) standard pNIPAAm, (b) iCVD pNIPAAm and (c) iCVD p(NIPAAm-co-DEGDVE) obtained using a heating rate of 1 °C/min. (d) provides a comparison of the  $\Delta H_{vH}$

obtained for each system from UV-vis (pNIPAAm) or QCM-D (p(NIPAAm-co-.....	96
Figure 4-4. Dissipation changes plotted against frequency changes for the 3 <sup>rd</sup> order harmonic response to a 50 nm p(NIPAAm-co-DEGDVE) coated QCM-D crystal when exposed to 10 mg/mL BSA in PBS both above (32 °C, red) and below (22 °C, black) the LCST. This figure .....	97
Figure 4-5. (a) Scaled transient 3 <sup>rd</sup> (black), 5 <sup>th</sup> (dark gray) and 7 <sup>th</sup> (light gray) order frequency and (b) dissipation response of 50 nm p(NIPAAm-co-DEGDVE) coated QCM-D crystal when exposed to 10 mg/mL BSA in PBS, at time 0, below the LCST (22 °C). The same system (c) frequency and (d) dissipation responses above the LCST (32 °C) depicting the transient 3 <sup>rd</sup> (dark red), 5 <sup>th</sup> (medium red) and 7 <sup>th</sup> (light red) order harmonics.....	99
Figure 5-1(a) Cross-sectional schematic of samples developed with dynamically switchable properties for both flat glass substrates and a track-etched PC membrane. The deposition steps for pEDOT and pEGDMA were performed from the top side, while the p(NIPAAm- co-DEGDVE) layer was deposited from the top side for the glass substrate and the bottom side for the PC track etched membrane. (b) Actual top down image of samples.....	111
Figure 5-2. (a) Temperature curves for pEDOT-coated glass substrates with varying resistances over a range of applied AC voltages. The data points were taken after allowing 10 min. of temperature equilibration at each voltage step. The dashed lines represent Equation 1 as fitted to the data using only one fitting parameter ( $h =$ $13 \pm 1 \text{ W m}^{-1} \text{ K}^{-1}$ ). (b) Set-up used to obtain static contact angle measurements of the responsive surface using pEDOT coating to provide resistive heating. Static contact angles for glass slides coated with pEDOT followed by pEGDMA and p(NIPAAm-co- DEGDVE) both (c) below the film's LCST (~22 °C) and (d) above the film's LCST (~ 35 °C) as achieved via application of 15 V AC across the substrate ( $R = 1,200 \Omega$ ).....	117
Figure 5-3. XPS survey scan taken of the top side (as in Figure 5-1) of a PC track etched membrane after (a) pEDOT deposition followed by (b) pEGDMA and (c) p(NIPAAm-co-DEGDVE). The important elemental peaks are highlighted where as expected S is present only after the pEDOT deposition, only C and O are present following the subsequent pEGDMA deposition and N is present only after the subsequent p(NIPAAm-co-DEGDVE) deposition.....	121

Figure 5-4. (a) Data representing the normalized (to the first low temperature measurement, Sample 1: 4.3 mL hr<sup>-1</sup>, Sample 2: 6.2 hr<sup>-1</sup>) DI water permeation rate of membrane Sample 1 (◆) and 2 (■). The temperature at which the measurements were taken are given in red open points on the second axis and the LCST of the polymer film is represented by the dashed line at 28 °C, illustrating that low temperature measurements were taken below this value and high temperature measurements above it. (b) Temperature changes as measured by a thermocouple affixed to the membrane in DI water from the base system temperature with applied AC voltage for the two different membrane samples. The dashed (sample 1) and solid (sample 2) lines are included merely as guides. (c) Transient temperature change profiles for a AC voltage jump of 0 to 12 V (open points) and 0 to 15 V (solid points) for sample 2. (d) Image of set-up for permeation study..... 123

## List of Tables

Table 1-1. Temperature responsive polymers initially identified for consideration. ....	18
Table 4-1. Summary of thermodynamic properties calculated using the van't Hoff relationship as well as the per monomer enthalpic contribution as determined from microcalorimetry. The estimated cooperative unit size based upon these values is also given. ....	91
Table 5-1. Details of deposition thickness as measured from profilometry for pEDOT and VASE for pEGDMA and p(NIPAAm-co-DEGDVE) on reference Si wafers for the two different 2 $\mu$ m track-etched PC membrane samples used in subsequent permeation studies. ....	120
Table 5-2. Expected and actual elemental compositions as calculated from XPS survey scans on the top side of 2 $\mu$ m pore size membranes after pEDOT, subsequent pEGDMA and subsequent p(NIPAAm-co-DEGDVE) depositions. ....	122

## List of Acronyms and Abbreviations

AAM	acrylamide
AC	alternating current
Bi	Biot number
BSA	bovine serum albumin
CVD	chemical vapor deposition
DEGDVE	di(ethylene glycol) divinyl ether
EDOT	3,4-ethylenedioxythiophene
DI water	deionized water
DSC	differential scanning calorimetry
DTGS	deuterated triglycine sulfate
EGDMA	ethylene glycol dimethacrylate
FTIR	Fourier transform infrared spectroscopy
HEMA	2-hydroxyethyl methacrylate
hwCVD	hot wire chemical vapor deposition
iCVD	initiated chemical vapor deposition
LCST	lower critical solution temperature
MEMS	microelectromechanical systems
MWCNT	multi-walled carbon nanotube
oCVD	oxidative chemical vapor deposition
p(NIPAAm-co-DEGDVE)	

poly(*N*-isopropylacrylamide-co-di(ethylene glycol) divinyl ether)

p(NIPAAm-co-EGDMA)

poly(*N*-isopropylacrylamide-co-ethylene glycol dimethacrylate)

PBS	phosphate buffer solution
PC	polycarbonate
PDMS	polydimethylsiloxane
PECVD	plasma enhanced chemical vapor deposition
pEGDMA	poly(ethylene glycol dimethacrylate)
PFM	pentafluorophenylmethacrylate
piCVD	photo-initiated chemical vapor deposition
pNIPAAm	poly( <i>N</i> -isopropylacrylamide)
QCM	quartz crystal microbalance
QCM-D	quartz crystal microbalance with dissipation monitoring
TBPO	tert-butyl peroxide
TEM	transmission electron microscopy
UV-vis	ultraviolet-visible spectroscopy
VASE	variable angle spectroscopic ellipsometry
XPS	X-ray photoelectron spectroscopy

# **1. CHAPTER ONE:**

*Introduction*

## 1.1 Motivation

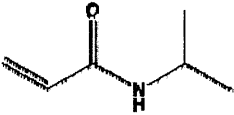
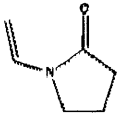
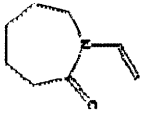

Stimuli-responsive polymers are a general class of polymers that exhibit properties that can change in response to external stimuli such as pH,<sup>1, 2</sup> light,<sup>3</sup> temperature,<sup>4-6</sup> electric or magnetic fields,<sup>7, 8</sup> or combinations thereof.<sup>9, 10</sup> This field is expanding at a rapid pace due to the many possibilities these polymers afford for system design. Specifically, surface modification of substrates with these polymers create so-called “smart” surfaces. This design gives additional functionality to previously-developed as well as novel substrates by providing dynamically switchable properties, which have applications ranging from separations,<sup>11-13</sup> sensors and actuators,<sup>14, 15</sup> drug delivery,<sup>16, 17</sup> and tissue engineering<sup>18</sup> among others.<sup>5, 19, 20</sup>

Many “smart” surface applications necessitate the integration of stimuli-responsive polymers with substrates that differ from the “ideal” surfaces typically employed in research work, such as glass slides or silicon wafers. Commercially relevant substrates, such as textiles and plastics, may exhibit damage when exposed to high temperature or harsh solvents. Micro-electrical and mechanical systems (MEMS) and medical devices typically represent 3D structures rather than simple planar surfaces. Uniform coverage of complex substrate geometry requires that the coating process be conformal. Thus, processes that avoid harsh solvents and high temperatures are desired for the synthesis conformal coatings of stimuli-response polymers on substrates of various compositions and geometries. The initiated chemical vapor deposition (iCVD) process is able to conformally coat these “non-ideal” substrates, while also allowing for control of chemistry necessary to dictate desired polymer film properties.



For this work, we focus on temperature as a stimulus. There are a number of different polymers that have been identified as having temperature-responsive properties, the great majority of which exhibit a lower critical solution temperature (LCST) whereby below this temperature the polymers are hydrophilic and as they pass through the LCST they undergo a rapid change in hydrophobicity, becoming hydrophobic. This means that surface-attached films would be in an extended, swollen conformation when immersed in an aqueous environment below the LCST and deswell by expelling water and collapsing to the surface when the temperature is increased above the LCST. Several different polymers of this nature were initially investigated as shown in Table 1-1. *N*-isopropylacrylamide (NIPAAm) was selected for several reasons including its ability to react via a free radical mechanism (needed for iCVD), its LCST lies near room temperature for facile switchability and it is relatively well-studied so has known utility and biocompatibility.

Table 1-1. Temperature responsive polymers initially identified for consideration.

Structure	Name	Polymerization Method	LCST	P <sup>vap</sup> (25 °C)
	N-isopropylacrylamide (NIPAAm)	Radical	32 °C	0.23 mTorr
	Vinyl pyrrolidone (VP)	Radical	170 °C	109 mTorr
	Vinylcaprolactam (VCL)	Radical	33 °C	49 mTorr
	Methyl vinyl ether (MVE)	Cationic	37 °C	1.5x10 <sup>6</sup> mTorr

Such stimuli-responsive / swellable polymers need to be cross-linked for stability. The cross-linkers di(ethylene glycol) divinyl ether (DEGDVE) as well as ethylene glycol dimethacrylate (EGDMA) will be investigated due to their successful use in previous cross-linked films deposited via iCVD. Both co-monomers will be investigated due to the unique properties each could provide the crosslinked film both in terms of comonomer hydrophobicity and vapor pressure allowing for different amounts of incorporation into the films.

The objective of this thesis work is three-fold. First, we wish to expand the cookbook of monomer functionalities accessible via iCVD to temperature-responsive polymers. Second, we wish to investigate the properties of the temperature-responsive polymers deposited by iCVD to better understand how their responsive properties behave and how to tune them for specific applications, such as the transition kinetics. Finally, we

want to put what we have learned into an application by integrating the temperature-responsive polymer deposited by iCVD with another complementary another vapor deposition technique, oxidative chemical vapor deposition (oCVD).

## **1.2 Initiated Chemical Vapor Deposition**

Chemical Vapor Deposition (CVD) is a general method used to coat a substrate with a thin polymer film. In CVD, monomer vapors are introduced into a reactor operating under a vacuum (typically 100 mTorr – 1 Torr), where they then react and form a solid film on the substrate's surface. Several different CVD technologies with differing energy sources and deposition characteristics are used to polymerize thin films, including Plasma Enhanced CVD (PECVD), photo-initiated CVD (piCVD), and hot wire CVD (hwCVD). Professor Gleason's research group has developed a novel offshoot of the hwCVD technology, iCVD. In iCVD, unlike hwCVD, initiator vapors as well as the monomer vapors are introduced into the reactor, where the hot wire filaments provide only enough energy (~200 – 300 °C) to cleave the initiator species into radicals, while leaving the monomer intact. This allows for the reaction to follow the well-defined free radical reaction pathway, preserving the functionality of the monomer side-groups in the polymer film, which is not the case for other higher-energy processes such as PECVD (Figure 1-1). Functional preservation is especially important for this project, as the functionality of the monomers is key to the polymer's responsive characteristics.

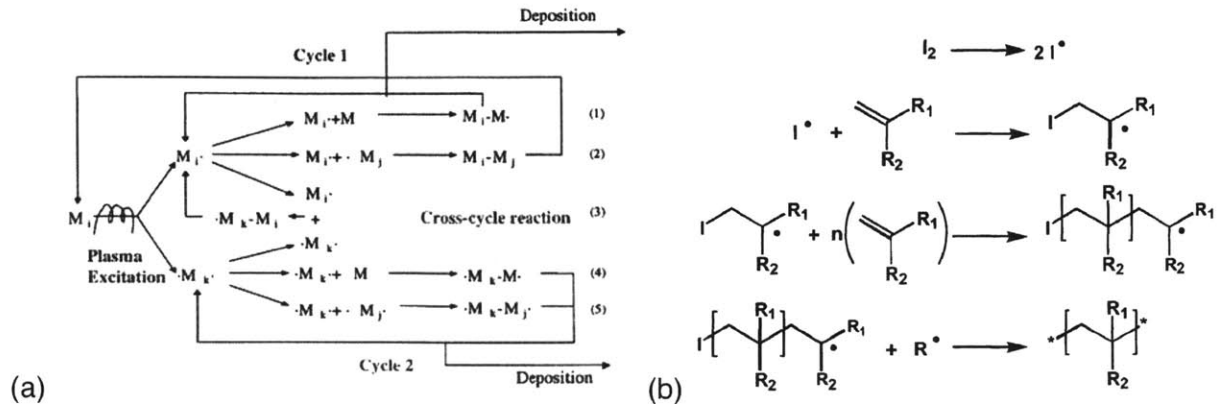


Figure 1-1. The reaction mechanisms of (a) PECVD and (b) iCVD. Panel (a) reproduced from <sup>21</sup>, copyright 2005 Taylor & Francis Group, LLC. Panel (b) reproduced from <sup>22</sup>, copyright 2009 the Owner Societies.

Figure 1-2 illustrates a schematic of the iCVD reaction system, which indicates that another important advantage to the system is its mild reaction conditions. The substrate is in contact with a cooling plate to keep it at near-ambient temperatures (generally from 25-45 °C). This allows for use of fragile substrates from paper to fabrics, and more importantly membranes, as they will be the focus of the final aspect of this project.

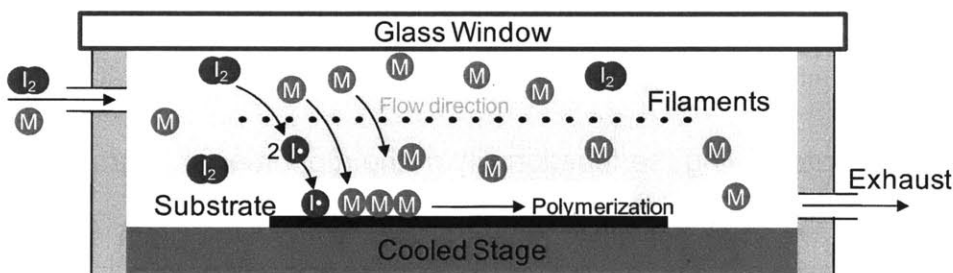


Figure 1-2. Schematic of cross-section of an iCVD reactor showing the initiation and surface-polymerization steps of the deposition process. This is not drawn to scale.

iCVD is also a solvent-free process, whereby it is possible to avoid environmentally-harmful solvents as well as solvent-removal processes that can be very time- and

energy-consuming. Finally, iCVD creates conformal films on the substrate, which may thereby be applied to substrates of varying geometries with micro- or nano-scaled features. Recently Sal Baxamusa has done work using trench wafers to look at the deposition characteristics within micro-scale features.<sup>23</sup> They have found that there are two primary reaction parameters that may be modified to increase the conformality of the coatings. The first is the ratio of monomer partial pressure to the saturation pressure of the monomer, which is directly related to the concentration of the monomer adsorbed on the substrate surface. As this value is decreased, conformality increases as the monomer will be able to travel farther into the trench before adsorbing on the surface. Also, an increase in the initiator to monomer feed ratio aids in conformality. The deposition characteristics may be modified through these parameters to correspond to the substrate and type of coverage required for a given application.

### **1.3 N-isopropylacrylamide**

As mentioned previously, polymers based on NIPAAm are part of a group of polymers that exhibit an LCST. The LCST for pNIPAAm occurs around 30-35 °C for pNIPAAm chains, depending on the polymer's molecular structure.<sup>5</sup> When immersed in an aqueous environment below the LCST, NIPAAm-based polymers become fully solvated by water with hydrogen bonding between the polar water molecule and the N-H group of NIPAAm, causing free chains to extend in a random coil configuration, while cross-linked gels swell. When temperatures are increased above the LCST, inter- and intra-molecular hydrogen bonds occurs between NIPAAm monomer units, causing free

chains to collapse into globular form and crosslinked gels to deswell and expel water, reverting back to a size comparable to their dry state.<sup>5</sup> A cartoon depiction of this event for grafted pNIPAAm chains is given in Figure 1-3. This drawing only serves as a conceptual understanding of the transition event, because the polymer chains do not in fact form helices above the LCST, but rather collapse into a more random state. It has been shown in fact that in the collapsed state above the LCST, only approximately 13% of the NIPAAm monomer units are participating in inter- or intra- chain bonding.<sup>24</sup>

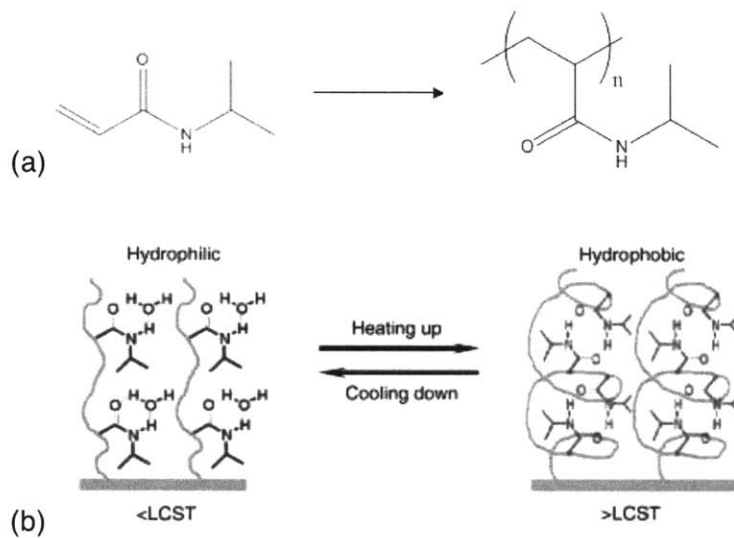


Figure 1-3. (a) structure of NIPAAm monomer and pNIPAAm. (b) schematic for understanding polymer conformational changes involved in the LCST transition from<sup>25</sup>.

The origin of this behavior is thermodynamic in origin and comes from the interaction of water molecules with the NIPAAm monomer. Due to hydrophobic effects, the isopropyl group of the monomer causes reorientation of the water molecules around the hydrophobic core, resulting in a negative entropy of mixing. At low temperatures however, the negative enthalpy of mixing due to hydrogen bonding between water and

the polar acrylamide group wins out, creating an overall negative free energy of mixing. As the temperature increases past the LCST, the entropy term becomes dominant and the free energy of mixing becomes positive and causes phase separation.

Because the LCST depends on hydrophobic interactions of the polymer with the solvent, the value of the LCST can be tuned through random copolymerization with other monomers. In general, copolymerization of NIPAAm with a more hydrophilic comonomer will cause an increase in LCST, while copolymerization with a more hydrophobic comonomer will cause a decrease in LCST.<sup>20</sup> In fact, copolymerization of NIPAAm with up to 20% acrylamide (AAm) has been shown to increase the LCST by as much as 20 °C as compared to copolymerization with up to 70% *N*-tertbutylacrylamide can decrease the LCST by as much as 35 °C. In the research presented here, we will utilize this understanding of the LCST transition to tailor the iCVD NIPAAm-based polymers to achieve specific aims.

## **1.4 Scope of Thesis**

This thesis utilizes iCVD as an enabling technology to create temperature-responsive thin films. By using this technique, we are able to control the properties of these temperature-responsive films as well as illustrate a specific application. The thesis concerns polymers primarily based on the monomer NIPAAm, but investigates different aspects of copolymers of NIPAAm throughout the chapters from proof of concept, to material properties and control, to application.

CHAPTER TWO describes the synthesis of a novel copolymer, p(NIPAAm-co-DEGDVE) and analysis of its responsive properties via QCM-D. We are able to illustrate That the temperature range of the transition region (sharpness of the transition) is as good or better than that observed for other surface-modification methods as well as providing thickness control from the nano- to micro-meter scale. This chapter illustrates the advantages of iCVD-deposited responsive polymer films where the subsequent chapters expand this theme, providing a more detailed picture of the polymer properties and how they can be controlled.

In CHAPTER THREE a method to improve the swelling / deswelling kinetics of the LCST transition through creation of a compositionally-graded responsive film. This is the first time both rapid swelling and deswelling kinetics have been presented. Additional analysis was performed via QCM-D measurements to determine time constants for the transition.

CHAPTER FOUR delves into the thermodynamic properties of the thin films as well as pNIPAAm chains using the similarities between the LCST coil to globule transition with protein folding and unfolding. A van't Hoff relationship was used to determine the enthalpy of transitions from UV-vis and QCM-D measurements. Analysis of the QCM-D data represents a novel technique by which thermodynamic properties of a surface-attached thin film can be obtained. Also illustrated here is a method to measure diffusion of molecules into a hydrogel matrix, which is especially applicable to the field of drug delivery.



CHAPTER FIVE utilizes the complementary techniques of oCVD and iCVD to develop membranes with dynamically-controlled permeability. oCVD pEDOT provides a conformal resistive heating property to the membranes, which can then be used to incite the hydrophobic change of the p(NIPAAm-co-DEGDVE) responsive layer deposited via iCVD on top.

CHAPTER SIX provides conclusions with respect to the synthesis of the temperature-responsive films. Emphasis is placed on how the techniques developed here have a wide range of applicability as well as what challenges are faced with further development of the technology. Several areas for future work are outlined both to better understand the polymer properties as well as what tailoring would be beneficial for future applications.

This material is based upon research supported by the DuPont MIT Alliance as well in part by the U.S. Army through the Institute for Soldier Nanotechnologies, under Contract DAAD-19-02-0002 with the US Army Research Office. The work also made use of the Center for Materials Science and Engineering shared facilities supported by NSF grant DMR-9400334.

## **1.5 References**

1. Ulbricht, M. *Reactive & Functional Polymers* **1996**, 31, 165-177.
2. Eichenbaum, G. M.; Kiser, P. F.; Simon, S. A.; Needham, D. *Macromolecules* **1998**, 31, 5084-5093.

3. Juodkazis, S.; Mukai, N.; Wakaki, R.; Yamaguchi, A.; Matsuo, S.; Misawa, H. *Nature* **2000**, 408, 178-181.
4. Tanaka, T.; Fillmore, D.; Sun, S.; Nishio, I.; Swislow, G.; Shah, A. *Physical Review Letters* **1980**, 45, 1636-1639.
5. Schild, H. G. *Progress In Polymer Science* **1992**, 17, 163-249.
6. Schmaljohann, D.; Byerlein, D.; Nitschke, M.; Werner, C. *Langmuir* **2004**, 20, 10107-10114.
7. Shiga, T. *Biopolymers/Pva Hydrogels/Anionic Polymerisation Nanocomposites* **1997**, 134, 131-163.
8. Irvin, D. J.; Goods, S. H.; Whinnery, L. L. *Chemistry of Materials* **2001**, 13, 1143-1145.
9. Yuan, W.; Jiang, G.; Wang, J.; Wang, G.; Song, Y.; Jiang, L. *Macromolecules* **2006**, 39, 1300-1303.
10. Chen, H.; Hsieh, Y. L. *Journal Of Polymer Science Part A-Polymer Chemistry* **2004**, 42, 6331-6339.
11. Kayaman, N.; Kazan, D.; Erarslan, A.; Okay, O.; Baysal, B. M. *Journal Of Applied Polymer Science* **1998**, 67, 805-814.
12. Kobayashi, J.; Kikuchi, A.; Sakai, K.; Okano, T. *Analytical Chemistry* **2001**, 73, 2027-2033.
13. Ulbricht, M. *Polymer* **2006**, 47, 2217-2262.
14. Chaterji, S.; Kwon, I. K.; Park, K. *Progress In Polymer Science* **2007**, 32, 1083-1122.

15. Kuckling, D.; Richter, A.; Arndt, K. F. *Macromolecular Materials And Engineering* **2003**, 288, 144-151.
16. Ichikawa, H.; Fukumori, Y. *Journal Of Controlled Release* **2000**, 63, 107-119.
17. Qiu, Y.; Park, K. *Advanced Drug Delivery Reviews* **2001**, 53, 321-339.
18. Idota, N.; Tsukahara, T.; Sato, K.; Okano, T.; Kitamori, T. *Biomaterials* **2009**, 30, 2095-2101.
19. Ahn, S.; Kasi, R. M.; Kim, S.; Sharma, N.; Zhou, Y. *Soft Matter* **2008**, 4, 1151-1157.
20. Gil, E.; Hudson, S. *Progress In Polymer Science* **2004**, 29, 1173-1222.
21. Yasuda, H., *Luminous Chemical Vapor Deposition and Interface Engineering*. Marcel Dekker: New York, 2005.
22. Baxamusa, S. H.; Im, S. G.; Gleason, K. *Physical Chemistry Chemical Physics* **2009**, 11, 5227-5240.
23. Baxamusa, S. H.; Gleason, K. *Chemical Vapor Deposition* **2008**, 14, 313-318.
24. Maeda, Y.; Higuchi, T.; Ikeda, I. *Langmuir* **2000**, 16, 7503-7509.
25. Sun, T.; Wang, G.; Feng, L.; Liu, B.; Ma, Y.; Jiang, L.; Zhu, D. *Angewandte Chemie-International Edition* **2004**, 43, 357-360.

## **2. CHAPTER TWO:**

***Sharp Hydrophilicity Switching and Conformality on Nanostructured Surfaces Prepared via Initiated Chemical Vapor Deposition (iCVD) of a Novel Thermally Responsive Copolymer***

Reproduced with permission from M. E. Alf, P. D. Godfrin, T. A. Hatton, K. K. Gleason, *Macromol. Rapid Commun.* **2010**, 31(24), 2166.

## 2.1 Abstract

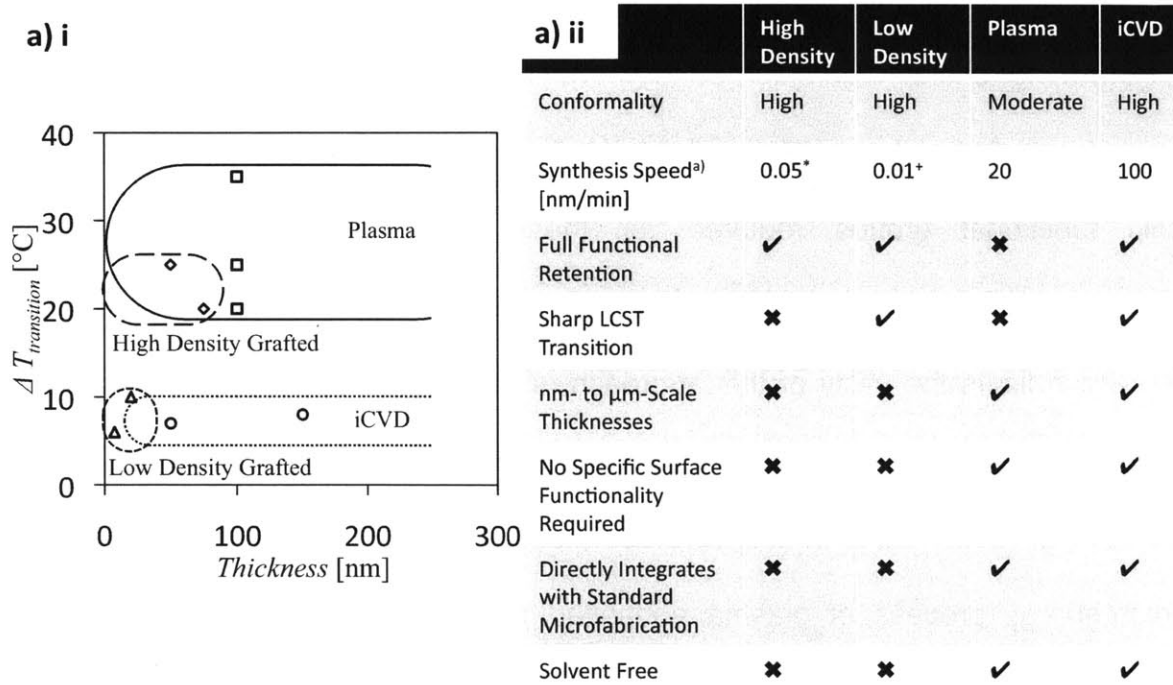
A novel thermally responsive copolymer p(NIPAAm-co-DEGDVE) is synthesized using the substrate independent method of iCVD and exhibits a sharp LCST transition centered at  $\sim 28.5 \pm 0.3$  °C determined via quartz QCM-D. Swelling with water below the LCST produces a reversible change of  $\sim 3x$  in film thickness. The layer is conformal on nanostructured surfaces including MWCNT forests and electrospun nanofiber mats. Modified planar substrates exhibit  $\sim 30^\circ$  change in static contact angle over the LCST, while through conformal coating on nanostructured substrates changes in static contact angle up to  $135^\circ$  are achieved. Additionally, coated surfaces exhibit temperature sensitive BSA adsorption measured by QCM-D and is reversible as shown through fluorescence imaging of a coated electrospun nanofiber mat.

## 2.2 Introduction

Integration of stimuli-responsive polymers<sup>1, 2</sup> with micro- and nano- structured substrates as “smart” surfaces for microelectrical and mechanical systems (MEMS), or medical devices, requires a surface modification process that provides conformal coverage. Additionally, substrates such as textiles and plastics that can be damaged by high temperatures or harsh solvents, ideally require low temperature, vapor phase deposition processes for their surface modification. These needs can be met by the process of initiated chemical vapor deposition (iCVD), as demonstrated in this paper in which we deposit a uniform layer of a novel thermally responsive copolymer on both flat as well as nano-structured substrates.

Poly(*N*-isopropylacrylamide) (pNIPAAm) belongs to a general class of temperature-responsive polymers that exhibit a lower critical solution temperature (LCST).<sup>3, 4</sup> The reversible hydrophilic/hydrophobic switch occurs at ~32 °C for bulk pNIPAAm.<sup>5</sup> Below its LCST, this polymer dissolves in aqueous solutions, such as cell culture media,<sup>6</sup> unless it is either grafted onto a substrate surface or is crosslinked to form a high molecular weight gel. However, these constraints on the chains often affect the value of the LCST transition and reduce its sharpness, as shown, for instance, by quartz crystal microbalance measurements with dissipation monitoring (QCM-D, Figure 2-1a i.).<sup>7-11</sup> A comparison of some of these surface modification techniques used to prepare NIPAAm-

based polymer surface functionalization are shown in Figure 2-1a ii. Both low-chain-density grafting-to and high-chain-density grafting-from methods allow for pNIPAAm coating of substrates from solution,<sup>9, 11, 12</sup> although not all substrates possess the specific functional groups required for these grafting approaches, even with pretreatment. Additionally, the polymer chain length limits the thickness of the grafted layers, which limits the utility of this approach, since much thicker films are desired to achieve a volumetric response for applications such as valves, actuators, and size-based separations. Thicker layers have been formed with NIPAAm as the monomer via the high-energy process of plasma enhanced chemical vapor deposition (PECVD), which inherently promotes cross-linking. With an increase in plasma excitation energy, cross-linking increases, but so does loss of polymer functionality, which can broaden and shift the LCST transition significantly from that of pure pNIPAAm (Figure 2-1a).<sup>7, 12-</sup>



\* Upper bound from literature + Not including surface preparation

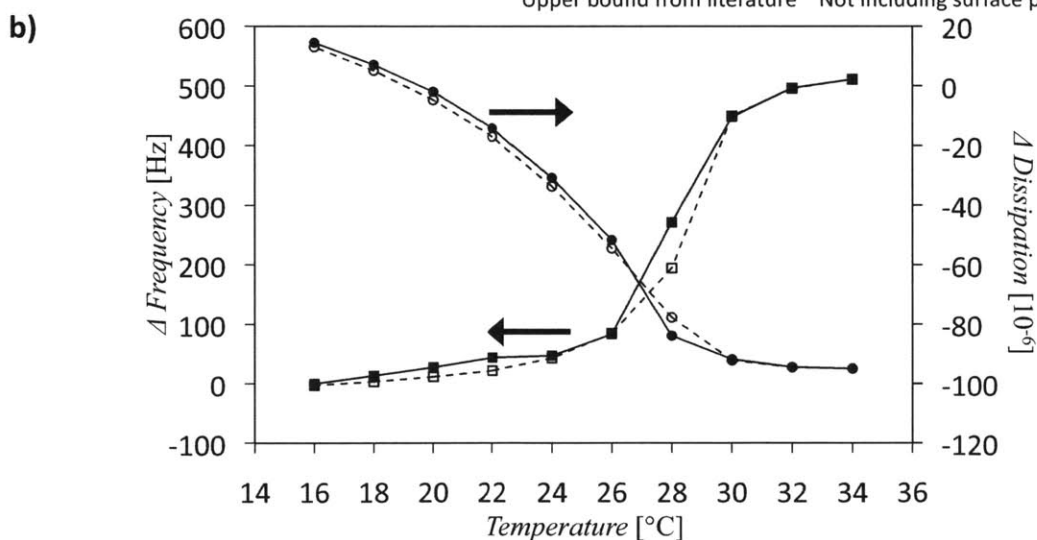


Figure 2-1. QCM-D LCST analysis a) i. schematic representation of achievable thickness range and LCST transition sharpness for pNIPAAm-based films from iCVD as compared to low density grafted layers,<sup>[8, 9]</sup> high density grafted layers,<sup>[9, 11]</sup> and plasma enhanced CVD<sup>[7]</sup> based on QCM-D data. a) ii. table comparing important characteristics of the same surface polymerization techniques. b) QCM-D data of the 7<sup>th</sup> harmonic from iCVD p(NIPAAm-co-DEGDVE) film at temperatures around the LCST. The solid lines correspond to data obtained ramping up temperature, while the dashed lines correspond to ramping down temperature.



In this paper, we demonstrate initiated chemical vapor deposition (iCVD) of lightly cross-linked films incorporating the NIPAAm monomer. The iCVD process is a solventless, low energy polymer deposition process, providing polymer structures equivalent to solution-phase polymerizations,<sup>15-17</sup> thus preserving the monomer functionality needed to achieve high-quality responsive behavior. We show that, unlike PECVD films, iCVD layers exhibit a sharp LCST transition (Figure 2-1a). The ability to deposit the polymer on virtually any substrate and create thick, cross-linked layers ranging from 25 nm to upwards of 1000 nm, makes iCVD an attractive alternative to grafting methods. The current work represents the first time a temperature-responsive film has been iCVD-polymerized, further expanding the capabilities of this versatile vapor synthesis method. Another key characteristic of iCVD is its ability to coat complex geometries conformally.<sup>18</sup> As designs for MEMs and other devices are becoming more complex, conformal coverage becomes increasingly important to assure that the desired chemical functionality is applied over the entire surface geometry.

## 2.3 Results and Discussion

Fourier Transform Infrared Spectroscopy (FTIR) confirmed successful iCVD homopolymerization of pNIPAAm. Peaks corresponding to the vinyl moieties of the monomer at  $1620\text{ cm}^{-1}$  and  $1405\text{ cm}^{-1}$  are clearly absent in the iCVD film (Figure 2-2). The peak intensities of the iCVD polymer spectrum match those for the pNIPAAm standard, indicating retention of each of the important functional groups of the polymer, including isopropyl C-H stretching between  $3000\text{ cm}^{-1}$  and  $2820\text{ cm}^{-1}$ , secondary amine

N-H stretching at  $3290\text{ cm}^{-1}$ , and amide C-N-H bending at  $1530\text{ cm}^{-1}$  and C=O stretching at  $1645\text{ cm}^{-1}$ .

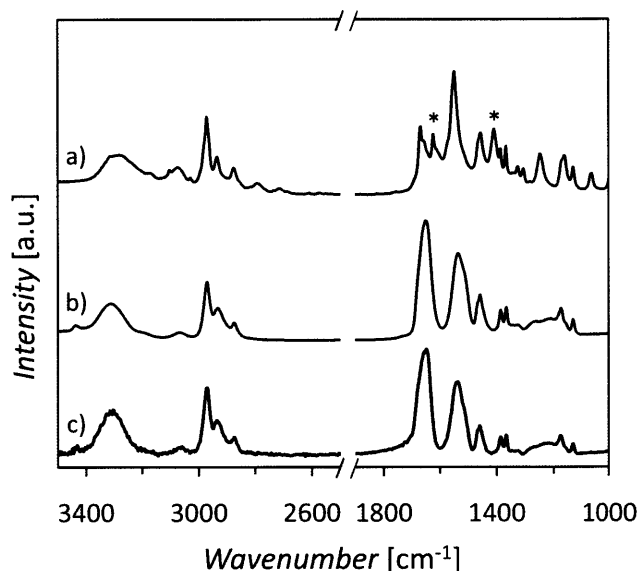


Figure 2-2. FTIR spectra of a) NIPAAm monomer, b) commercial pNIPAAm reference sample, and c) iCVD pNIPAAm homopolymer. Peaks associated with the vinyl bonds of the monomer are marked (\*) and are absent in the polymer spectra. Additionally, no differences between the conventionally synthesized and iCVD-polymerized materials can be resolved by FTIR.

In order to produce a film which resists dissolution, the crosslinker di(ethylene glycol) divinyl ether (DEGDVE) was added to the iCVD process, chosen because of its proven compatibility with the iCVD system<sup>19</sup> and relatively high vapor pressure, which limits adsorption on the growth surface, and hence limits cross-linking. Reduced crosslinking is anticipated to result in responsive properties closer to those of pure pNIPAAm. To our knowledge, this represents the first synthesis of p(NIPAAm-co-DEGDVE) copolymer reported by any method. Due to the lack of strong FTIR absorption peaks for DEGDVE quantification of the small amount of the crosslinker in the film was difficult. An analysis

based on the area under the C=O stretching peak indicates that there is approximately 5 - 10% DEGDVE in the copolymer films (Figure 2-3). Although it was difficult to determine the exact composition, the presence of the crosslinker was confirmed via a simple washing step, where the iCVD pNIPAAm homopolymer completely dissolved when rinsed for 15 seconds with water and p(NIPAAm-co-DEGDVE) survived such rinsing.

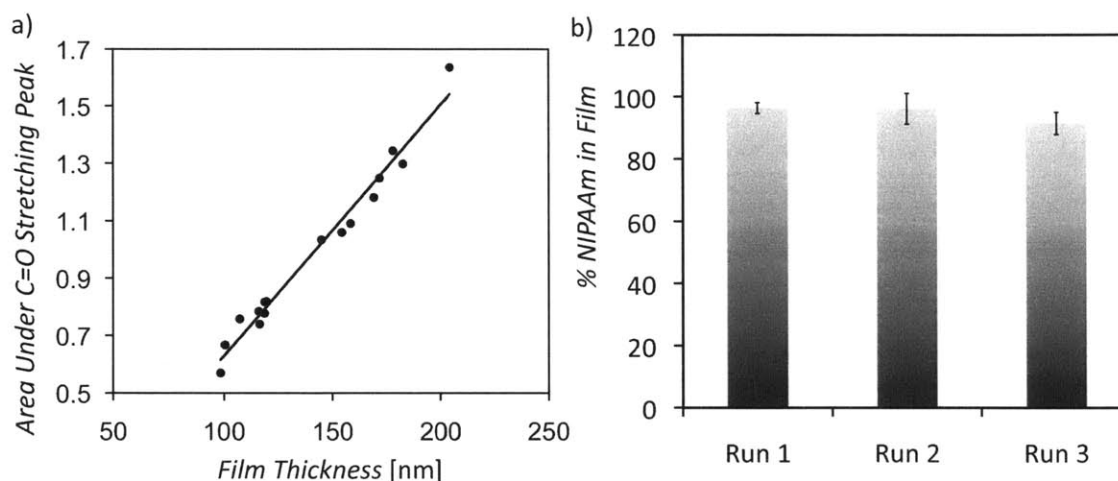


Figure 2-3. a) Correlation between pNIPAAm film thickness and area under the FTIR spectra C=O stretching peak centered at  $1645\text{ cm}^{-1}$ . Solid line represents linear fit to this data. b) Composition of three representative p(NIPAAm-co-DEGDVE) films deposited under the same conditions (as given in methods). The small compositional differences seen here are due to slight NIPAAm flow rate variations during the deposition. Compositions were calculated from area under the C=O stretching peak compared to the pNIPAAm calibration.

QCM-D measurements showed a sharp LCST transition for the iCVD film (Figure 2-1b). The higher frequencies observed with increasing temperature indicate the expulsion of absorbed water from the polymer layer, which reduced the viscoelasticity of

the layer, and hence the observed dissipation decreased.<sup>9</sup> The frequency data are well described by a non-linear least squared errors fit to an “s”-curve of the form

$$\Delta F = \frac{A}{1 + \exp(-B(T - T_{LCST}))} + C, \quad (1)$$

where A, B, C, and  $T_{LCST}$  (°C) are fit parameters (Figure 2-4). The inflection point corresponds to an LCST of  $28.5 \pm 0.3$  °C, slightly lower than the 32 °C value for bulk pNIPAAm homopolymer, most likely as a result of the incorporation of the DEGDVE units and constraints imposed by the consequent crosslinking.

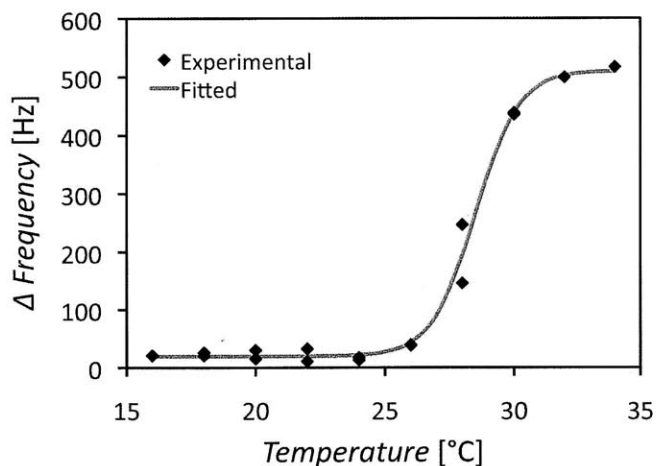


Figure 2-4. QCM-D frequency data with the fitted s-curve of the form given in Equation 1. The fitted parameters of the curve shown here are  $490 \pm 30$  Hz,  $1.2 \pm 0.3$  °C<sup>-1</sup>,  $20 \pm 3$  Hz and  $28.5 \pm 0.3$  °C for A, B, C and  $T_{LCST}$  respectively.

The swollen iCVD hydrogel formed below the LCST was a factor of  $3.0 \pm 0.3$  thicker than in its dry state as determined by Variable Angle Spectroscopic Ellipsometry

(VASE). This swelling ratio is comparable to that achieved with bulk hydrogels,<sup>20</sup> which is notable because the geometrical constraints imposed by the substrate would generally be expected to limit the swellability of hydrogel thin films.<sup>21</sup> We believe that the low cross-linker density and high functional retention of the polymer both contribute to the high swelling ratio, and transition sharpness. When the film was heated to above the LCST while still immersed in DI water, the layer thickness reverted to the dry state value, indicating essentially complete expulsion of water from the gel, in agreement with previous studies.<sup>22</sup> The VASE measurements were reproducible over at least three heating / cooling cycles.

iCVD is a mild process, which can successfully coat practical substrates that may lack solvent or thermal resistance or have non-planar geometries.<sup>23</sup> Figure 2-5a and b display the conformality of iCVD p(NIPAAm-co-DEGDVE) deposited over micron-scale trenches etched in silicon. In agreement with results for other iCVD polymers,<sup>18</sup> conformality improved on reduction of the monomer partial pressure. Conformality can also be achieved on the nano-scale features of both electrospun nanofiber mats and multi-walled carbon nanotube (MWCNT) forests. The morphology of the nanofiber mat remained unchanged after deposition (Figure 2-5c), without the merging of individual fibers at crossover points seen many times with solution processing methods, thus retaining the high surface area of the mat. Figure 2-5d verifies that p(NIPAAm-co-DEGDVE) can successfully coat MWCNT forests, preserving the CNT morphology while providing responsive surface properties.

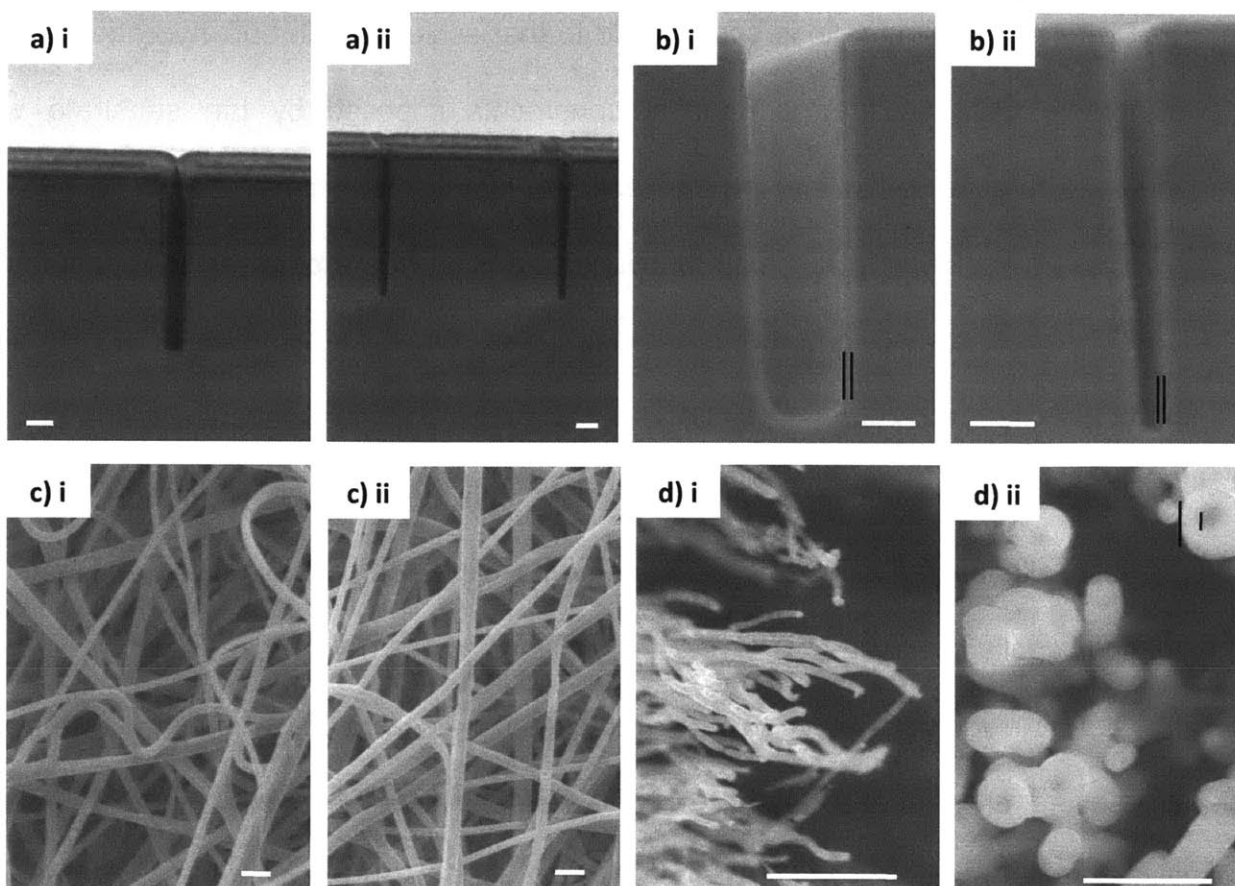


Figure 2-5. SEM images of a cross-section of iCVD p(NIPAAm-co-DEGDVE) coated trenches cut into a silicon wafer with aspect ratios of a) i. and b) i. 7:1, and a) ii. and b) ii. 14:1. a) represents poor conditions for conformality, where b) represents improved conditions for conformality on a complex geometry. The black lines are guides to highlight film thickness. SEM images of c) i. uncoated and ii. 200 nm coated electrospun nanofiber mats, and d) i. uncoated and ii. coated carbon nanotube forests. The scale bar on each image represents 1  $\mu\text{m}$ . The black lines in image d) ii. highlight polymer film thickness of approximately 150 nm.

Figure 2-6a shows switchable surface properties imparted by the p(NIPAAm-co-DEGDVE) film as investigated via static contact angle measurements. For a p(NIPAAm-co-DEGDVE) coating on a flat silicon wafer, a  $30^\circ$  change in contact angle is seen as the temperature increases from 25  $^\circ\text{C}$  to a temperature of 40  $^\circ\text{C}$ , above the LCST. This change in contact angle is comparable to the values previously reported in literature.<sup>24,</sup>

<sup>25</sup> The effect of the conformal coating of p(NIPAAm-co-DEGDVE) on the rough surfaces

of an electrospun nanofiber mat and a MWCNT forest are also shown. At 25 °C, the water droplet was pulled into the nanofiber mat via capillary forces. When a droplet is introduced at a substrate temperature of 40°C, the contact angle increased dramatically to 125° due to the combined surface characteristics of roughness and hydrophobic functionalization, which is comparable to what has been previously reported.<sup>26</sup> The same contact angles above and below the LCST were seen on both the top and bottom sides of the mats, indicating that monomers penetrated the mat, coating the entire thickness. The contact angle on the coated CNT forest increased from 50° to 135° as the temperature is increased above the LCST; in contrast to the nanofiber mats, this process was reversible under several heating and cooling cycles. These contact angle measurements illustrate the dramatic effect a NIPAAm based polymer coating can have on the surface properties of a device.

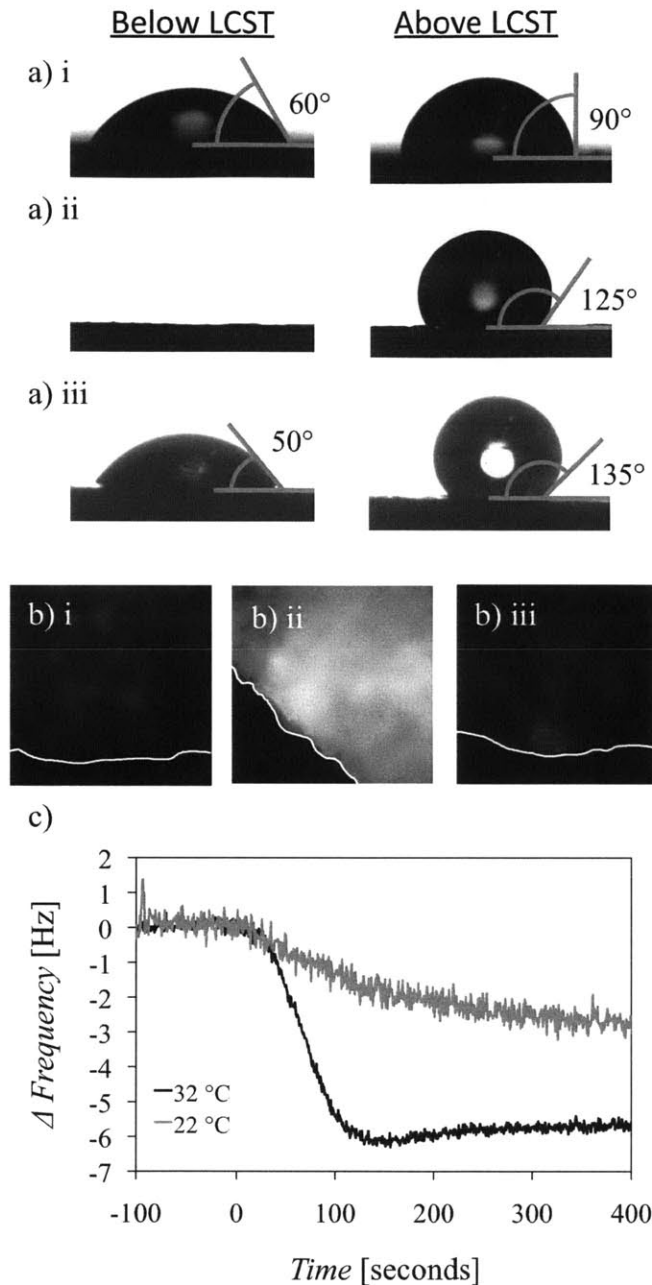


Figure 2-6. a) Static contact angles both below and above the LCST on various coated substrates including i. flat Si wafer, ii. electrospun nanofiber mat and iii. MWCNT forest. b) Fluorescence images at 40x magnification of p(NIPAAm-co-DEGDVE) coated nanofiber mats after soaking for 30 minutes in tetramethylrhodamine-labeled BSA in PBS at i.  $25^\circ\text{C}$  and ii.  $40^\circ\text{C}$ . The mat at  $40^\circ\text{C}$  was rinsed at  $25^\circ\text{C}$  resulting in image iii. The white lines represent the edge of the mat. c) QCM-D data depicting frequency vs. time as BSA was introduced to the system at time 0 at two different temperatures.



The reversible hydrophilic / hydrophobic switch can be utilized in practice for applications such as cell growth and protein separations. iCVD p(NIPAAm-co-DEGDVE) has reversible protein adsorption properties as illustrated by Figure 2-6b and c. Panel b represents a set of fluorescence imaging experiments showing the adsorption and desorption of tetramethylrhodamine-labeled bovine serum albumin (BSA) to p(NIPAAm-co-DEGDVE)-coated electrospun nanofiber mats. There was a marked increase in fluorescence on the mat at temperatures above the LCST, which was lost once the mat was cooled again to below the LCST (Figure 2-6b iii ), an important observation that indicates the reversibility of protein adsorption simply through temperature change.

QCM-D, which has been used to study protein adsorption onto surfaces,<sup>27</sup> was used here to monitor the adsorption of BSA on the p(NIPAAm-co-DEGDVE) films, which, to our knowledge, is the first time the technique has been used for NIPAAm-based polymers. The frequency change of the QCM-D crystal was monitored while a solution of 10 mg/mL BSA in PBS was passed through the QCM-D cell at temperatures above (32 °C) and below (22 °C) the LCST of the polymer film. The frequency changes depicted in Figure 2-6c, which reflect changes in the mass of the film, record the rapid adsorption of protein to the film at temperatures above the LCST, when the film is hydrophobic. At short times, the adsorption of BSA at temperatures below the LCST is much lower, because hydrophobic interactions are suppressed. These results demonstrate our ability to control protein adsorption on a surface afforded by a p(NIPAAm-co-DEGDVE) thin film.

## 2.4 Conclusions

We have shown the successful deposition of conformal thin films of both pNIPAAm and the novel copolymer p(NIPAAm-co-DEGDVE) via iCVD. Complete functional retention and conformal coating of geometrically complex surfaces were achieved via this one step, solventless process. Compared to grafting, the iCVD technique affords the ability to control overall film thicknesses ranging from the nanometer to micron scale. The bulk responsive properties of the copolymer were shown to be equal or superior to grafted pNIPAAm chains based on QCM-D measurements. The LCST of the iCVD polymer was determined to be  $28.5 \pm 0.3$  °C, with the transition occurring over a narrow temperature range, where 80% of the change happened over 4 °C. Swollen film thickness was ~3 times the dry film thickness below the LCST, and reversibly reduced to the dry film thickness above the LCST. Coated surface properties showed responsive wettability with a static contact angle change around the LCST of 30° for flat surfaces to up to 135° for conformally-coated, nanostructured surfaces. The combined effects of surface and bulk responsive behavior provided variable BSA adsorption properties with small changes in temperature as measured via QCM-D. Fluorescence imaging shows that this adsorption is also reversible, indicating that this polymer could be viable for applications involving protein separation or adsorption. We believe that the combined characteristics of a sharp LCST transition and conformal coverage make these films ideal for smart surface applications such as in MEMS devices.

## 2.5 Experimental

### 2.5.1 iCVD Polymerization

The polymerization took place in a custom built cylindrical reactor described previously.<sup>15</sup> Depositions were performed on several substrates including 100 mm diameter Si wafers (WaferWorld), nylon-6,6 electrospun nanofiber mats (DuPont) and multi walled carbon nanotube (MWCNT) forests (Nanolabs). NIPAAm (Acros, 99%), EGDA (Aldrich, 99%), and *tert*-butyl peroxide initiator (TBPO) (Aldrich, 98%) were purchased and used without further purification. NIPAAm (0.15 sccm) and DEGDVE (1.7sccm) were heated to 75 °C and 40 °C respectively and vapors were fed to the reactor. TBPO (1.0 sccm) was kept at room temperature and its vapors were fed into the reactor via a mass flow controller (MKS 1490A). For the pure pNIPAAm films, NIPAAm and TBPO were fed into the reactor concurrently with a reactor pressure of 100 mTorr. For the cross-linked films, DEGDVE was added to the other two with the reactor at a pressure of 200 mTorr. The same deposition conditions were used for all films analyzed in this paper.

### 2.5.2 Film Characterization

FTIR (Nicolet Nexus 870 spectrometer) spectra were obtained in normal transmission mode using a deuterated triglycine sulfate (DTGS) KBr detector over 400-4000  $\text{cm}^{-1}$  at 4  $\text{cm}^{-1}$  resolution averaged over 64 scans. All spectra were baseline corrected. pNIPAAm (Aldrich,  $M_n$  20,000 – 25,000) was purchased and used as an FTIR reference standard. Film thicknesses were measured using VASE (JA Woollam M-2000) for both dry and swollen films by mounting coated wafers in a liquid cell (JA Woollam). An incident angle of 75° was used and the data were fit to a Cauchy-Urbach

isotropic model with an ambient water layer using commercial modeling software (WVASE32, JA Woollam). Film thicknesses were taken dry, after 5 minutes in DI water, and 5 minutes after heating to 40 °C. Contact angle measurements were performed on a goniometer equipped with an automatic dispenser (Model 500, Ramé-Hart) using a 4 µL DI water droplet. Measurements were taken both at room temperature (~25 °C) and after heating the substrate to 40 °C.

LCST behavior was determined using QCM-D (Model E4, Q-sense). Gold-coated QCM-D sensors with a fundamental frequency of 5 MHz (QSX-301, Q-sense) were used as a deposition substrate. Duplicate coated sensors and blank reference were placed in flow cells with DI water flowing at a rate of 100 µL/min. The Peltier heating element was programmed to equilibrate for 20 minutes at each temperature starting from 16 °C and allowing 1 minute to ramp the temperature by 2 °C up to 34 °C and back down. The values obtained from the blank crystal were subtracted from that of the coated crystal to remove the inherent dependence of the system on temperature.

### **2.5.3 Protein Adsorption**

Fluorescence measurements were performed by coating the electrospun nanofiber mats with 200 nm of p(NIPAAm-co-DEGDVE) and soaking samples in albumin from bovine serum (BSA), tetramethylrhodamine conjugate (Invitrogen, 0.5 mg/mL) in phosphate buffer solution (PBS) at either 25 °C or 40 °C. The mats were then removed and rinsed with PBS at the same temperature. The samples were imaged using a Zeiss Axiovert inverted microscope using a rhodamine filter set. The 40 °C mat was then rinsed for 30 seconds at 25 °C and reimaged. The QCM-D protein adsorption

measurements were done using the same equipment and films as the LCST measurements. The films were allowed to equilibrate at either 22 °C or 32 °C for 30 minutes while flowing PBS (100  $\mu$ L/min). Then the solution was changed to BSA in PBS (10 mg/mL), and monitored at constant temperature.

## 2.6 Acknowledgements

We thank the *DuPont MIT Alliance* for financial support. We thank the *MIT CMSE* shared facilities supported in part by the *MRSEC program* of the *National Science Foundation* under Award DMR 02-13282. We also thank Dr. *Edward Gleason* of *Analog Devices* for providing the trench structures.

## 2.7 References

1. Huber, D. L.; Manginell, R. P.; Samara, M. A.; Kim, B. I.; Bunker, B. C. *Science* **2003**, 301, 352-354.
2. Richter, A.; Paschew, G. *Adv. Mater.* **2009**, 21, 979-+.
3. Ahn, S.; Kasi, R. M.; Kim, S.; Sharma, N.; Zhou, Y. *Soft Matter* **2008**, 4, 1151-1157.
4. Gil, E.; Hudson, S. *Prog. Polym. Sci.* **2004**, 29, 1173-1222.
5. Schild, H. G. *Prog. Polym. Sci.* **1992**, 17, 163-249.
6. Idota, N.; Tsukahara, T.; Sato, K.; Okano, T.; Kitamori, T. *Biomaterials* **2009**, 30, 2095-2101.
7. Tamirisa, P. A.; Hess, D. W. *Macromolecules* **2006**, 39, 7092-7097.

8. Ishida, N.; Biggs, S. *Langmuir* **2007**, *23*, 11083-11088.
9. Zhang, G.; Wu, C. *Macromolecular Rapid Communications* **2009**, *30*, 328-335.
10. Ma, H.; Fu, L.; Li, W.; Zhang, Y.; Li, M. *Chemical Communications* **2009**, 3428-3430.
11. Annaka, M.; Yahiro, C.; Nagase, K.; Kikuchi, A.; Okano, T. *Polymer* **2007**, *48*, 5713-5720.
12. Teare, D. O. H.; Barwick, D. C.; Schofield, W. C. E.; Garrod, R. P.; Beeby, A.; Badyal, J. P. S. *Journal Of Physical Chemistry B* **2005**, *109*, 22407-22412.
13. Pan, Y. V.; Wesley, R. A.; Luginbuhl, R.; Denton, D. D.; Ratner, B. D. *Biomacromolecules* **2001**, *2*, 32-36.
14. Cheng, X. H.; Canavan, H. E.; Stein, M. J.; Hull, J. R.; Kweskin, S. J.; Wagner, M. S.; Somorjai, G. A.; Castner, D. G.; Ratner, B. D. *Langmuir* **2005**, *21*, 7833-7841.
15. Chan, K.; Kostun, L. E.; Tenhaeff, W. E.; Gleason, K. *Polymer* **2006**, *47*, 6941-6947.
16. Martin, T. P.; Kooi, S. E.; Chang, S. H.; Sedransk, K. L.; Gleason, K. K. *Biomaterials* **2007**, *28*, 909-915.
17. Tenhaeff, W. E.; Gleason, K. *Langmuir* **2007**, *23*, 6624-6630.
18. Ozaydin-Ince, G.; Gleason, K. *Chem. Vap. Deposition* **2010**, *16*, 1-9.
19. Tenhaeff, W. E.; Gleason, K. *Chem. Mater.* **2009**, 1-9.
20. Kayaman, N.; Kazan, D.; Erarslan, A.; Okay, O.; Baysal, B. M. *J. Appl. Polym. Sci.* **1998**, *67*, 805-814.
21. Toomey, R.; Freidank, D.; Ruhe, J. *Macromolecules* **2004**, *37*, 882-887.

22. Maeda, Y.; Higuchi, T.; Ikeda, I. *Langmuir* **2000**, 16, 7503-7509.
23. Baxamusa, S. H.; Im, S. G.; Gleason, K. *PCCP* **2009**, 11, 5227-5240.
24. Sun, T.; Wang, G.; Feng, L.; Liu, B.; Ma, Y.; Jiang, L.; Zhu, D. *Angew. Chem. Int. Ed.* **2004**, 43, 357-360.
25. Tamirisa, P. A.; Koskinen, J.; Hess, D. W. *Thin Solid Films* **2006**, 515, 2618-2624.
26. Fu, G. D.; Xu, L. Q.; Yao, F.; Zhang, K.; Wang, X. F.; Zhu, M. F.; Nie, S. Z. *ACS Applied Materials and Interfaces* **2009**, 1, 239-243.
27. Baxamusa, S. H.; Gleason, K. *Adv. Funct. Mater.* **2009**, 19, 3489-3496.

# **3. CHAPTER THREE:**

***Novel N-isopropylacrylamide Based  
Polymer Film Architecture for Faster  
LCST Transition Kinetics***



### 3.1 Abstract

Temperature-responsive p(N-isopropylacrylamide-co-ethylene glycol dimethacrylate) (p(NIPAAm-co-EGDMA) films, graded in composition to provide a NIPAAm-rich surface, were synthesized successfully via initiated chemical vapor deposition (iCVD). Their dynamic response to temperature changes as monitored using quartz crystal microbalance with dissipation monitoring (QCM-D) was clearly distinguishable from the response of control iCVD-prepared films of homogeneous composition. The lower critical solution temperature (LCST) of the homogeneous copolymer (15 °C) was less than that reported for pure NIPAAm (32 °C) due to the hydrophobicity of the comonomer, EGDMA. The graded films displayed a broader transition over the range from 16 to 28 °C. The time constants associated with the response to small step changes in temperature around the LCST transition were significantly smaller in the graded (<143 s) than in the homogeneous films (1000 to 8000 s). The novel graded film architecture is promising for facilitating fast switching in applications requiring responsiveness to temperature swings.

## 3.2 Introduction

Stimuli-responsive or “smart” polymers exhibit a change in their properties in response to the application of an appropriate environmental stimulus such as light,<sup>1-3</sup> temperature,<sup>4, 5</sup> pH,<sup>6, 7</sup> redox potentials,<sup>8</sup> and magnetic or electric field,<sup>9, 10</sup> among others.<sup>11, 12</sup> These “smart” materials can be integrated into devices where their responsive behavior can be harnessed to achieve a functional, mechanical or chemical response in applications ranging from separations to mechanical actuation.<sup>13-17</sup> Temperature responsive polymers have been studied extensively, particularly those that exhibit a lower critical solution temperature (LCST), below which the polymer chains are fully hydrated when in aqueous solution, and above which the polymer chains undergo a sharp change in hydrophobicity and collapse into a globular state. N-isopropylacrylamide (NIPAAm)-based polymers are of particular interest as the LCST of polyNIPAAm (pNIPAAm) is approximately 32 °C,<sup>4</sup> which is close to body temperature and thus suitable for many biological applications.

The use of these polymers in systems such as membrane separations or MEMS devices requires surface modification of a base substrate, which many times has a micro- or nano-structure important to the application. Several techniques have been shown to provide surface functionalization including common solution-phase methods such as polymer grafting-to<sup>18, 19</sup> or grafting-from,<sup>20-22</sup> and vapor-phase methods that

include initiated chemical vapor deposition (iCVD)<sup>23</sup> and plasma enhanced chemical vapor deposition (PECVD).<sup>24-26</sup> The LCST properties of the thin films must be well understood in order to be of use in a given application and it is notoriously difficult to characterize thin films on modified surfaces due to substrate constraints. In many cases, however, thin film properties and behavior can be elucidated successfully using quartz crystal microbalance with dissipation monitoring (QCM-D).

We describe in this paper a novel, compositionally-graded film generated by iCVD (Figure 3-1) that greatly improves both the swelling and deswelling kinetics in response to small temperature changes within the LCST transition range even for films that are substantially thicker than conventionally synthesized grafted layers. The LCST deswelling kinetics of pNIPAAm gels have been shown previously to be improved through the grafting of free chains onto a cross-linked pNIPAAm matrix, which form hydrophobic cores to enhance the aggregation of the networks and prevent the formation of a surface skin layer that would hinder mass transfer.<sup>27, 28</sup> Incorporation of voids in the gels also improves the deswelling transition kinetics by reducing mass transfer resistances.<sup>29</sup> The graded film developed here functions by creating a range of local LCST's distributed over the film that enhance not only the deswelling kinetics, as observed in the aforementioned works, but also aid in speeding up the swelling kinetics of the cross-linked film. We also show that QCM-D provides a useful platform to gain insight into the kinetics of this transition through suitable modeling of the frequency and dissipation response of the films to small thermal disturbances.

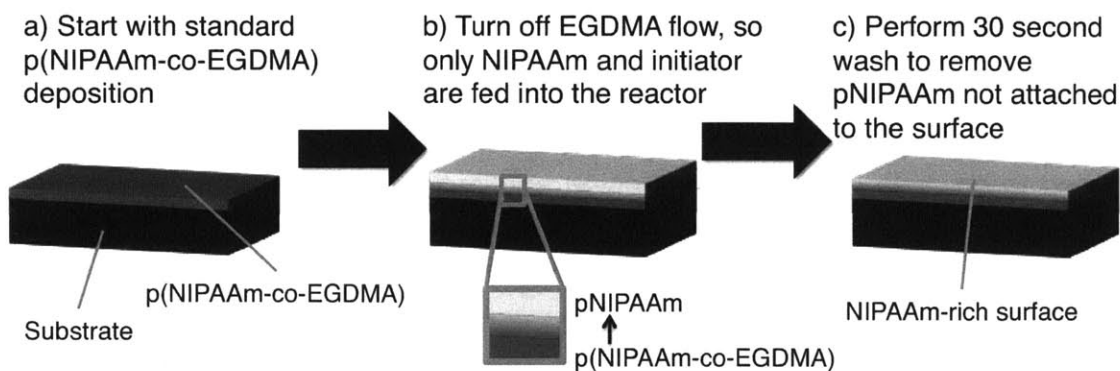


Figure 3-1. Schematic of the process used to synthesize graded polymer films with a NIPAAm-rich surface. Preparation of (a) the copolymer base layer of homogeneous composition, (b) the as-deposited graded film, and (c) the graded film after rinsing.

We compare directly the temperature responses of p(NIPAAm-co-EGDMA) copolymer films that are homogeneous in composition throughout, to films of comparable thickness, which are graded to create a NIPAAm-rich surface on top of a base layer of higher cross-linker content (comparable to that in the homogeneous films). The LCST behavior of the homogenous copolymer (Figure 3-1(a)) and graded films after rinsing (Figure 3-1(c)) was evaluated primarily through an analysis of transient QCM-D responses following small step changes in temperature. The latter novel film architecture shows faster LCST transition kinetics, attributed to the grafting of the surface pNIPAAm chains to the cross-linked base film.

### 3.2.1 iCVD Background

iCVD was used as the novel synthesis method as it is a solvent-free process that provides high thin film conformality and complete functional retention.<sup>30</sup> Additionally, the iCVD film deposition rates are fast (up to around 100 nm/min depending on the polymer

system and conditions) and can be measured *in situ* by interferometry or with a quartz crystal microbalance (QCM), allowing control of the final film thickness since the film growth can be stopped once the desired thickness has been achieved. Finally, and most importantly, since iCVD films grow from the substrate interface outwards, dynamic control over the concentration of gaseous reactants during the deposition period opens up the possibility to prepare films with tailored compositional gradients through the thickness of the film, i.e., variable film properties in the direction normal to the substrate surface can be introduced in real-time during the deposition process. Indeed, iCVD compositionally graded films have been synthesized successfully from the monomers 2-hydroxyethyl methacrylate (HEMA) and pentafluorophenylmethacrylate (PFM) to create swellable bulk HEMA-rich hydrogel films with PFM-rich surface functionalities for reaction with growth factors.<sup>31</sup> We used this same principle to form a polymer film with a base of poly(*N*-isopropylacrylamide-co-ethylene glycol dimethacrylate) (p(NIPAAm-co-EGDMA)) having a NIPAAm-rich surface functionality, as shown in Figure 1.

### 3.2.2 QCM-D Background

In QCM-D, a quartz crystal is coated with the thin film and exposed to a surrounding fluid. Multiple orders of the crystal vibration harmonics are measured in real-time to determine the changes in frequency and dissipation relative to the starting point. Because the crystal vibrations are induced electrically with different charges on each side of the crystal, only odd order harmonics can be measured. The temperature of the film and the surrounding liquid is controlled to within  $\pm 0.1$  °C, making QCM-D an ideal

tool to study the temperature-responsive behavior of thin films. Observed frequency shifts primarily measure changes in mass of the load on the crystal, and can therefore be used to monitor swelling of a hydrogel film or the adsorption of materials to its surface. Dissipation measures the time it takes for the harmonic vibrations to dissipate after the electrical stimulus is removed, thus giving information on the viscoelastic properties of the coating and surrounding fluid. There is some correlation between these two measurements, but, in general, frequency and dissipation can be attributed primarily to mass and viscoelasticity, respectively.

Also important when studying the temperature behavior of a sample is the inherent temperature response of the QCM-D system to temperature due mostly to viscoelastic changes in the surrounding fluids, which is given by

$$\Delta f = -C_T f_0 \Delta T, \quad (1)$$

where  $\Delta f$  is the frequency change,  $C_T$  is a constant based on the crystal manufacturing process,  $f_0$  is the fundamental frequency of the crystal and  $\Delta T$  is the temperature change. This effect must be accounted for in any analysis performed on data taken at different temperatures.

The QCM-D technique measures the transient response to whatever stimulus is applied to the system, in our case to a step change in temperature. This transient response provides kinetic information, while the final state gives the equilibrium response of the system to the stimulus. Both grafted pNIPAAm and plasma-polymerized pNIPAAm have been studied in the QCM-D system and exhibit distinctly different

signatures that are characteristic of the type of polymer film examined. Densely grafted and highly cross-linked films tend to exhibit hysteresis and have a broader LCST transition.<sup>20, 32</sup> In some cases evaluation of the transient data reveals that the hysteresis can be attributed partially to the fact that the system may not have reached equilibrium during the allotted measurement time. Polymeric layers with fewer steric constraints (e.g. low grafting and/or crosslinking density) generally respond rapidly to stimuli, with a sharper transition and minimal hysteresis.<sup>21, 23, 32</sup> An understanding of the effect of polymer chain architecture of a pNIPAAm-based film on its kinetic response to an applied stimulus will permit the tailoring of modified surfaces to provide the desired overall response time for a wide range of applications.<sup>1</sup>

### **3.3 Experimental**

#### **3.3.1 iCVD Polymerization**

All reactions took place in a custom-built reactor as described previously.<sup>33</sup> NIPAAm (Acros, 99%), EGDMA (Aldrich, 98%), and *tert*-butyl peroxide (TBPO) initiator (Aldrich, 98%) were purchased and used without further purification.

For the base cross-linked films, TBPO vapors (room temperature) were fed into the reactor through a mass flow controller (MKS 1490A) at a flow rate of 1.0 sccm. The monomers NIPAAm and EGDMA were kept at 80 °C and 50 °C respectively and fed into the reactor via fully open diaphragm valves at respective flow rates of 0.3 sccm and 0.6 sccm. All three vapors were fed concurrently while keeping the reactor pressure at 150

---

<sup>1</sup> For more information on QCM-D, please refer to the Q-Sense website (<http://www.q-sense.com/>) and their listed publications.

mTorr. The substrate was kept at a temperature of 45 °C to promote monomer adsorption and the filaments were held at 200 °C throughout the course of the deposition. Both gold-coated QCM-D crystals with a fundamental frequency of 5 MHz (QSX-301, Q-sense) and bare Si wafers (WaferWorld) were included as substrates during each deposition. The Si wafers were used for in situ interferometry with a 633 nm HeNe laser source (JDC Uniphase) to monitor and achieve film thicknesses of approximately 50 nm.

The graded films with a NIPAAm-rich surface were formed by initially growing a homogeneous film to a thickness of approximately 50 nm. Then, without delay or breaking vacuum, and keeping all other reaction conditions constant, the EGDMA inlet flow was stopped, allowing the polymerization to continue with only pNIPAAm growing from the radical sites on the surface of the film, or from any pNIPAAm polymer chains that may have formed on the surface. The reaction was stopped after an additional 50 nm of film growth, and, following removal of the substrate from the reaction chamber, the non-bonded pNIPAAm chains were removed by a 30 second DI water rinse.

Pure pNIPAAm and pEGDMA films were deposited on Si wafers in the same iCVD unit to serve as reference standards for Fourier transform infrared spectroscopy (FTIR). The flow rate of each of the individual components was the same as before, but in these cases only TBPO and NIPAAm, or TBPO and EGDMA, were fed into the reactor, where the pressure was maintained at 100 mTorr for the pNIPAAm film, or 175 mTorr for the pEGDMA deposition. Approximately 200 nm of polymer film was deposited in each case.



### 3.3.2 Film Characterization

FTIR (Nicolet Nexus 870 spectrometer) spectra were obtained in normal transmission mode using a deuterated triglycine sulfate (DTGS) KBr detector over 400-4000  $\text{cm}^{-1}$  at 4  $\text{cm}^{-1}$  resolution averaged over 256 scans. All spectra were baseline corrected. pNIPAAm (Aldrich,  $M_n$  20,000 – 25,000) was purchased and used as an FTIR reference standard. Film thicknesses were measured using variable angle spectroscopic ellipsometry (VASE) (JA Woollam M-2000).

LCST behavior was evaluated using a QCM-D unit (Model E4, Q-sense). Duplicate coated sensors and blank reference were placed in flow cells with DI water flowing at a rate of 100  $\mu\text{L}/\text{min}$ . The Peltier heating element was programmed to equilibrate for 20 minutes at each temperature. Changes in both frequency and dissipation for harmonics of order 1, 3, 5, 7 and 9 were monitored to provide the transient response profiles, although only the 3<sup>rd</sup>, 5<sup>th</sup>, and 7<sup>th</sup> order harmonics were used in subsequent analyses, as they were most consistently reliable for all polymer systems studied. The equilibrium frequency and dissipation curves with respect to temperature were obtained using the transient value for each harmonic order at the end of the 20 min equilibration period. There is an inherent linear dependence of the QCM-D system on temperature, so the equilibrium data obtained from the blank crystal were subtracted from those of the coated crystals to get the final equilibrium curve form.

## 3.4 Results and Discussion

### 3.4.1 QCM-D of the homogeneous copolymer film

Thin p(NIPAAm-co-EGDMA) films of approximately 80 nm dry thickness, as measured by VASE on a reference Si wafer, were deposited on QCM-D crystals. The frequency and dissipation responses were monitored following a series of step changes in temperature over the temperature range of 10 to 30 °C in order to cover the LCST range of the polymer (Figure 3-2).

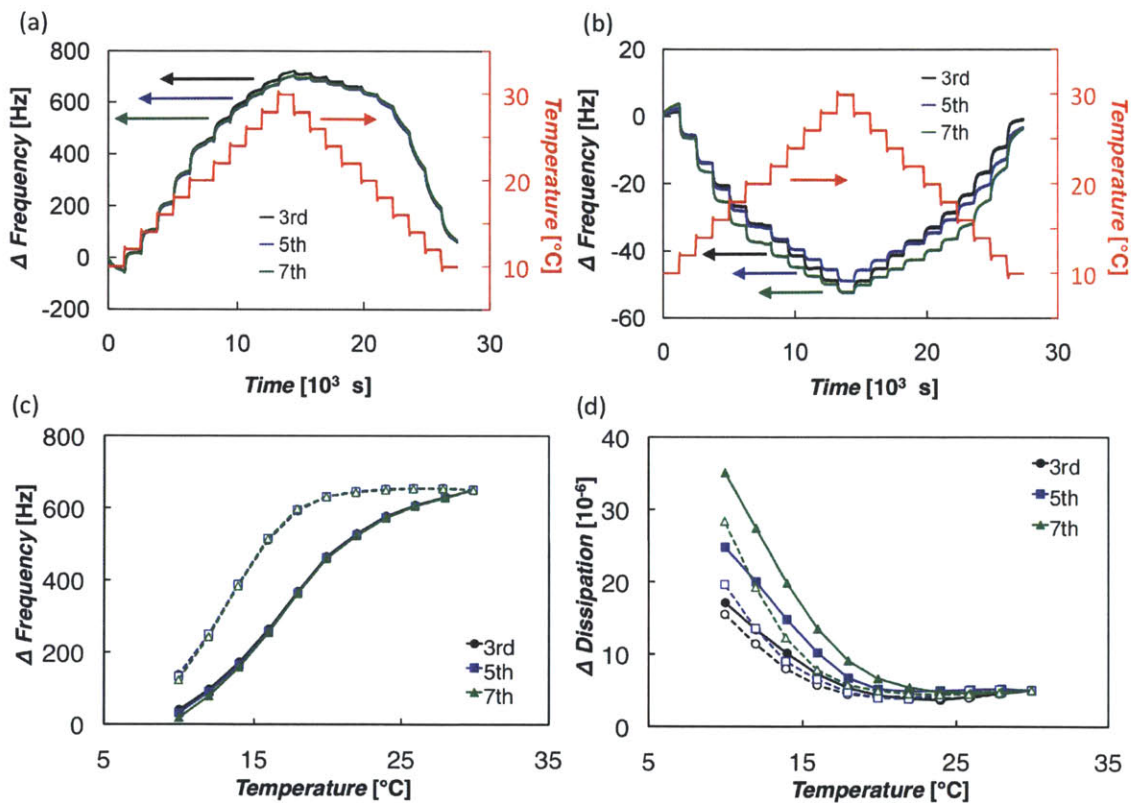


Figure 3-2. The QCM-D transient (a) frequency and (b) dissipation curves of the 3<sup>rd</sup>, 5<sup>th</sup> and 7<sup>th</sup> order harmonics for an iCVD film of p(NIPAAm-co-EGDMA) having a uniform composition. These data show the kinetic response of the system to each temperature step given on the second y-axis. Panels (a) and (b) are then used to form the (c) frequency and (d) dissipation curves after 20 minutes of equilibration time at each temperature step. Solid lines correspond to data points taken as the temperature was stepped up, while the dashed lines correspond to decreasing temperature.

The curves in Figure 3-2 provide important insights into the LCST behavior of the copolymer film. First, frequency increases with increasing temperature, in accord with the expected decrease in mass as the film became hydrophobic and expelled water. The LCST was estimated to be  $15 \pm 1$  °C, determined from the inflection point for each of the frequency curves. This value is significantly lower than that typically reported for pure pNIPAAm,<sup>4</sup> though it is known that copolymerization of NIPAAm with a more hydrophobic comonomer has the effect of lowering the LCST, while copolymerization with a more hydrophilic comonomer increases the LCST.<sup>4, 15</sup> Indeed, iCVD copolymerization of NIPAAm with a more hydrophilic crosslinking monomer, di(ethylene glycol) divinyl ether, was previously reported to result in an LCST of  $\sim 28.5$  °C.<sup>23</sup> Therefore, a lowering of the LCST in the present case was expected due to the relatively high hydrophobicity of the crosslinking co-monomer, EGDMA, which contains a pendant methyl group.

Frequency data for all three harmonic orders lie on the same curve, indicating the polymer film was securely attached to the vibrating crystal and all harmonic orders measured the full thickness of the film, as would be expected for a fully cross-linked polymer, and is discussed in more detail later. Dissipation decreased with increasing temperature (Figure 3-2(d)), consistent with an expected increase in the shear modulus of the film as it changed from a swollen hydrogel to a collapsed film.<sup>34</sup> The dissipation also underwent a transition at lower temperatures than did the frequency, which is consistent with previous results for other iCVD-polymerized NIPAAm-based polymer films.<sup>23</sup> Unfortunately 10 °C was the practical lower limit of the QCM-D instrument used,

but if lower temperatures could have been achieved, the dissipation curve (Figure 3-2(d)) would have been anticipated to flatten out at a higher a dissipation value, indicating minimal change in film properties at temperatures well below the transition point.

Finally, Figure 3-2(c) and (d) indicate some apparent hysteresis in the LCST transition, which occurred because the 20 minutes allowed at each time step were insufficient to attain full equilibration of the system as illustrated by the transient data in Figure 3-2(a) and (b). This behavior is analogous to that seen for high-density grafted films,<sup>20, 32</sup> and is attributed to the steric constraints imposed by the large number of polymer chains per area, or, in the case of this p(NIPAAm-co-EGDMA) film, to the cross-linking.

#### **3.4.2 QCM-D of the graded film**

An iCVD graded film with a copolymer base of p(NIPAAm-co-EGDMA) and a NIPAAm-rich surface (Figure 3-1(c)) was investigated to test the hypothesis that the expected desirable, faster response of the surface region could improve the overall response kinetics for the entire film. The total dry thickness of the graded film was 65 nm, of which the first ~55 nm base layer is of the same homogeneous copolymer composition as that investigated by QCM-D above.

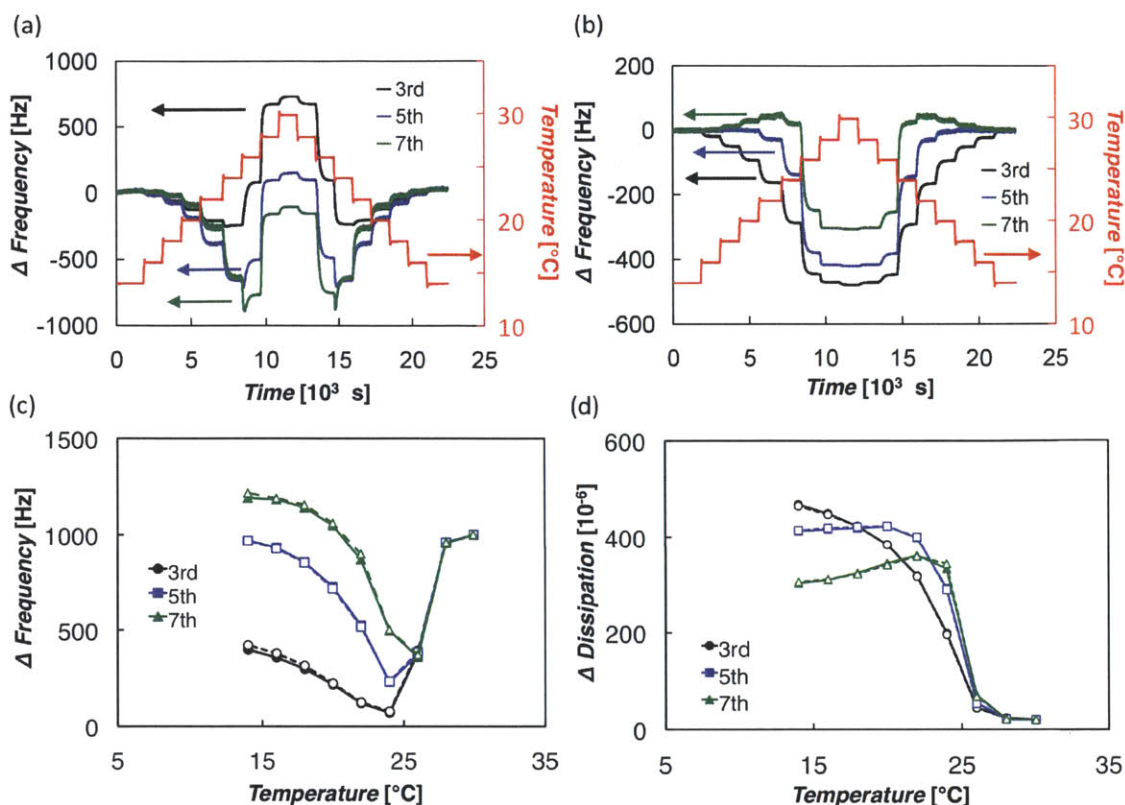


Figure 3-3. The QCM-D transient (a) frequency and (b) dissipation curves of the 3<sup>rd</sup>, 5<sup>th</sup> and 7<sup>th</sup> order harmonics for graded iCVD film having a p(NIPAAm-co-EGDMA) base beneath a NIPAAm-rich surface layer. These data show the kinetic response of the system to each temperature step given on the second y-axis. Panels (a) and (b) were used to prepare the curves for the (c) frequency and (d) dissipation after 20 minutes of equilibration time at each temperature step. Solid lines correspond to data taken as the temperature was stepped up, while the dashed lines correspond to decreasing temperature steps.

The transition behavior of the graded film, as reflected in the responses of the odd harmonics shown in Figure 3-3, is significantly different from that of the base case of the homogenous film (Figure 3-2). The frequency response curves in Figure 3-3(c) do not have the monotonically increasing S-curve form observed in Figure 3-2(c), and indeed, at temperatures lower than about 25°C, decrease with increasing temperature. Moreover, the curves for the different harmonics in Figure 3-3(c) do not coincide over much of the temperature range investigated, in contrast to the results shown in Figure

3-2(c). As discussed in more detail later, these differences can be attributed to differences in the sampling of different regions in the films by the different harmonics; for homogeneous films, all regions are sampled equivalently, but for graded films the sampling varies across the film. In addition, the curve for the 3rd harmonic below 25°C is lower than those for the 5th and 7th harmonics, and would be expected to be flat, as in Figure 3-2(c), if the entire graded film were to be sampled adequately. Indeed, the results for the 1st harmonic do show this behavior, but because of the noise in those results, they have not been included in our analyses. Interestingly, similar deviations from the S-curve response have been reported for low-density grafted films,<sup>21</sup> which suggests that the NIPAAm-rich surface of the graded iCVD film consists of relatively mobile pNIPAAm chains grafted to the base p(NIPAAm-co-EGDMA) film.

For this system, it is difficult to determine the absolute value of the LCST, which is expected vary with depth in the sample due to the compositional variations. The base polymer would have a lower LCST than the NIPAAm-rich surface as the additional hydrophobic EGDMA in the film should lower the LCST. A further indication toward this hypothesis is that the range for the entire transition is around 14 °C, which is significantly larger than the 8 °C found for a hysteresis-free iCVD film of p(NIPAAm-co-DEGDVE).<sup>23</sup> The most significant part of the LCST transition for the graded film geometry occurs from 26 – 28 °C with the largest frequency shift. This part of the transition can be attributed to the surface layer of the film because that composition is expected to give a higher LCST as well as swell the most due to the decreased x-linker density, so as it collapses or swells, it would induce the greatest frequency change. The

majority of the LCST transition is also shifted up towards the LCST value reported for pure pNIPAAm (32 °C)<sup>4</sup> from that determined for the homogenous p(NIPAAm-co-EGDMA) film (15 °C), which is in agreement with the effects a NIPAAm-rich surface layer would have on the polymer film.

Above the LCST, the frequency data for all the harmonic orders displayed were coincident (Figure 3-3(c)) and the dissipation was low (Figure 3-3(d)). This supports the expectation that above the LCST the graded film was dehydrated and collapsed due to hydrophobic effects, allowing even the higher order harmonics to penetrate the sample entirely. However, the data from different harmonic orders (Figure 3-3(c) and (d)) diverge below the LCST, where the more hydrophilic film absorbed water, thereby causing a consequent increase in the measured viscoelastic dissipation (Figure 3-3(d)). These differences between the curves for the different harmonics, as well as the distinct shape of each curve, resulted from the variation in effective depth of penetration for each QCM-D harmonic order, as illustrated schematically in Figure 3-4. As opposed to a fully cross-linked film, where the full mass of the film vibrates with and is considered part of the crystal mass, for the graded film, when swollen, there is a threshold above which the film is too lightly cross-linked to vibrate with (i.e., behave as part of) the crystal. From this threshold, the harmonics penetrate a defined distance into the surrounding fluid, and this distance decreases with increasing harmonic order. This threshold moves as the film collapses, due to hydrophobic effects, so that more of the film becomes “fully attached” and vibrates with the crystal. At some point, the threshold moves to the film’s

surface so that all harmonic orders penetrate the film to the same depth and the curves coincide.

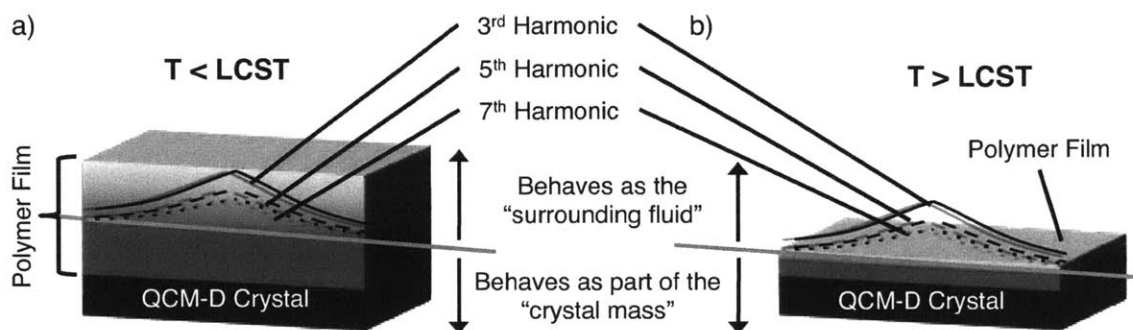


Figure 3-4. Schematic depicting qualitatively the physical area of QCM-D sampling for the 3<sup>rd</sup>, 5<sup>th</sup> and 7<sup>th</sup> order harmonics of the graded p(NIPAAm-co-EGDMA) film along a cross-section of a coated quartz crystal both (a) below and (b) above the film's LCST. Note that the vertical axis is not drawn to scale but is merely a schematic to illustrate the differences in the harmonic order sampling within the film. The gray horizontal line represents the threshold below which the film is sufficiently attached to the crystal to be considered part of the crystal's mass and the labeled 3<sup>rd</sup>, 5<sup>th</sup>, and 7<sup>th</sup> order harmonic curves represent how far past this threshold each of the harmonic orders penetrate. The penetration depth varies from harmonic to harmonic as well as depending on radial distance from the edge of the crystal as depicted qualitatively by the shapes of the curves. Each of the harmonic orders samples the amount of film and fluid below each of their respective curves, thus illustrating the difference in sample size for the different harmonic orders, especially for the swollen polymer below its LCST.

Although we were unable to determine the exact penetration height for these harmonic orders, this insight into the sampling of the harmonic orders helps to explain the curves shown in Figure 3-3 with respect what is occurring at different temperatures and heights within the film. The curve for the 3<sup>rd</sup> order harmonic in Figure 3-3(c) is most similar to the "typical" s-curve seen for fully cross-linked films,<sup>23</sup> as it samples from a greater fraction of the film than the 5<sup>th</sup> or 7<sup>th</sup> order harmonics. In Figure 3-3(d), the 7<sup>th</sup> order harmonic gives a curve that has lower viscous dissipation than the others because



its sampling depth does not reach the lightly cross-linked, high NIPAAm composition chains at the surface; these chains have a higher viscous dissipation that is included in the sampling of the lower order harmonics. Therefore, these data provide further evidence that composition varied throughout the height of the film, and specifically that there was a decrease in the cross-linker (increasing NIPAAm concentration) present near the surface.

Furthermore, the graded film structure did not display hysteresis (Figure 3-3(c) and (d)). Through inspection of the transient data (Figure 3-1(a) and (b)), it can be concluded that 20 minutes following a given temperature step was sufficient time to attain equilibrium, and that the kinetics of the LCST transition were significantly faster for the graded structure with the NIPAAm-rich surface than for the homogeneous films, indicating that the novel architecture aids with the LCST transition.

### **3.4.3 Kinetic Analysis**

Comparison of Figure 3-2(a) to Figure 3-3(a) and of Figure 3-2(b) to Figure 3-3(b) clearly demonstrates that the transient QCM-D response to the temperature steps differed sharply between the homogeneous and graded film architectures. In order to provide an improved quantitative understanding of the temperature responses, models were developed to describe the systems and quantify the time constants of their responses.

The QCM-D system itself has an inherent temperature response, as given by Eq. 1, which must be understood prior to extending the model to more complex systems such as those with attached polymer films. In our analysis, the temperature jump is

approximated as a step change for each system studied. For the base case of the blank crystal, we are able to approximate the system as first order, where the system response to a step change is defined as,

$$\Delta f = Ak \left( 1 - \exp \left[ \frac{-(t - t_d)}{\tau} \right] \right), \quad (2)$$

with  $A$  being the system gain,  $k$  the magnitude of the step input,  $t_d$  the response delay time, and  $\tau$  the time constant.<sup>35</sup> The fact that the input was not a true step function, and that there was some variation associated with the beginning of the response curve, was accounted for via the effective time delay,  $t_d$ .

This model fit the transient data obtained for the blank crystal very well, yielding a time constant for the base system of  $143 \pm 10$  s (Figure 3-5), with strong agreement between the data for all three harmonic orders, as well as at all the temperature steps investigated. In practice, it takes a slightly longer time to lower temperature than to increase it, which is manifested slightly in the system response time when decreasing temperature.

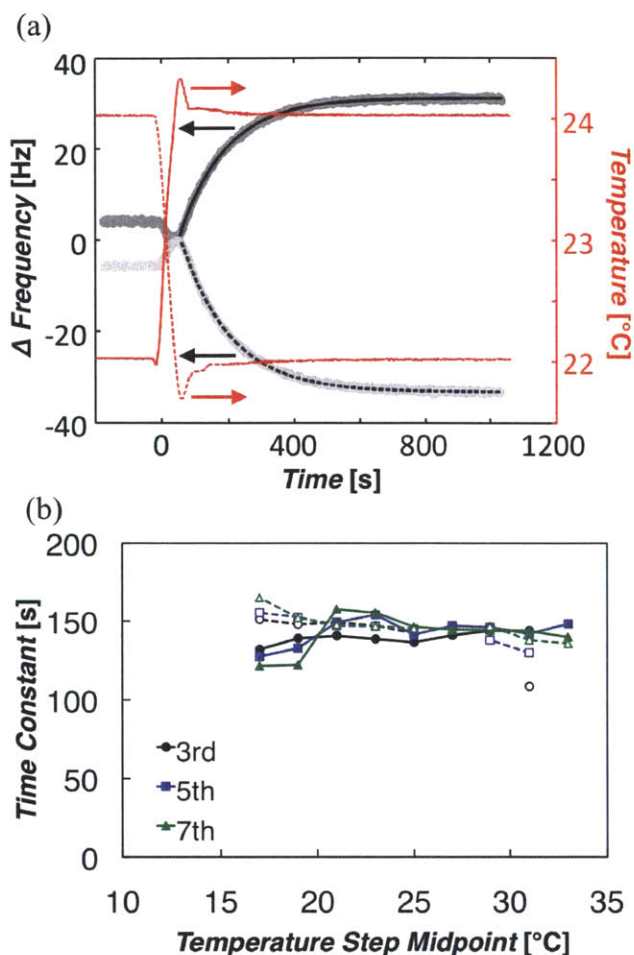


Figure 3-5. (a) The QCM-D transient responses of the 3rd order harmonic of a blank crystal to stepping the temperature up (dark grey, solid lines) and down (light grey, dashed lines). Each response is well described by Eq. 2, allowing extraction of a single first-order time constant. (b) Time constants obtained using Eq. 2 to fit the transient responses for the 3<sup>rd</sup>, 5<sup>th</sup> and 7<sup>th</sup> order harmonics of the blank QCM-D crystal. Solid lines correspond to stepping the temperature up, while dotted lines indicate that the temperature is being stepped down.

The effect of an attached homogeneous copolymer film on the response characteristics of the QCM-D crystal can be accounted for by the incorporation of an additional first-order response term in Eq. 2 to represent the mass flux of water into and out of the film owing to temperature-induced changes in its hydrophobic/philic properties. The resulting equation is

$$\Delta f = A_1 k \left( 1 - \exp \left[ \frac{-(t - t_{d,1})}{\tau_1} \right] \right) + A_2 k \left( 1 - \exp \left[ \frac{-(t - t_{d,2})}{\tau_2} \right] \right), \quad (3)$$

where the definitions of the variables are as in Eq. 2, and the subscripts 1 and 2 correspond to the base QCM-D system and the polymer film respectively. Figure 3-6 shows the nonlinear least squares regression of Eq. 3 to one set of raw data for homogeneous p(NIPAAm-co-EGDMA) film. For all the data sets analyzed, the average value of  $\tau_1$  obtained from Eq. 3 was  $97 \pm 10$  s, which is comparable to the value of  $143 \pm 10$  s found using the blank crystal for the QCM-D system using Eq. 2. The approximately 40 s difference between the blank crystal and the  $\tau_1$  values is within the range of typical crystal-to-crystal variations (of 4 blank crystals studied, the time constant was seen to vary from 100 - 200 s). Thus, we can be confident that  $\tau_1$  does correspond to the QCM-D system.

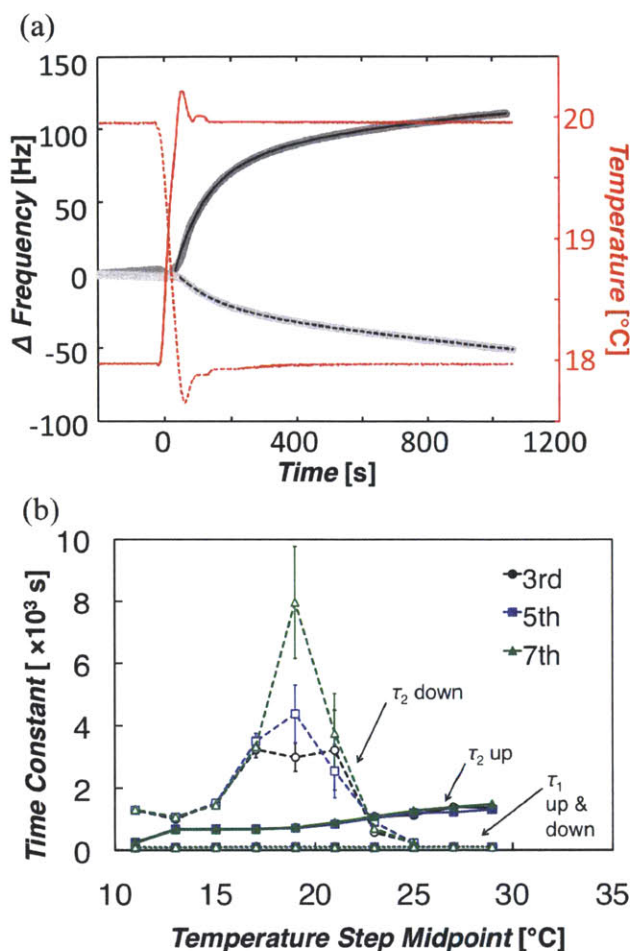


Figure 3-6. (a) The QCM-D transient responses of the 3rd order harmonic of a quartz crystal coated with 80 nm of homogeneous p(NIPAAm-co-EGDMA) to stepping the temperature up (dark grey) and down (light grey). Each response is well described by Eq. 3, allowing extraction of two first-order time constants. (b) Time constants obtained using Eq. 3 to fit the transient responses for the 3<sup>rd</sup>, 5<sup>th</sup> and 7<sup>th</sup> harmonics of the coated QCM-D crystal. Arrows on the figure indicate those data points corresponding to  $\tau_1$  (QCM-D system) and  $\tau_2$  (polymer film). Solid lines correspond to stepping the temperature up, while dotted lines indicate that the temperature is being stepped down. The error bars represent 95% confidence intervals for the fits.

Figure 3-6(b), shows that the time constant for the copolymer,  $\tau_2$ , exceeds that of the QCM-D crystal,  $\tau_1$ , at temperatures below 25 °C. The most prominent characteristic of Figure 3-6(b) is the spike in  $\tau_2$  at temperatures around the upper edge of the LCST when the temperature was stepped down, which is physically where the gel began to re-

swell. Early demonstrations that diffusion of the polymer network into the solvent is the limiting process in polymer gel swelling<sup>29, 36, 37</sup> were based on results when the temperature jump was large, from a temperature at which the equilibrium gel was totally collapsed to a temperature at which the gel was fully expanded under equilibrium conditions, i.e., at temperatures well-moved from the LCST. Under these conditions, the swelling is diffusion controlled and there are limited segment-segment interactions. The diffusion coefficient of the polymer network is proportional to the ratio of the polymer longitudinal bulk modulus to the friction coefficient between the polymer and solvent,<sup>36</sup>. Based upon this analysis, a possible reason for the time constant spike at the upper end of the LCST transition is the large amount of inter- and intra-chain hydrogen bonding at this point, making the effective crosslinking much higher than that represented by just the chemical crosslinks. As the temperature decreases toward and past the LCST, the inter- and intra-chain hydrogen bonding is overcome by hydration, decreasing the effective crosslinking to that represented by the chemical crosslinks and increasing chain mobility.

A similar kinetic analysis was performed on the graded p(NIPAAm-co-EGDMA) films with NIPAAm-rich surfaces. In contrast to the homogeneous p(NIPAAm-co-EGDMA) film, the graded films dynamic response curves could be described by the simple first order response model as given by Equation 2. The results of this fit are shown in Figure 3-7.

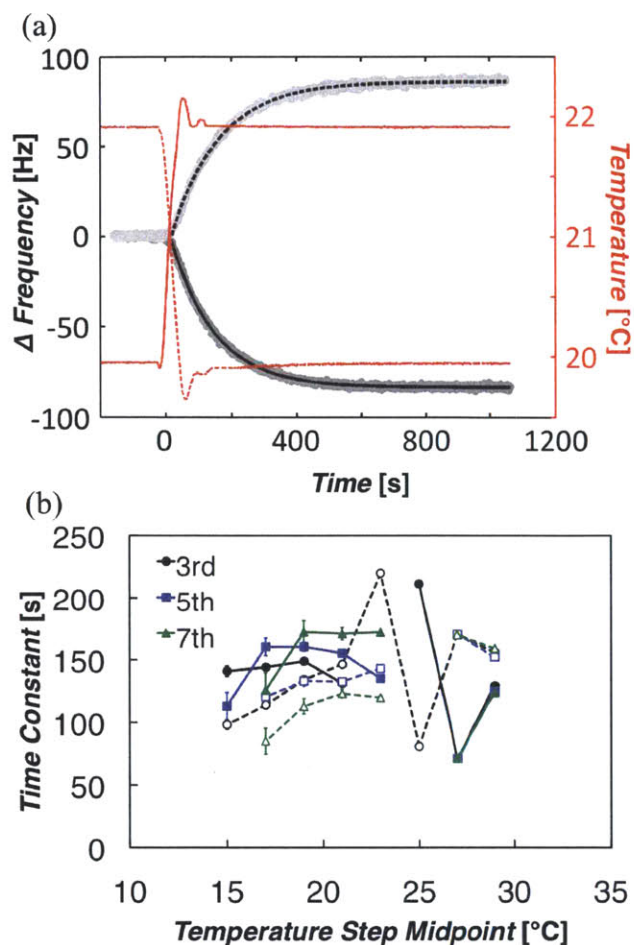


Figure 3-7. (a) The QCM-D transient responses of the 3rd order harmonic of a quartz crystal coated with 65 nm of a p(NIPAAm-co-EGDMA) film with a NIPAAm-rich surface to stepping the temperature up (dark grey) and down (light grey). Each response is well described by Eq. 2, allowing extraction of a single first-order time constant. (b) Time constants obtained using Eq. 2 to fit the transient responses for the 3<sup>rd</sup>, 5<sup>th</sup> and 7<sup>th</sup> order harmonics of the coated QCM-D crystal. Solid lines connecting points correspond to stepping the temperature up, while dashed lines indicate that the temperature is being stepped down. The error bars represent 95% confidence intervals for the fits.

The fact that the response to the temperature jumps could be described by a single first order response model indicates that the time constant for the polymer chain diffusion and subsequent diffusion of water into and out of the film was fast with respect to the QCM-D system time constant, and can therefore essentially be neglected when

modeling the combined QCM-D plus polymer film system. This is confirmed by the average fitted time constant of  $137 \pm 34$  s, which is identical within experimental error to that for the blank crystal system,  $143 \pm 10$  s. Also, although the spread of time constant values found for the graded film system is larger than that seen for the blank crystal system, there is no significant trend around the LCST.

We hypothesize that the reason the graded film transition kinetics are significantly faster than the homogeneous p(NIPAAm-co-EGDMA) films is due to the gradient in NIPAAm content, and hence in the LCST, across the graded film. The increased NIPAAm content at the surface of the film ensures that the LCST is slightly higher there than in its bulk. The range of LCST values aids in the swelling and deswelling of the films. For example, when the temperature is stepped down, the film surface begins to swell at a higher temperature than if the film were homogeneous, and the consequent opening of the pores at the surface helps to pull open the pores in the layers below, thereby facilitating the film swelling.

#### **3.4.4 Structural Analysis**

Figure 3-8 shows the FTIR spectra of the homogeneous and graded p(NIPAAm-co-EGDMA) copolymer films, and the iCVD pNIPAAm and pEGDMA homopolymer films. Incorporation of both NIPAAm and EGDMA into the films is confirmed by the presence of characteristic peaks corresponding to each co-monomer. In spectra (i), (ii) and (iii), peaks corresponding to the NIPAAm secondary amine N-H stretching are present at approximately  $3330\text{ cm}^{-1}$ , and amide C-N-H bending (amide II band) at  $1530\text{ cm}^{-1}$  and



C=O stretching (amide I band) at 1654 -1645  $\text{cm}^{-1}$ . In spectra (ii), (iii) and (iv), a representative peak corresponding to C=O stretching of the methacrylate group in EGDMA occurs at 1732  $\text{cm}^{-1}$ . The presence of peaks representing both NIPAAm and EGDMA demonstrates successful incorporation of both co-monomers into the film.

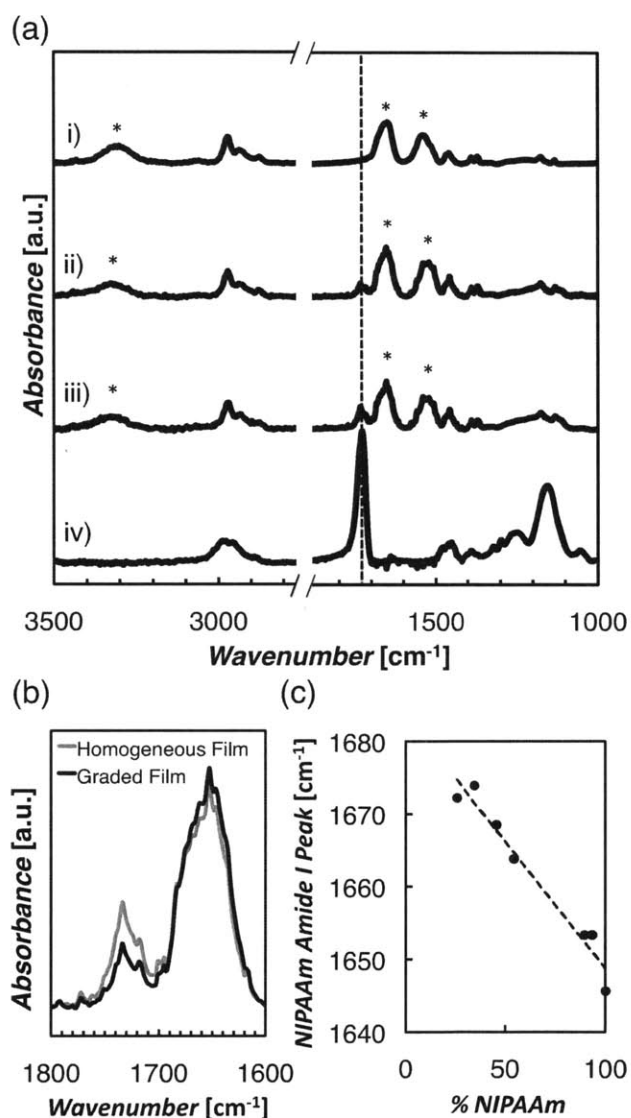


Figure 3-8. (a) FTIR spectra for iCVD films of (i) pNIPAAm, (ii) graded p(NIPAAm-co-EGDMA) with NIPAAm-rich surface, (iii) p(NIPAAm-co-EGDMA) homogeneously crosslinked film, and (iv) pEGDMA. The asterisks correspond to peaks uniquely associated with NIPAAm, while the dashed line corresponds to the C=O stretching peak uniquely associated with EGDMA. These

can be used to confirm the presence of each monomer in both (i) and (ii). (b) Overlay of (a.ii) (black) and (a.iii) (gray) zoomed in around the C=O stretching peaks for EGDMA and NIPAAm, depicting the increased NIPAAm content (decreased EGDMA content) in the graded film. (c) Location of the NIPAAm C=O stretching peak for different compositions of p(NIPAAm-co-EGDMA). The shift in wavenumber with composition is direct evidence of copolymerization.

The FTIR spectra were used to determine the overall composition of the two different p(NIPAAm-co-EGDMA) films by comparing the areas of the C=O stretching peaks for NIPAAm and EGDMA. The homogeneous film contained approximately 89% NIPAAm, while the overall composition of the graded film with the NIPAAm-rich surface contained approximately 93% NIPAAm. The peak corresponding to the NIPAAm amide I band shifts from  $1645\text{ cm}^{-1}$  in pure pNIPAAm to  $1654\text{ cm}^{-1}$  for the two p(NIPAAm-co-EGDMA) films, which indicates a copolymer was formed instead of individual polymer chains of each monomer.<sup>38</sup> The shift occurred due to close range interactions that affected bond vibrations. When the bond was in a more electronegative environment, the vibration frequency and therefore wavenumber increased. Since EGDMA is more electronegative than NIPAAm, as EGDMA content increased the amide I band of NIPAAm shifted to a higher wavenumber. Figure 3-8(b) illustrates this shift for increasing EGDMA content and how it can be used as a simple method to determine the composition of p(NIPAAm-co-EGDMA) films.

### 3.5 Conclusions

We have developed a novel temperature-responsive p(NIPAAm-co-EGDMA) film of graded composition, with a NIPAAm rich surface, that has rapid response times to temperature perturbations near the LCST. QCM-D was used to study the thin film

behavior around the LCST, which was compared to that of a homogeneous p(NIPAAm-co-EGDMA) film. The equilibrium QCM-D data show evidence of the graded film composition as reflected in the analysis of multiple order harmonics, which sampled through different heights into the film. These data also show that the LCST of the homogeneous film and the LCST range for the graded film were both shifted to lower values (15 °C and 16 - 28 °C respectively) than that reported for pure pNIPAAm (32 °C), attributed to the hydrophobicity of the co-monomer, EGDMA. The LCST for the graded film varies over a wide range because the variation in composition across the thickness of the film. A kinetic analysis of the transient QCM-D data indicated that the response time of the graded polymer film around the LCST was significantly faster than that of the homogeneous film, and that for the graded system the QCM-D system itself was the limiting factor and not diffusion. This novel film architecture opens up the possibility for producing polymer films with fast-switching temperature response properties, which are desirable for many applications including separations, or micro valves and pumps in microreactors or MEMS devices.

### **3.6 Acknowledgments**

We thank the *DuPont MIT Alliance* for financial support. We thank the *MIT CMSE* shared facilities supported in part by the *MRSEC program* of the *National Science Foundation* under Award DMR 02-13282.

### **3.7 References**

1. Juodkazis, S.; Mukai, N.; Wakaki, R.; Yamaguchi, A.; Matsuo, S.; Misawa, H. *Nature* **2000**, 408, 178-181.
2. Yuan, W.; Jiang, G.; Wang, J.; Wang, G.; Song, Y.; Jiang, L. *Macromolecules* **2006**, 39, 1300-1303.
3. Deshmukh, S.; Bromberg, L.; Smith, K. A.; Hatton, T. A. *Langmuir* **2009**, 25, 3459-3466.
4. Schild, H. G. *Prog. Polym. Sci.* **1992**, 17, 163-249.
5. Bromberg, L.; Temchenko, M.; Moeser, G. D.; Hatton, T. A. *Langmuir* **2004**, 20, 5683-5692.
6. Eichenbaum, G. M.; Kiser, P. F.; Simon, S. A.; Needham, D. *Macromolecules* **1998**, 31, 5084-5093.
7. Geismann, C.; Ulbricht, M. *Macromol. Chem. Phys.* **2005**, 206, 268-281.
8. Akhoury, A.; Hatton, T. A. *ACS Applied Materials and Interfaces* **2011**, In Press.
9. Boker, A.; Elbs, H.; Hansel, H.; Knoll, A.; Ludwigs, S.; Zettl, H.; Zvelindovsky, A. V.; Sevink, G. J. A.; Urban, V.; Abetz, V.; Muller, A. H. E.; Krausch, G. *Macromolecules* **2003**, 36, 8078-8087.
10. Majumder, M.; Zhan, X.; Andrews, R.; Hinds, B. J. *Langmuir* **2007**, 23, 8624-8631.
11. Ahn, S.; Kasi, R. M.; Kim, S.; Sharma, N.; Zhou, Y. *Soft Matter* **2008**, 4, 1151-1157.
12. Bromberg, L.; Temchenko, M.; Alakhov, V.; Hatton, T. A. *Langmuir* **2005**, 21, 1590-1598.

13. Irvin, D. J.; Goods, S. H.; Whinnery, L. L. *Chem. Mater.* **2001**, 13, 1143-1145.
14. Ulbricht, M. *Polymer* **2006**, 47, 2217-2262.
15. Gil, E.; Hudson, S. M. *Prog. Polym. Sci.* **2004**, 29, 1173-1222.
16. Chaterji, S.; Kwon, I. K.; Park, K. *Prog. Polym. Sci.* **2007**, 32, 1083-1122.
17. Yoshida, M.; Langer, R.; Lendlein, A.; Lahann, J. *Polymer Reviews* **2006**, 46, 347-375.
18. Takei, Y. G.; Aoki, T.; Sanui, K.; Ogata, N.; Sakurai, Y.; Okano, T. *Macromolecules* **1994**, 27, 6163-6166.
19. Cunliffe, D.; Alarcon, C.; Peters, V.; Smith, J.; Alexander, C. *Langmuir* **2003**, 19, 2888-2899.
20. Annaka, M.; Yahiro, C.; Nagase, K.; Kikuchi, A.; Okano, T. *Polymer* **2007**, 48, 5713-5720.
21. Ishida, N.; Biggs, S. *Langmuir* **2007**, 23, 11083-11088.
22. Ma, H.; Fu, L.; Li, W.; Zhang, Y.; Li, M. *Chem. Commun.* **2009**, 3428-3430.
23. Alf, M. E.; Godfrin, P. D.; Hatton, T. A.; Gleason, K. K. *Macromol. Rapid Commun.* **2010**, 31, 2166-2172.
24. Tamirisa, P. A.; Hess, D. W. *Macromolecules* **2006**, 39, 7092-7097.
25. Cheng, X. H.; Canavan, H. E.; Stein, M. J.; Hull, J. R.; Kweskin, S. J.; Wagner, M. S.; Somorjai, G. A.; Castner, D. G.; Ratner, B. D. *Langmuir* **2005**, 21, 7833-7841.
26. Teare, D. O. H.; Barwick, D. C.; Schofield, W. C. E.; Garrod, R. P.; Beeby, A.; Badyal, J. P. S. *J. Phys. Chem. B* **2005**, 109, 22407-22412.

27. Yoshida, R.; Uchida, K.; Kaneko, Y.; Sakai, K.; Kikuchi, A.; Sakurai, Y.; Okano, T. *Nature* **1995**, 374, 240-242.
28. Annaka, M.; Tanaka, C.; Nakahira, T.; Sugiyama, M.; Aoyagi, T.; Okano, T. *Macromolecules* **2002**, 35, 8173-8179.
29. Chu, L.; Kim, J.; Shah, R. K.; Weitz, D. A. *Adv. Funct. Mater.* **2007**, 17, 3499-3504.
30. Baxamusa, S. H.; Im, S. G.; Gleason, K. *PCCP* **2009**, 11, 5227-5240.
31. Montero, L.; Baxamusa, S. H.; Borros, S.; Gleason, K. *Chem. Mater.* **2009**, 21, 399-403.
32. Zhang, G.; Wu, C. *Macromol. Rapid Commun.* **2009**, 30, 328-335.
33. Chan, K.; Kostun, L. E.; Tenhaeff, W. E.; Gleason, K. *Polymer* **2006**, 47, 6941-6947.
34. Zhang, Y.; Du, B.; Chen, X.; Ma, H. *Anal. Chem.* **2009**, 81, 642-648.
35. Ogunnaike, B. A.; Ray, W. H., *Process Dynamics, Modeling, and Control*. Oxford University Press, Inc.: New York, 1994.
36. Tanaka, T.; Fillmore, D. J. *J. Chem. Phys.* **1979**, 70, 1214-1218.
37. Matsuo, E. S.; Tanaka, T. *J. Chem. Phys.* **1988**, 89, 1695-1703.
38. Lau, K. K. S.; Gleason, K. *Macromol. Biosci.* **2007**, 7, 429-434.

# **4. CHAPTER FOUR:**

## ***Insights into Thin,***

***Thermally-Responsive Polymer  
Layers Through Quartz Crystal  
Microbalance with Dissipation  
Monitoring (QCM-D)***

## 4.1 Abstract

The thermodynamics of temperature-responsive polymeric layers were analyzed using a two state coil to globule model to which the van't Hoff relationship was applied. For soluble homopolymer poly(*N*-isopropylacrylamide (pNIPAAm), enthalpies of transition,  $\Delta H_{VH}$ , were calculated using ultraviolet-visible (UV-vis) spectroscopy data to be  $2,008 \pm 7$  and  $395 \pm 1$  kcal mol<sup>-1</sup> for standard synthesis and initiated chemical vapor deposition (iCVD) respectively. For the insoluble surface bound layer of crosslinked iCVD poly(*N*-isopropylacrylamide-co-di(ethylene glycol) divinyl ether) (p(NIPAAm-co-DEGDVE)),  $\Delta H_{VH}$  was determined to be  $194 \pm 6$  kcal mol<sup>-1</sup> using quartz crystal microbalance with dissipation monitoring (QCM-D). Microcalorimetry measurements showed the enthalpy per mole NIPAAm monomer to be 1.3, 0.85 and 0.8 kcal mol<sup>-1</sup>, resulting in cooperative unit sizes of 1,500, 470 and 240 monomer units for the standard pNIPAAm, iCVD pNIPAAm and p(NIPAAm-co-DEGDVE) systems respectively. These values indicate that both per monomer enthalpic contribution as well as cooperative unit size are primary factors contributing to the variations in van't Hoff enthalpies for the three systems studied. Diffusion of bovine serum albumin (BSA) into swollen p(NIPAAm-co-DEGDVE) films below its LCST was elucidated via QCM-D measurements. These data provided a calculated diffusion coefficient of  $3.5 \pm 0.1 \times 10^{-14}$  cm<sup>2</sup> s<sup>-1</sup> of BSA into the swollen hydrogel film with a mesh size of  $6.0 \pm 0.2$  nm (compared to the hydrodynamic radius of BSA,  $r_H = 3.36$  nm).



## 4.2 Introduction

Interest in thermally responsive polymers as surface modification layers is driven by potential applications including, but not limited to, drug delivery,<sup>1</sup> tissue engineering<sup>2, 3</sup> and sensors and actuators for microelectromechanical systems (MEMS).<sup>4-6</sup> These substrate-attached films can display properties deviating significantly from those of their free chain or bulk hydrogel forms.<sup>7</sup> While, traditional characterization methods provide great insight into polymers solutions and macroscopic samples, many of these approaches are not compatible with thin surface layers. Thus, there is a need for new characterization approaches specifically applicable to thin films.

An emerging method for analyzing thermal responsive surfaces is quartz crystal microbalance with dissipation monitoring (QCM-D). To date, QCM-D has been primarily used to determining the lower critical solution temperature (LCST) values of these films.<sup>8-10</sup> Recently, we reported the ability to follow the kinetics of the LCST transition of thin responsive layers using QCM-D.<sup>8</sup> Here, we extend the utility of QCM-D analysis to provide additional thermodynamic insight into the LCST transition of thin, thermally responsive layers. Specifically, the equilibrium fractional conversion of the film to the hydrophobic state as a function of temperature was determined by QCM-D, allowing the enthalpy of the LCST transition to be calculated via a van't Hoff relationship. Thus, QCM-D provides the same insight from surface layers that traditional Ultraviolet-visible (UV-vis) spectroscopy provides for transition occurring in solutions, such as the

denaturing (unfolded state) of proteins<sup>11</sup> or collapse to the globule state for NIPAAm-based polymers.<sup>12</sup> pNIPAAm chains in solution exhibit high transmission of UV and visible light below their LCST, characteristic of lack of absorption by the random coil state. As temperature increases, these chains exhibit a cloud point at the LCST as they transition into the globular state. The precipitation of these chains results in light scattering from suspended pNIPAAm globules and loss of UV-vis transmission at temperatures above the LCST. However, temperature-controlled UV-vis spectroscopy is a challenging experiment for cross-linked films on substrates because attached thin films do not become opaque above the LCST resulting in essentially no contrast between the two states. Other methods that have been successfully used to determine fractional conversion between the two states include <sup>1</sup>H NMR spectroscopy<sup>13</sup> and differential scanning calorimetry (DSC).<sup>14</sup>

Additionally, QCM-D provides insight into the how a protein or molecule interacts with a surface, e.g. monolayer vs. multilayer adsorption and deposition onto the surface vs. penetration into a film, as well as providing information pertaining to the kinetics of each of these processes. Previously, Hook, *et al.* showed through QCM-D measurements that the binding of hemoglobin to a hydrophobic methyl-terminated surface occurred in two kinetic steps. First, a tightly bound initial monolayer formed, followed by adsorption of more loosely bound proteins. This study illustrates the utility of the method to elucidate protein interactions with a conventional hydrophobic surface. Here, we will extend this type of QCM-D analysis to demonstrate the differences in

protein interactions with our thermally responsive films both below and above the LCST and the different kinetic processes operative in each regime.

#### **4.2.1 Responsive Surfaces Selected**

For the current work, we chose to examine *N*-isopropylacrylamide (NIPAAm) and its copolymers because their LCST behavior has been extensively investigated. Below their LCST, these polymers are hydrophilic in aqueous solution, their free chains exhibit a solvated extended coil configuration while cross-linked gels swell. Increasing the temperature above the LCST induces a sharp change in hydrophobicity, where free chains collapse into a globule conformation, while hydrogels expel water and de-swell to an extent comparable to the dry state.<sup>12</sup>

In order for surface modification layers containing NIPAAm to be stable in water, these polymers must either be grafted to the underlying substrate or be rendered insoluble below the LCST by a sufficient degree of crosslinking. For this work, thin, insoluble crosslinked layers of poly(NIPAAm-co-di(ethylene glycol) divinyl ether) (p(NIPAAm-co-DEGDVE)) were prepared via initiated chemical vapor deposition (iCVD). The iCVD method is a solvent-free, all-dry technique for producing thin, cross-linked hydrogel layers directly on a surface. In iCVD polymerization from a vapor-phase mixture of monomers and crosslinkers and film formation occur in a single step. We utilize in situ growth rate monitoring by interferometry during the deposition to achieve cross-linked hydrogel thin films of a predefined thickness. Unlike some other vapor phase deposition techniques such as plasma enhanced CVD, the composition of the

resulting polymer films are well defined and comparable to similar solution-polymerized polymers, as iCVD follows traditional free-radical polymerization pathways even for relatively fast deposition (up to  $> 100$  nm/min).<sup>15</sup> These capabilities make iCVD extremely advantageous for this system, where complete functional retention is needed to preserve the temperature-responsive behavior of the resulting polymer films.

The iCVD method can be applied to virtually any substrate which is a marked contrast to traditional solution-based grafting methods, which require substrates specifically functionalized with reactive chemical moieties to act as the anchoring sites. Additionally, the iCVD method produces films that are conformal, providing a uniform layer thickness on all the surfaces of 3D object. Thus, iCVD is particularly desirable for “real-world” substrates that may differ significantly from the traditional glass and silicon planar surfaces generally used for experimentation and analysis.

We have previously shown that p(NIPAAm-co-DEGVE), exhibited a sharp LCST transition and significant swelling below the LCST ( $\sim 3x$  dry thickness),<sup>8</sup> and as such is an intriguing candidate for applications where a high degree of switchable behavior is desired along with minimal energy input and thickness, such as for sensor and actuator applications in microelectromechanical systems (MEMS) or cell encapsulation and drug delivery. To this end, iCVD NIPAAm-based thin film gels on micro-structured poly(dimethylsiloxane) (PDMS) substrates have been used to successfully grow and retrieve cell aggregates, which retrain the microstructure of the PDMS substrate.<sup>2</sup> This has important implications for the future of tissue engineering and creation of 3D cell constructs.

## 4.3 Experimental

### 4.3.1 iCVD Polymerization

All reactions took place in a custom-built reactor as described previously.<sup>31</sup> NIPAAm (Acros, 99%), DEGDVE (Aldrich, 99%), and *tert*-butyl peroxide (TBPO) initiator (Aldrich, 98%) were purchased and used without further purification.

To deposit the iCVD polymer films, TBPO vapors (room temperature) were fed into the reactor through a mass flow controller (MKS 1490A) at a flow rate of 1.0 sccm. The monomers NIPAAm and DEGDVE were kept at 75 °C and 40 °C respectively and fed into the reactor via fully open diaphragm valves at respective flow rates of 0.15 sccm and 1.7 sccm. For the pNIPAAm film only NIPAAm and TBPO were fed into the reactor kept at a pressure of 100 mTorr. For the cross-linked films, all three vapors were fed concurrently while keeping the reactor pressure at 200 mTorr. The substrate was kept at a temperature of 45 °C to promote monomer adsorption and the filaments were held at 200 °C throughout the course of the deposition. For the samples used in subsequent UV-vis spectroscopy and DSC analysis, bare Si wafers (WaferWorld) were used as deposition substrates and could also be used for in situ interferometry with a 633 nm HeNe laser source (JDC Uniphase) to monitor and achieve film thicknesses between 200 nm – 1000 nm depending on the sample size needed. For the samples used in subsequent QCM-D analysis, both gold-coated QCM-D crystals with a fundamental frequency of 5 MHz (QSX-301, Q-sense) and bare Si wafers were included as substrates during depositions.

### 4.3.2 Characterization

Film thicknesses were measured using variable angle spectroscopic ellipsometry (VASE) (JA Woollam M-2000) for both dry and swollen films by mounting coated Si wafers in a liquid cell (JA Woollam). An incident angle of 75° was used and the data were fit to a Cauchy-Urbach isotropic model with an ambient water layer using commercial modeling software (WVASE32, JA Woollam). Film thicknesses were taken dry, after 5 minutes in DI water, and 5 minutes after heating to 40 °C. LCST behavior of both the iCVD pNIPAAm and standard solution polymerized pNIPAAm (Aldrich,  $M_n$  20,000 – 25,000) were investigated using UV-vis spectroscopy (Hewlett-Packard HP 8453 spectrophotometer). The transmittance of 0.25 wt% aqueous polymer solutions was measured at 500 nm at various temperatures. The solution was allowed to equilibrate at each temperature for 20 min before taking the transmittance measurements. The thermodynamics of the LCST transition were investigated via conventional differential scanning calorimetry (DSC) measurements using a Micro DSC III (SETARM, France). For all systems studied, a 500 mg sample with a 0.25 wt% polymer concentration in DI water was used with 500 mg pure DI water as a reference. The heating rate used was 1 °C/min. Using PeakFit Version 4.11 (SYSTAT, Inc., Richmond, CA) software, all thermograms were fitted with a linear baseline determined from the entire temperature range and then subtracted from the signal.

LCST behavior of the cross-linked films was evaluated using a QCM-D unit (Model E4, Q-sense). Duplicate coated sensors and blank reference were placed in flow cells

with DI water flowing at a rate of 100  $\mu\text{L}/\text{min}$ . The Peltier heating element was programmed to equilibrate for 20 minutes at each temperature. Changes in both frequency and dissipation for harmonics of order 3, 5, and 7 were monitored to provide the transient response profiles. The behavior of the 1<sup>st</sup> harmonic was inconsistent and was excluded from the analysis as has been done in other studies<sup>16</sup>. The equilibrium frequency and dissipation curves with respect to temperature were obtained using the transient value for each harmonic order at the end of the 20 min equilibration period. There is an inherent approximately linear dependence of the QCM-D system on temperature,<sup>9</sup> so the equilibrium data obtained from the blank crystal were subtracted from those of the coated crystals to get the final equilibrium curve form. The QCM-D protein adsorption measurements were done using the same equipment and films as the LCST measurements. The films were allowed to equilibrate at either 22 °C or 32 °C for 30 minutes while flowing PBS (100  $\mu\text{L}/\text{min}$ ). Then the solution was changed to albumin from bovine serum (BSA, Aldrich) in PBS (10 mg/mL), and monitored at constant temperature.

## **4.4 Results and Discussion**

### **4.4.1 Thermodynamic Analysis**

#### ***Two State Transition Model***

We have found that a common approach for analyzing protein folding, the two state transition model,<sup>17</sup> can be successfully extended to the calculation of enthalpy changes associated with the coil to globule transition of NIPAAm-based chains and crosslinked

gels, as Kato, *et al.* have similarly extended this analogy to pressure effects using a Clausius-Clapeyron form.<sup>18</sup> This model assumes the change from coil to globule involves only two states where  $f_G$  and  $(1-f_G)$  are the fraction of the chains in the globule and coil states, respectively. Thus, the equilibrium constant at each temperature is of the form,

$$K = \frac{f_G}{1-f_G}, \quad (1)$$

where  $K=0.5$  represents the LCST. For a series of temperatures,  $f_G$  was experimentally measured by UV-vis spectroscopy for soluble chains, such as pNIPAAm homopolymer, or by QCM-D for insoluble films, such as crosslinked p(NIPAAm-co-DEGDVE).

Previous studies reveal the transition from the coil to globular state proceeds through “cooperative units” which are subsegments of the full polymer chain.<sup>14</sup> The monomers belonging to the same cooperative unit display correlated behavior during the transition. Typically, a full pNIPAAm chain will be comprised of multiple cooperative units, where the size of the cooperative units depends on several factors. Physically, chain branching and crosslinking can shorten the length of cooperative units. There is also an influence of the transition kinetics, with a faster heating rate decreasing the cooperative unit size and slower heating increases its size.

The van't Hoff enthalpy change associated with the LCST transition,  $\Delta H_{vH}$ , has units of energy per mole of cooperative units. Thus determination of  $\Delta H_{vH}$  provides insight into the variation of the extent of the cooperative units as a function of composition and



experimental conditions. Indeed,  $\Delta H_{vH}$  can be related to the temperature dependence of  $K$  through integration the van Hoff equation to give

$$\ln K = \left( \frac{-\Delta H_{vH}}{R} \right) \frac{1}{T} + C, \quad (2)$$

where,  $R$  is the gas constant,  $T$  is the absolute temperature, and  $C$  is an arbitrary constant. Therefore,  $\Delta H_{vH}$  can be determined directly from the slope of  $\ln(K)$  vs.  $T^{-1}$ . Our measurements with UV-vis and QCM-D are all taken after allowing the system to approach equilibrium at a given temperature step ( $\sim 20$  minutes for every  $2^\circ\text{C}$  step). Thus, we will assume that the cooperative unit size, and therefore the  $\Delta H_{vH}$  calculated are both the largest possible for the given physical polymer system.

### ***UV-vis Analysis***

Figure 4-1 compares UV-vis transmittance at 500 nm for iCVD pNIPAAm to a solution-polymerized standard. Both samples exhibit high transmission below their LCSTs, characteristic of lack of absorption by the random coil state. Transition into the globular state at high temperature causes the chains to precipitate, resulting in loss of transmission at temperatures above the LCST. Significant differences between the two materials are observed both in the LCST values and in the sharpness of this transition. The LCST of  $34^\circ\text{C}$  for the standard corresponds to the value expected for an equilibrated system,<sup>12</sup> while the value of  $31^\circ\text{C}$  obtained for the iCVD polymer is slightly lower than expected. Because the initiator tert-butyl peroxide (TBPO) is used, the iCVD

NIPAAm have tert-butyl groups as the chain ends. These strongly hydrophobic groups would be expected to shift the LCST to lower values.<sup>19, 20</sup>

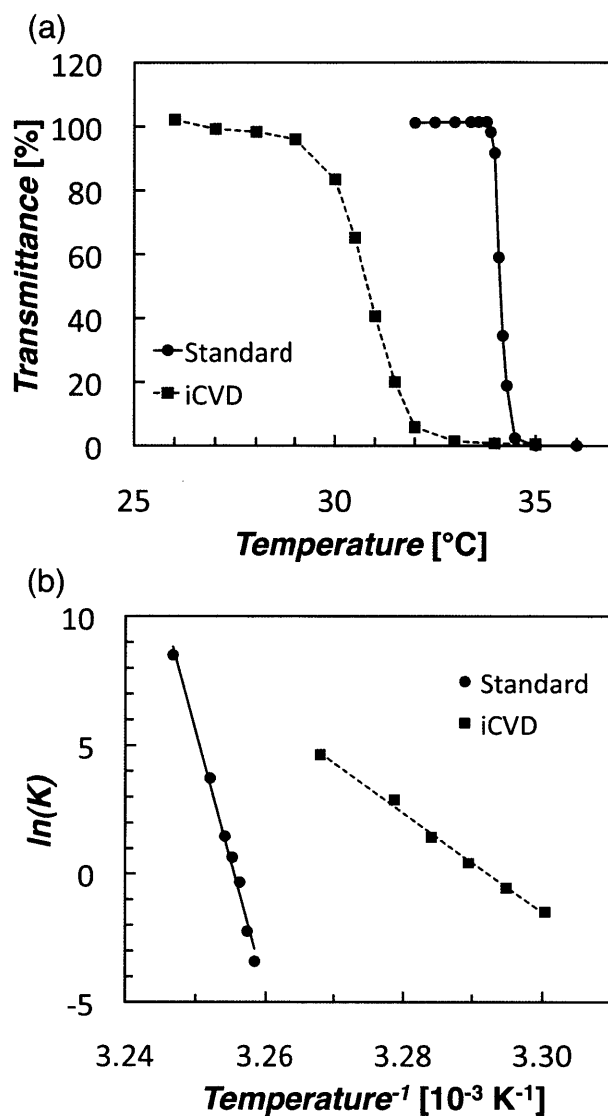


Figure 4-1. (a) UV-vis transmission at 500 nm for pNIPAAm standard solution polymerized and iCVD chains around their LCST's. (b) The van't Hoff form (Eq. 2) of data from (a). The solid and dashed lines depict the regression lines used to calculate the enthalpy change associated with the LCST transition for the pNIPAAm standard and iCVD sample respectively. Data points taken below the LCST transition region are excluded because variations seen at such a low fractional conversion are not significant because they are within the experimental error of the instrument. Only those points taken through the transition region provide the slope proportional to the enthalpy of the transition.

These data in Figure 4-1(a) are of a similar form to that previously observed for protein folding<sup>11</sup> and were subsequently analyzed via the procedure outlined above as shown in Figure 4-1(b). First we see that these data give a good fit to the van't Hoff form as a distinct linear trend is seen in the data for those points corresponding to the transition region. From this region, the calculated enthalpies are  $2,008 \pm 7$  kcal/mol and  $395 \pm 1$  kcal/mol for the standard and iCVD-polymerized pNIPAAm respectively (Table 4-1). Both values are endothermic as expected.<sup>21-23</sup> The higher enthalpy change for the standard sample indicates that its cooperative units are larger than in the iCVD polymer, but also that the enthalpy per monomer unit may be lower for the iCVD polymer. The end groups of the iCVD polymer are likely very hydrophobic t-butyl group which we hypothesize could reduce the number of water molecules hydrating each NIPAAm monomer unit. Additionally, the iCVD polymerization occurs from a surface adsorbed layer of 100% NIPAAm, whereas the standard is produced from the monomer in dilute aqueous solution. We hypothesize that at the high monomer concentrations present during iCVD synthesis, branching reactions are more likely, resulting in a reduction in the cooperative unit size.

Table 4-1. Summary of thermodynamic properties calculated using the van't Hoff relationship as well as the per monomer enthalpic contribution as determined from microcalorimetry. The estimated cooperative unit size based upon these values is also given.

Polymer	$\Delta H_{VH}$ [kcal / mol-coop. unit]	$\Delta H_{cal}$ [kcal / mol- NIPAAm]	Coop. Unit Size [# NIPAAm]
Standard pNIPAAm	$2008 \pm 7$	1.3	1500
iCVD pNIPAAm	$395 \pm 1$	0.85	470
iCVD p(NIPAAm-co- DEGDVE)	$194 \pm 6$	0.80	240

The range of values obtained here for the  $\Delta H_{vH}$  bracket the extrapolated value of  $\sim 900$  kcal/mol obtained via DSC by Tictopulo, *et al.*<sup>14</sup> for free pNIPAAm chains in an SDS solution. Importantly, all of these values are of the same order of magnitude as those obtained using the UV-vis measurements, with differences as expected caused by differences in polymer and solution properties. Tictopulo, *et al.* used SDS to segregate the chains and inhibit interchain interactions, while the polymer solutions used here are in DI water, thus allowing for interchain cooperativity, artificially increasing the enthalpy values.

### **QCM-D Analysis**

iCVD crosslinked films of p(NIPAAm-co-DEGDVE) were analyzed around the LCST transition region using QCM-D as depicted in Figure 4-2(a). These films were previously shown to exhibit an LCST of  $28.5 \pm 0.3$  °C<sup>8</sup> and is confirmed here through analysis of the 3<sup>rd</sup>, 5<sup>th</sup> and 7<sup>th</sup> order harmonics. At low temperatures, frequency is relatively low because the films are swollen and therefore contain additional mass in the form of bound water. Above the LCST, the frequency increases as the films deswelled and expelled water, which would be expected through the Sauerbrey relationship,

$$\Delta m = -C \frac{1}{n} \Delta f, \quad (3)$$

where  $\Delta m$  is the change in mass,  $C$  is a constant dependent on the crystal ( $17.7 \text{ ng s cm}^{-2}$ ),  $n$  is the harmonic overtone and  $\Delta f$  is the frequency change.<sup>24, 25</sup> Although dissipation changes, relating to viscoelasticity of the films, were also tracked, only frequency changes are analyzed here because the fraction of swollen coils is linearly related to the amount of adsorbed water, while viscoelastic properties of the film are nonlinear functions of the water content. For every NIPAAm monomer that undergoes the transition, it dehydrates and releases water molecules, thus decreasing the effective mass of the film, and thereby relating the frequency changes directly to the number of chains (or cooperative chain units) that underwent the LCST transition.

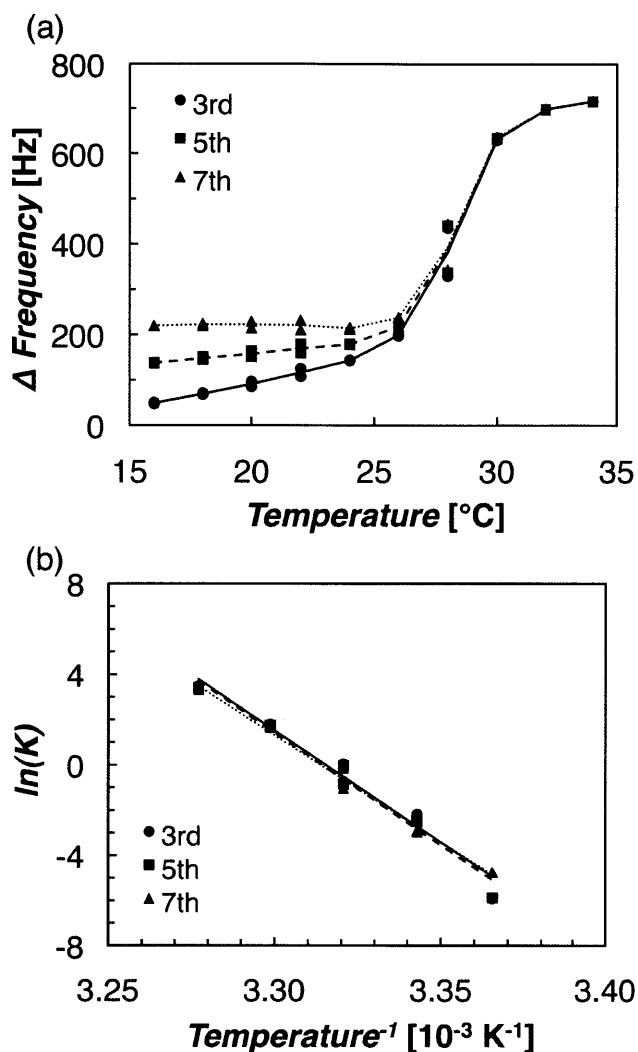


Figure 4-2. (a) QCM-D data for 50 nm iCVD p(NIPAAm-co-DEGVE) films around the LCST. Data from the 3<sup>rd</sup>, 5<sup>th</sup> and 7<sup>th</sup> order harmonics are included for comparison. (b) van't Hoff form of data from (a) used to calculate the enthalpy change associated with the LCST transition. The solid, dashed and dotted lines correspond to the linear fits for the 3<sup>rd</sup>, 5<sup>th</sup> and 7<sup>th</sup> harmonics respectively.

Data analysis done to determine  $\Delta H_{VH}$  shows good agreement between all three harmonics as well as the linear form expected (Figure 4-2(b)). The calculated enthalpy for the transition is  $194 \pm 6$  kcal/mol (Table 4-1). This value is lower than the calculated enthalpy ( $395 \pm 1$  kcal/mol) for the iCVD pNIPAAm chains, which is expected due to the

increased restrictions on chain mobility created by cross-linking, thus reducing the cooperative unit size in crosslinked films. The cross-linking can also create steric hindrances, which inhibit solvent interaction with the monomer units and therefore decrease the enthalpic contribution per monomer unit as changes in hydration state of the monomer is the primary contributor to the enthalpy change of the LCST transition.<sup>26</sup>

### **Microcalorimetry**

For all three systems studied, generally there were two different effects noted as possible causes for differences in  $\Delta H_{vH}$ , variations in cooperative unit size and variations in enthalpic contribution per monomer unit. In order to better understand if one or both of these are reasons for the enthalpy differences, a microcalorimetry study was performed to determine the enthalpic contribution per mole of monomer unit as depicted in Figure 4-3. The enthalpies per monomer were thus determined to be endothermic with values of 1.3, 0.85 and 0.80 kcal/mol-NIPAAm for the standard pNIPAAm, iCVD pNIPAAm and iCVD p(NIPAAm-co-DEGDVE) respectively (Table 4-1). These values are comparable to the reported value of 0.858 kcal/mol-NIPAAm reported in by Shibayama, *et al.*,<sup>26</sup> and indicate that the  $\Delta H_{vH}$  differences are partially caused by the differences in enthalpic contribution per monomer unit. However, as Figure 4-3(d) illustrates, this is not the only contributing factor, because there is a greater percentage decrease in the  $\Delta H_{vH}$  than is seen for the per monomer enthalpic contribution. Therefore, we can conclude that cooperative unit size also decreases from the standard to iCVD pNIPAAm to the iCVD p(NIPAAm-co-DEGDVE). From these data the calculated cooperative unit sizes are 1,500, 470 and 240 for the standard pNIPAAm, iCVD

pNIPAAm and iCVD p(NIPAAm-co-DEGDVE) respectively (Table 4-1). These values are comparable to those reported previously in literature for pNIPAAm chains by Tiktopulo, *et al.*<sup>14</sup> In fact, when comparing the iCVD pNIPAAm to the cross-linked copolymer, cooperative unit size appears to be the primary contributing factor to the decrease in  $\Delta H_{VH}$  as the per monomer enthalpic contribution does not vary significantly between the two.

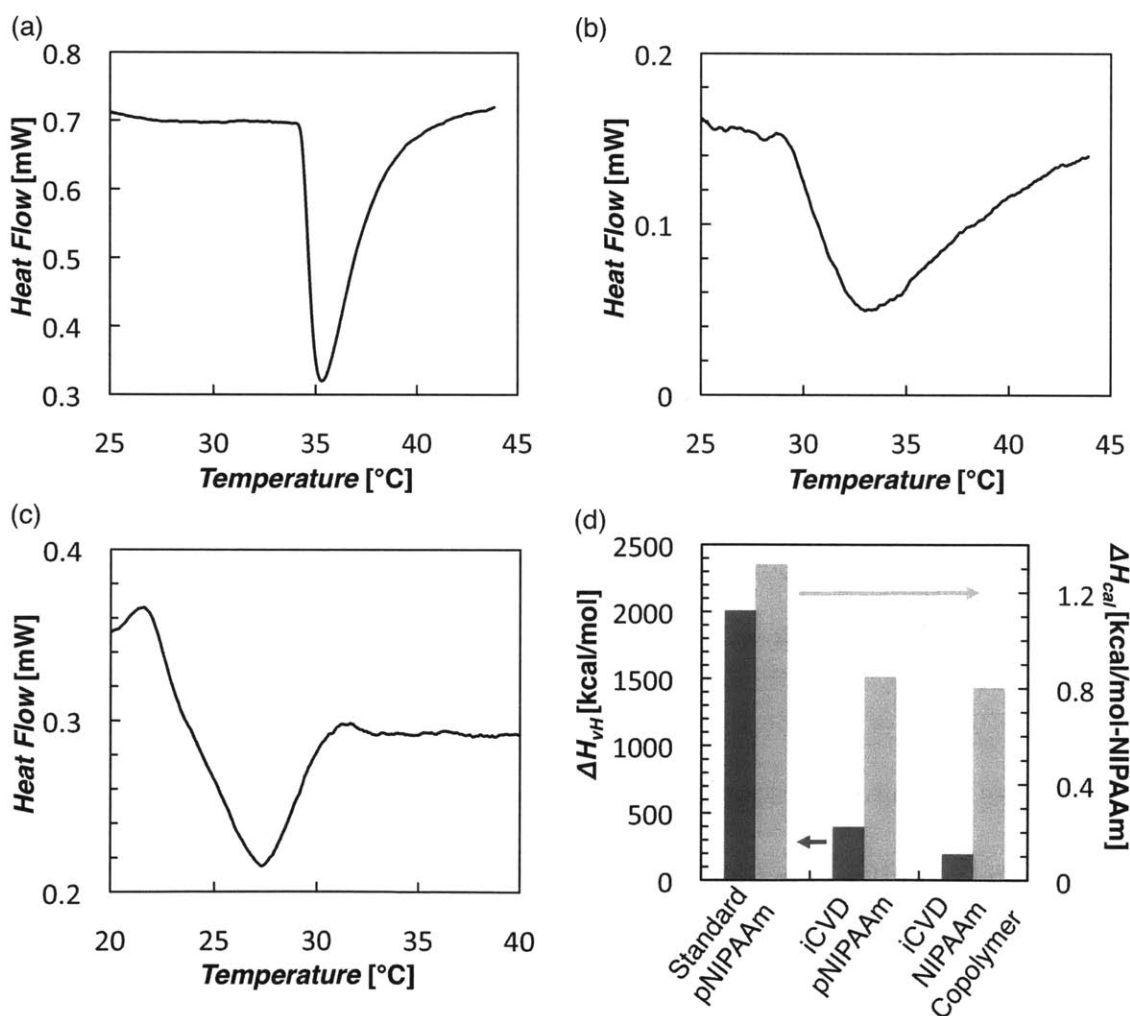


Figure 4-3. DSC thermograms for (a) standard pNIPAAm, (b) iCVD pNIPAAm and (c) iCVD p(NIPAAm-co-DEGDVE) obtained using a heating rate of 1 °C/min. (d) provides a comparison of the  $\Delta H_{VH}$  obtained for each system from UV-vis (pNIPAAm) or QCM-D (p(NIPAAm-co-



DEGDVE)) measurements with  $\Delta H_{cal}$  obtained for each system from calorimetry. The left y-axis is therefore the enthalpy per mole of cooperative units, while the right y-axis is in terms of enthalpy per mole of NIPAAm monomer units, specifically showing the fraction of change in  $\Delta H_{vH}$  can be explained by variations in contribution per monomer unit versus cooperative unit size.

#### 4.4.2 QCM-D for Protein Adsorption

We have previously investigated the adsorption of BSA onto p(NIPAAm-co-DEGDVE) surfaces using QCM-D, showing that at short times the adsorption of BSA is much higher on the film at temperatures above the LCST as compared to below.<sup>8</sup> The kinetic processes involved in the protein-polymer interaction above and below the LCST become evident by plotting the dissipation response versus the frequency response as shown in Figure 4-4. We are able to distinguish two distinct kinetic processes involved in the interaction of BSA with the polymer surface at temperatures below the LCST, whereas only a single kinetic process is noted at temperatures above the LCST.

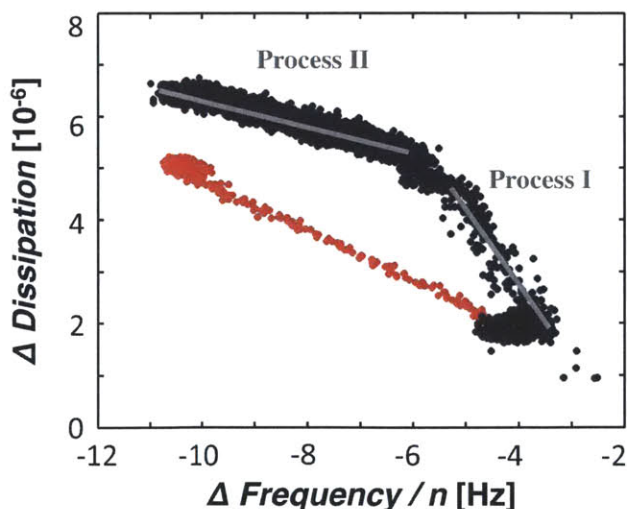


Figure 4-4. Dissipation changes plotted against frequency changes for the 3<sup>rd</sup> order harmonic response to a 50 nm p(NIPAAm-co-DEGDVE) coated QCM-D crystal when exposed to 10 mg/mL BSA in PBS both above (32 °C, red) and below (22 °C, black) the LCST. This figure

form provides insight into the kinetic processes occurring during protein adsorption. The gray lines illustrate the dual kinetic processes below the LCST.

To better understand what is occurring during each of these kinetic processes, the transient response for the 3<sup>rd</sup>, 5<sup>th</sup> and 7<sup>th</sup> harmonic orders is also useful and provided in Figure 4-5. From the frequency response below the LCST (Figure 4-5(a)), we see that at longer times, there is additional mass increase after the initial adsorption event, which is not seen for the compact film above the LCST (Figure 4-5(c)). Above the LCST, the analysis of these data is relatively straightforward, where we believe that approximately a monolayer of BSA adsorbs on the polymer surface, after which no further interaction is observed. This corresponds well with the BSA adsorption step expected with a NIPAAm-based polymer surface in its hydrophobic state as reported in literature.<sup>27</sup> There is some difference in the scaled frequency response (Figure 4-5(c)) owing to the relatively large dissipation changes (Figure 4-5(d)) Also, although there is some dissipation increase for the adsorption event above the LCST, Figure 4-4 illustrates the slope of the curve in above the LCST is shallower than that for process I (surface adsorption) below the LCST, indicating the BSA is more tightly bound to the hydrophobic film than the swollen hydrophilic polymer layer, which would be expected due to the relatively strong hydrophobic interactions between the protein and the polymer above the polymer's LCST.

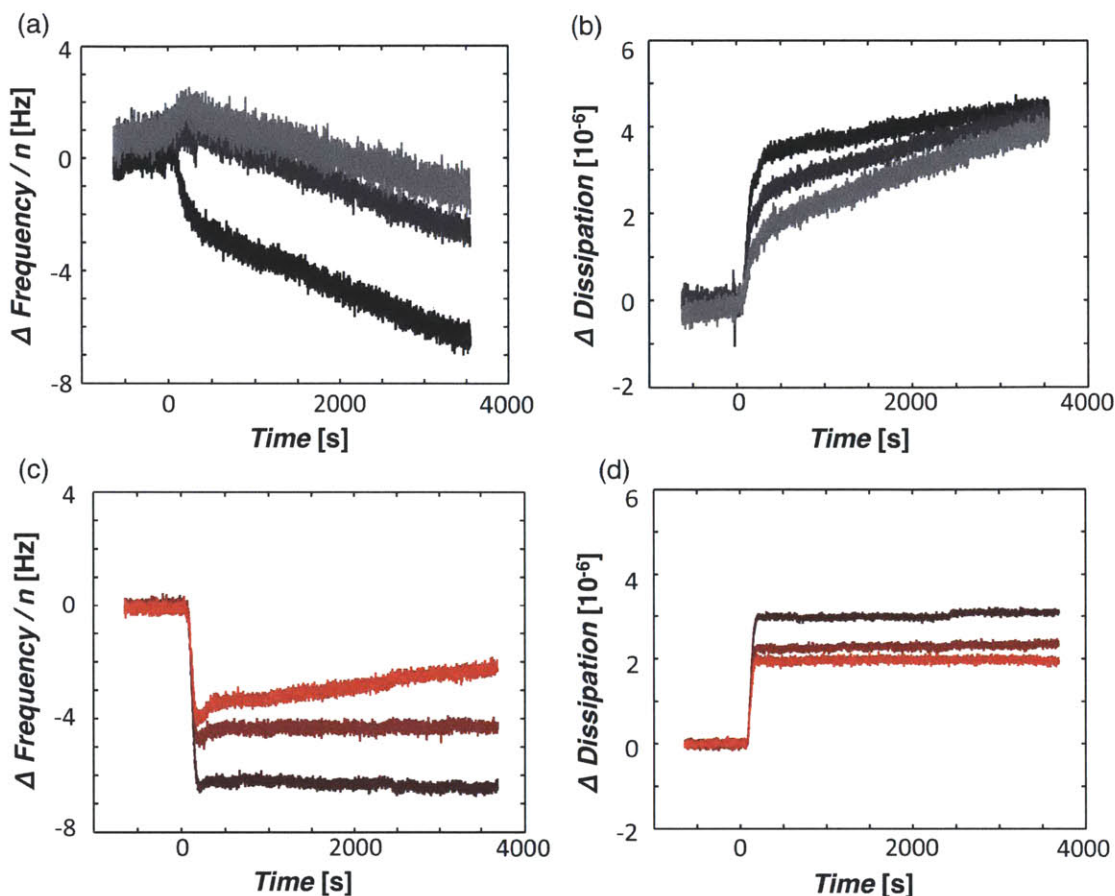


Figure 4-5. (a) Scaled transient 3<sup>rd</sup> (black), 5<sup>th</sup> (dark gray) and 7<sup>th</sup> (light gray) order frequency and (b) dissipation response of 50 nm p(NIPAAm-co-DEGDVE) coated QCM-D crystal when exposed to 10 mg/mL BSA in PBS, at time 0, below the LCST (22 °C). The same system (c) frequency and (d) dissipation responses above the LCST (32 °C) depicting the transient 3<sup>rd</sup> (dark red), 5<sup>th</sup> (medium red) and 7<sup>th</sup> (light red) order harmonics.

However, the interaction of the swollen hydrogel film below its LCST with BSA is more complex. The behavior in process I corresponds to the initial adsorption of BSA to the surface. Although there is some initial adsorption, even in process I, the response can be seen to be slower than that for the LCST through direct comparison of the frequency responses (Figure 4-5(a) and (c)). This is consistent with antifouling properties of more hydrophilic surfaces.<sup>28</sup> For hydrophilic surfaces, more water needs to

be displaced in order for the protein to adsorb, which has a significant energy penalty, and thus slows the adsorption process.

The behavior seen in process II is less straight forward and could be attributed to several behaviors: (i) Additional complexation and multi-layer formation at the surface, (ii) conformational changes of BSA after it adsorbs to the surface, (iii) conformational changes of the NIPAAm coils (e.g. swelling) as the BSA adsorbs, or (iv) diffusion into the swollen hydrogel layer. To better understand this behavior, we first note that for kinetic process I, the slope of the trend line in Figure 4-4 is steeper than for process II. This indicates that during the constant mass gain of process II, there is less viscoelastic change in the film properties associated with a given change in mass. This is opposite of what is observed for proteins, such as hemoglobin, that form multilayers after initial adsorption,<sup>25</sup> and implies effect (i) is not what we are observing. Additionally, such complexation to form multilayers is not an expected behavior for BSA.<sup>27</sup> As for effect (ii), if we observe the scaled frequency response of three different harmonic orders (Figure 4-5(a)), only the 3<sup>rd</sup> order harmonic shows the initial surface adsorption step. This can be attributed to the fact that the film in this state is swollen and not completely coupled to the oscillating crystal. Because the 3<sup>rd</sup> order harmonic has the greatest penetration depth from the crystal interface outward, its penetration reaches the surface, so can monitor the initial adsorption steps, while the higher order harmonics do not fully penetrate to the film's surface. Interestingly, although these harmonics do not show the process I behavior, they do show the process II behavior, indicating that process II is not the result of changes at the surface of the polymer film. This effectively shows that

neither (i) or (ii) are the observed behavior. Behavior (iii) is also not likely as the interaction of a hydrophobic protein with the polymer chains would be expected to compress the film further if anything due to hydrophobic effects and shear forces. This leaves option (iv), diffusion of BSA into the swollen hydrogel, as the most likely behavior to cause the frequency and dissipation responses observed in Figure 4-5.

Two effects can further corroborate diffusion into the hydrogel film. First, the decreased slope of process II compared to process I (Figure 4-4) indicates that dissipation is changing less per comparable change in frequency. This means that although there is additional mass uptake, the viscoelastic properties of the film are not changing to as large an extent. This is what we would qualitatively expect from a solute diffusing through a hydrogel matrix. Secondly, the slope of Process II behavior (the slope at longer times) in the frequency response (Figure 4-5(a)), which corresponds to material flux, decreases as the harmonics increase. This would make sense, as the flux of solute particles would be lower as the sampling distance is moved farther from the film surface. Because of these reasons, as well as elimination of options (i), (ii) and (iii) in the previous paragraph, we believe the behavior we are observing is the diffusion of BSA into the p(NIPAAm-co-DEGDVE) polymer film.

In order to show this diffusion is physically possible, the mesh size of the swollen polymer matrix was calculated using the mean-field Flory-Rehner swelling modified for uniaxial swelling<sup>29</sup> and using a composition averaged interaction parameter.<sup>30, 31</sup> Ellipsometry measurements in a swelling cell gave a swelling ratio of  $3.0 \pm 0.3$ ,<sup>8</sup> which resulted in an average mesh size of  $6.0 \pm 0.2$  nm. This value is significantly larger than

the hydrodynamic radius of BSA ( $r_H = 3.36$  nm),<sup>32</sup> confirming BSA could penetrate the mesh as indicated by the QCM-D data. Using these data, we were then able to estimate the rate of protein diffusion into the film using the Sauerbrey equation (Equation 3). This results in a molar flux of  $1.1 \times 10^{-14}$  mol cm<sup>-2</sup> s<sup>-1</sup>. It should be noted that we used the Sauerbrey equation here although there is some dissipation change in the system, therefore this is a slight underestimation of the true mass change. Using the solution to Fick's Second Law for 1-D diffusion with a constant solute concentration at the interface,

$$\phi(x,t) = \text{erfc}\left[\frac{x}{\sqrt{Dt}}\right], \quad (4)$$

where  $\phi$  and  $\phi_0$  are the solute concentration at a given distance from the film surface,  $x$ , and time,  $t$ , and at the film's surface respectively, and  $D$  is the diffusion constant of the solute, and Equation 3, we were able to derive an equation relating the frequency change over time to the diffusion constant,

$$\Delta f = \frac{4\phi_0 n}{C} \sqrt{\frac{Dt}{\pi}}. \quad (3)$$

Fitting this equation to the 3<sup>rd</sup> order harmonic frequency response gives an approximate diffusivity of  $3.5 \pm 0.1 \times 10^{-14}$  cm<sup>2</sup> s<sup>-1</sup>. This value seems to be reasonable as compared to diffusivities of BSA in other polymers given the properties of the p(NIPAAm-co-DEGDVE) matrix and the free diffusion of BSA in solution ( $6.0 \times 10^{-8}$  cm<sup>2</sup> s<sup>-1</sup>).

Decreases in gel diffusivity from that of free diffusion of BSA of up 6 orders of magnitude have been seen in gels of various compositions that have greater swelling ratio than the value of  $3.0 \pm 0.3$  our films exhibit.<sup>32</sup> Therefore a diffusivity on the lower end of this spectrum would be expected based on the swelling and thus expected mesh size of the p(NIPAAm-co-DEGDVE) polymer studied here.

## 4.5 Conclusions

This work demonstrates that QCM-D, previously used to determine only LCST value,<sup>9, 10</sup> can also elucidate the thermodynamic behavior of surface-bound pNIPAAm-based films. Using the van't Hoff relation in conjunction with both UV-vis and QCM-D data,  $\Delta H_{VH}$  was calculated for standard pNIPAAm, iCVD pNIPAAm and iCVD p(NIPAAm-co-DEGDVE) as  $2,008 \pm 7$ ,  $395 \pm 1$ , and  $194 \pm 6$  kcal mol<sup>-1</sup> respectively. The variation in enthalpies was caused by both differences in cooperative unit size as well as enthalpic contribution per NIPAAm monomer unit. The later was determined by microcalorimetry to be 1.3, 0.85 and 0.80 kcal mol<sup>-1</sup> for the standard, iCVD homopolymer, and iCVD copolymer respectively. Thus, the cooperative unit size varied with values of 1,500, 470 and 240 monomer units for the standard pNIPAAm, iCVD pNIPAAm and p(NIPAAm-co-DEGDVE) respectively.

Finally, QCM-D was used to illustrate the interaction between the surface attached p(NIPAAm-co-DEGDVE) polymer film and BSA. Above the LCST of the film, simple monolayer adsorption was seen, while below the LCST, a secondary behavior was noted where QCM-D results indicated protein diffusion into the swollen hydrogel matrix

with an estimated diffusion constant of  $3.5 \pm 0.1 \times 10^{-14} \text{ cm}^2 \text{ s}^{-1}$ . This further illustrates the utility of QCM-D to analyze the absorption of macromolecules into a hydrogel matrix, which is of considerable interest currently as applied to the burgeoning field of drug delivery.

## 4.6 Acknowledgments

This research was supported by, or supported in part by, the US Army through the Institute for Soldier Nanotechnologies, under Contract DAAD-19-02-0002 with the US Army Research Office. We thank the *MIT CMSE* shared facilities supported in part by the *MRSEC program* of the *National Science Foundation* under Award DMR 02-13282.

## 4.7 References

1. Qiu, Y.; Park, K. *Advanced Drug Delivery Reviews* **2001**, 53, 321-339.
2. Tekin, H.; Ozaydin-Ince, G.; Tsinman, T.; Gleason, K.; Langer, R.; Khademhosseini, A.; Demirel, M. C. *Langmuir* **2011**.
3. Cole, M. A.; Voelcker, N. H.; Thissen, H.; Griesser, H. J. *Biomaterials* **2009**, 30, 1827-1850.
4. Huber, D. L.; Manginell, R. P.; Samara, M. A.; Kim, B. I.; Bunker, B. C. *Science* **2003**, 301, 352-354.
5. Chaterji, S.; Kwon, I. K.; Park, K. *Progress In Polymer Science* **2007**, 32, 1083-1122.



6. Stuart, M. A. C.; Huck, W. T. S.; Genzer, J.; Mueller, M.; Ober, C.; Stamm, M.; Sukhorukov, G. B.; Szleifer, I.; Tsukruk, V. V.; Urban, M.; Winnik, F.; Zauscher, S.; Luzinov, I.; Minko, S. *Nat Mater* **2010**, 9, 101-113.
7. Vidyasagar, A.; Smith, H. L.; Majewski, J.; Toomey, R. G. *Soft Matter* **2009**, 5, 4733-4738.
8. Alf, M. E.; Godfrin, P. D.; Hatton, T. A.; Gleason, K. K. *Macromolecular Rapid Communications* **2010**, 31, 2166-2172.
9. Ishida, N.; Biggs, S. *Langmuir* **2007**, 23, 11083-11088.
10. Zhang, G.; Wu, C. *Macromolecular Rapid Communications* **2009**, 30, 328-335.
11. Ginsburg, A.; Carroll, W. R. *Federation Proceedings* **1965**, 24, 412-&.
12. Schild, H. G. *Progress In Polymer Science* **1992**, 17, 163-249.
13. Burba, C. M.; Carter, S. M.; Meyer, K. J.; Rice, C. V. *Journal Of Physical Chemistry B* **2008**, 112, 10399-10404.
14. Tiktopulo, E. I.; Bychkova, V. E.; Ricka, J.; Ptitsyn, O. B. *Macromolecules* **1994**, 27, 2879-2882.
15. Baxamusa, S. H.; Im, S. G.; Gleason, K. *Physical Chemistry Chemical Physics* **2009**, 11, 5227-5240.
16. Cho, N.; Frank, C. W.; Kasemo, B.; Hook, F. *Nature Protocols* **2010**, 5, 1096-1106.
17. Engel, T.; Drobny, G.; Reid, P. J., *Physical chemistry for the life sciences*. Pearson Prentice Hall: 2008.
18. Kato, E. *Journal Of Applied Polymer Science* **2005**, 97, 405-412.

19. Gil, E.; Hudson, S. M. *Progress In Polymer Science* **2004**, 29, 1173-1222.
20. Xia, Y.; Burke, N. A. D.; Stover, H. D. H. *Macromolecules* **2006**, 39, 2275-2283.
21. Kano, M.; Kokufuta, E. *Langmuir* **2009**, 25, 8649-8655.
22. Afroze, F.; Nies, E.; Berghmans, H. *Journal Of Molecular Structure* **2000**, 554, 55-68.
23. Grinberg, V. Y.; Dubovik, A. S.; Kuznetsov, D. V.; Grinberg, N. V.; Grosberg, A. Y.; Tanaka, T. *Macromolecules* **2000**, 33, 8685-8692.
24. Sauerbrey, G. *Zeitschrift Fur Physik* **1959**, 155, 206-222.
25. Hook, F.; Rodahl, M.; Kasemo, B.; Brzezinski, P. *Proceedings Of The National Academy Of Sciences Of The United States Of America* **1998**, 95, 12271-12276.
26. Shibayama, M.; Mizutani, S.; Nomura, S. *Macromolecules* **1996**, 29, 2019-2024.
27. Dolatshahi-Pirouz, A.; Rechendorff, K.; Hovgaard, M. B.; Foss, M.; Chevallier, J.; Besenbacher, F. *Colloids And Surfaces B-Biointerfaces* **2008**, 66, 53-59.
28. Baxamusa, S. H.; Gleason, K. *Advanced Functional Materials* **2009**, 19, 3489-3496.
29. Vidyasagar, A.; Majewski, J.; Toomey, R. *Macromolecules* **2008**, 41, 919-924.
30. Dinc, C. O.; Kibarer, G.; Guner, A. *Journal Of Applied Polymer Science* **2010**, 117, 1100-1119.
31. Caykara, T.; Kiper, S.; Demirel, G. *Journal Of Applied Polymer Science* **2006**, 101, 1756-1762.
32. Amsden, B. *Macromolecules* **1998**, 31, 8382-8395.

# **5. CHAPTER FIVE:**

***Facile Vapor Phase Method to  
Prepare Dynamically Switchable  
Membranes***

## 5.1 Abstract

We successfully develop a vapor-phase method using the complementary techniques of oxidative and initiated chemical vapor deposition (oCVD and iCVD) to modify substrate surfaces to achieve direct heating of temperature-responsive films. This modification involves oCVD poly(3,4-ethylenedioxythiophene) (pEDOT) for resistive heating, followed by an insulating layer of iCVD poly(ethylene glycol dimethacrylate) (pEGDMA), and a subsequent iCVD layer of poly(*N*-isopropylacrylamide-co-di(ethylene glycol) divinylether) (p(NIPAAm-co-DEGDVE)) that provides the temperature-responsive surface properties. We achieve heating of flat surfaces in air up to temperatures of 70 °C for applied voltage of 20 V AC and successfully model this heating behavior through a simple energy balance. Flat surfaces show a static contact angle shift of 30° when heated above the responsive film's lower critical solution temperature (LCST). X-ray photoelectron spectroscopy (XPS) survey scans confirm successful functionalization steps on 2 μm polycarbonate (PC) track-etched membranes. These membranes show temperature changes of 10 °C heating in water, sufficient for temperature control on both sides of the LCST transition and a corresponding change in flux of 50 – 150 % when the temperature is controlled below and above the LCST.

## 5.2 Introduction

Poly(*N*-isopropylacrylamide) (pNIPAAm) and its copolymers are thermally responsive materials exhibiting a lower critical solution temperature (LCST).<sup>1, 2</sup> In water below the LCST, free polymer chains exhibit a hydrated coil conformation and cross-linked gels are swollen. A sharp change in hydrophilicity occurs above the LCST, resulting in a hydrophobic, collapsed globule conformation for free chains and a dehydrated, collapsed gel for cross-linked polymers. Polymers containing NIPAAm have been studied and explored for applications in widely varying arenas including drug delivery, sensors, actuators, pumps, and separations.<sup>3-5</sup> For all of these applications, a method to apply the external change temperature must be designed in order induce the polymer's response. In some cases, the temperature change is inherent in actual application, such as a temperature increase from ambient conditions to body-temperature for drug delivery systems. However, this is not as straightforward for all systems and can be difficult to achieve direct heating of the polymer needed to create a fast response. Several methods that have been explored include heating of pNIPAAm-modified gold nanocages via near infrared radiation,<sup>6</sup> attachment of pNIPAAm-modified PDMS to a black substrate which can subsequently be heated by a strong light beam,<sup>7</sup> as well as the more common methods of simply heating the entire system by an external heating source or metal deposition on substrate backing for resistive heating used mainly for MEMS devices or micro-reactors.<sup>3</sup>

Here, we propose simple, three-step method to provide direct heating and temperature-responsive characteristics to both flat and micro-structured surfaces. A schematic of the surface functionalization is depicted in Figure 5-1, which utilizes both oxidative and initiated chemical vapor deposition (oCVD and iCVD) as surface modification methods. First, oCVD is used to deposit of the conductive polymer poly(3,4-ethylenedioxythiophene) (pEDOT), which provides resistive heating capabilities. A thin (~200 nm) layer of poly(ethylene glycol dimethacrylate) (pEGDMA) follows to provide an electrically insulating layer between the conductive pEDOT and the environment. Ideally, this layer is thick enough to provide electrical insulation, but thin enough to minimize thermal conduction resistance to the subsequent temperature responsive poly(*N*-isopropylacrylamide-co-di(ethylene glycol) divinyl ether) (p(NIPAAm-co-DEGDVE)) layer. Silver paint was added along the length on opposite sides of the substrates as electrodes to facilitate conduction across the full surface area. Using these structures we are successfully able to prepare substrates, which show responsive surface and membrane permeation properties to applied AC voltage. These specific deposition methods and polymers were chosen with the understanding that the same technique developed here can be applied to wide range of surfaces for a variety of applications.

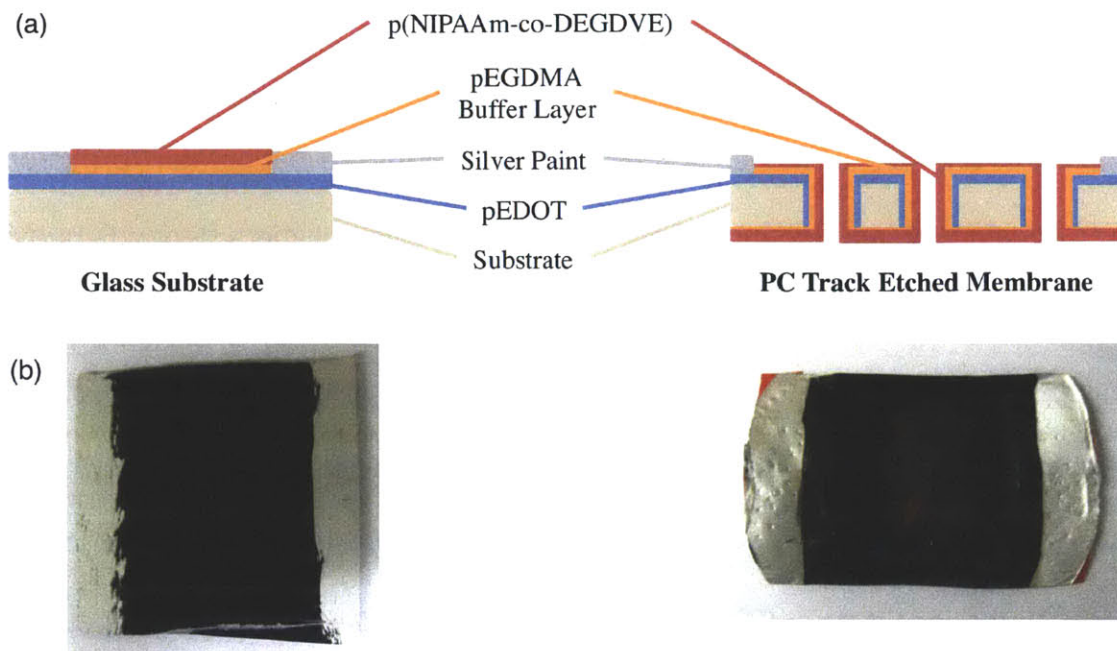


Figure 5-1(a) Cross-sectional schematic of samples developed with dynamically switchable properties for both flat glass substrates and a track-etched PC membrane. The deposition steps for pEDOT and pEGDMA were performed from the top side, while the p(NIPAAm-co-DEGDVE) layer was deposited from the top side for the glass substrate and the bottom side for the PC track etched membrane. (b) Actual top down image of samples.

### 5.2.1 Deposition Methods

Many of the varied applications for NIPAAm-based polymers require surface modification, which gives the polymer's responsive characteristics to a base substrate. Several methods have been used to provide this functionalization including solution-phase methods such as "grafting-to"<sup>8-10</sup> and "grafting-from,"<sup>11-13</sup> as well as vapor phase methods such as plasma enhanced chemical vapor deposition (PECVD)<sup>14-16</sup> and initiated CVD (iCVD).<sup>17</sup> We have chosen the iCVD deposition method because it has been shown to have several distinct advantages over other surface functionalization methods. Between the substrate independent nature of the process and its ability to conformally coat structured surfaces, iCVD is a technique with applicability that spans a

broad range of arenas. Also from a processing standpoint, iCVD provides dynamic control over film composition and thickness, with achievable deposition rates upwards of  $100 \text{ nm min}^{-1}$  and film thicknesses that can range from the nanometer to micrometer range.<sup>18</sup> Additionally, surface modification with responsive polymers depends heavily on functional retention to preserve desired polymer properties. iCVD follows the traditional free radical reaction pathway, which is equivalent to the solution phase process and therefore provides complete functional retention, which is not the case with other higher energy vapor phase processes (e.g. PECVD). For these reasons, we have chosen iCVD to form both the insulating (pEGDMA) and responsive (p(NIPAAm-co-DEGDVE)) layers of the structure in Figure 5-1.

While iCVD is very useful for monomers that react via free-radical polymerization, oCVD is a complementary technique that capitalizes on monomers that react via step polymerization, which includes conductive polymers. Here we utilize oCVD to deposit the conductive polymer pEDOT to provide resistive heating properties to our substrates due to some of the same important characteristics the deposition method shares with iCVD, including its compatibility with a wide range of substrates and is conformal in nature.<sup>18</sup> Although evaporated metals have previously been used to resistively heat substrates to induce temperature-responsive behavior,<sup>3</sup> oCVD, due to the conformal nature of the polymer films it deposits,<sup>19, 20</sup> has the ability to provide targeted heating even in confined geometries. Therefore, instead of needing to provide enough energy to heat the entire substrate, it is possible to merely provide enough energy to heat the responsive polymer it is close thermal contact with. Here, we utilize its conformality to



provide targeted heating across a membrane, while being able to preserve the base membrane structure.

## 5.3 Experimental

### 5.3.1 Deposition Conditions

Following pEDOT depositions, films of both pEGDMA and p(NIPAAm-co-DEGDVE) were subsequently deposited on all substrates using iCVD. All iCVD depositions took place in a custom-built reactor as described previously.<sup>31</sup> NIPAAm (Acros, 99%), DEGDVE (Aldrich, 99%), EGDMA (Aldrich, 98%) and *tert*-butyl peroxide (TBPO) initiator (Aldrich, 98%) were purchased and used without further purification. To deposit the iCVD polymer films, TBPO vapors (room temperature) were fed into the reactor through a mass flow controller (MKS 1490A) at a flow rate of 1.0 sccm. The monomers EGDMA, NIPAAm and DEGDVE were kept at 85 °C, 75 °C and 50 °C respectively and fed into the reactor via fully open diaphragm valves at respective flow rates of 0.5 sccm, 0.15 sccm and 1.7 sccm. For the pEGDMA films, only EGDMA and TBPO were fed into the reactor kept at a pressure of 140 mTorr. For the cross-linked p(NIPAAm-co-DEGDVE) films, NIPAAm, DEGDVE and TBPO vapors were fed concurrently, while keeping the reactor pressure at 200 mTorr. For all depositions, the substrate was kept at a temperature of 45 °C to promote monomer adsorption and the filaments were held at 200 °C throughout the course of the deposition. For each deposition, the sample substrates (coated glass slides or membranes) were included along with a reference Si wafer (WaferWorld) to be used for subsequent variable angle spectroscopic ellipsometry

(VASE) thickness measurements, and which could also be used for in situ interferometry with a 633 nm HeNe laser source (JDC Uniphase) to monitor to achieve approximate desired film thicknesses.

### **5.3.2 Sample Preparation**

For the flat surface samples, glass slides (2.5 cm x 25 cm) were used as substrates for the depositions. First pEDOT was deposited in varying thicknesses (~50 – 200 nm) in order to achieve different resistances (400 – 3,000  $\Omega$ ). For the preliminary resistive heating tests, silver paint was then applied along the length of the sample on opposite sides to act as electrodes, leaving approximately an area 2 cm x 2.5 cm for conduction and power generation in PEDOT between the electrodes. To prepare samples for contact angle measurements, the silver electrodes were masked and followed by subsequent pEGDMA followed by p(NIPAAm-co-DEGDVE) depositions.

To prepare the membrane samples, similar processing was used. The substrates were 4.7 cm diameter track-etched PC membranes with 2  $\mu\text{m}$  pores (Millipore) for the pEDOT depositions (~200 nm). Prior to pEGDMA depositions, masking of opposite membrane edges was performed, leaving approximately 4 cm between the masked edges open for deposition. pEGDMA was then deposited from the same direction as the pEDOT. After the deposition was performed, the mask was removed and the membrane flipped. A new mask was placed on the edges, masking the same membrane area prior to the p(NIPAAm-co-DEGDVE) deposition (150 – 500 nm). After this deposition, the membrane was removed and silver paint was painted on the side where the pEDOT

deposition was performed to assure contact with the PEDOT and therefore conduction and heat generation across the membrane.

### **5.3.3 Sample Characterization**

Film thicknesses of pEGDMA and p(NIPAAm-co-DEGDVE) were measured using variable angle spectroscopic ellipsometry (VASE) (JA Woollam M-2000). An incident angle of 65° was used and the data were fit to a Cauchy-Urbach isotropic model. Contact angle measurements on the fully-functionalized flat substrates were performed on a goniometer equipped with an automatic dispenser (Model 500, Ramé-Hart) using a 4 µL DI water droplet. Measurements were taken both at room temperature (~23 °C) and after heating the substrate to ~35 °C through application of 15 V AC. X-ray photoelectron spectroscopy (XPS) (SSX-100, Surface Science Instruments) survey scans measured the surface composition of the membrane samples after each deposition step. Scans were carried out at 150 eV pass energy with an electron emission angle of 55°.

### **5.3.4 Membrane Permeation**

The membrane permeation experiments were performed by mounting a membrane between two pieces of glass tubing with o-rings and keeping a constant water head to provide back-pressure for permeation over an area of 4.5 cm<sup>2</sup>. Water height was maintained at 28 cm, providing a backpressure of 2.7 kPa. Water was allowed to permeate through the membrane for 1 hour prior to taking the first measurement, but

was allowed to equilibrate for only 20 minutes after each change of condition (e.g. heating or cooling cycle). An AC voltage was applied across the membrane using a variac to provide heating and for cooling, the sample was simply allowed to dissipate heat to the atmosphere. For data analysis, a baseline shift was applied to account for a small amount of drift in the base permeation values.

## 5.4 Results and Discussion

### 5.4.1 Proof of Concept on Flat surfaces.

To first investigate the heating properties of conductive pEDOT, we began by heating various resistances of PEDOT film on glass slides with AC current (Figure 5-2(a)). Data points were taken after allowing the temperature to come to equilibrium for approximately 10 minutes after each voltage step. We were able to model this heating behavior by performing a basic energy balance on the glass slide system. By making the assumptions that the glass temperature is the same as the pEDOT temperature, that there is only convective heat loss to the air, and that data points are taken at equilibrium, the energy balance of temperature as a function of applied voltage reduces to,

$$T = \frac{V^2}{2RhA} + T_{am}, \quad (1)$$

where  $T$  and  $T_{atm}$  are the temperatures of the surface and atmosphere respectively,  $V$  is the applied voltage,  $R$  is the resistance across the pEDOT film,  $h$  is the convective heat transfer coefficient to stagnant air, and  $A$  is the area of the glass surface.

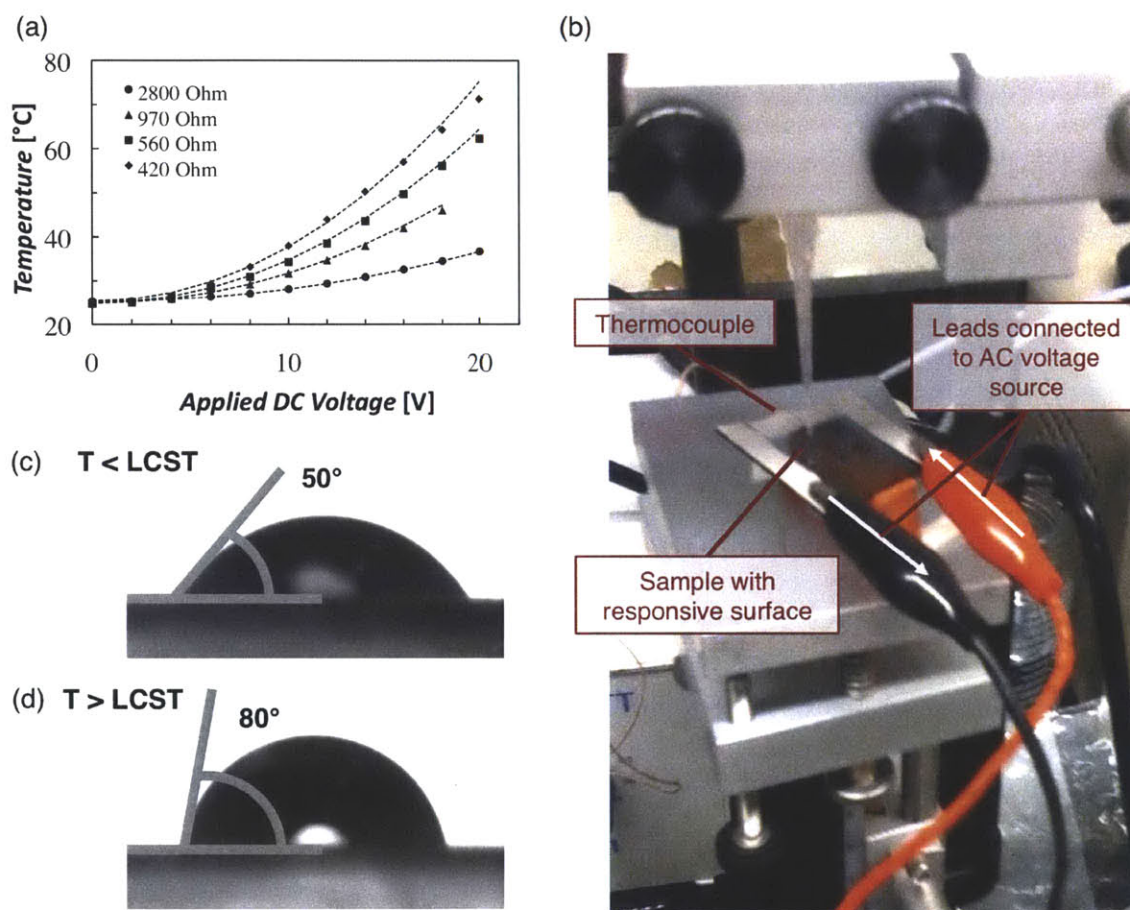


Figure 5-2. (a) Temperature curves for pEDOT-coated glass substrates with varying resistances over a range of applied AC voltages. The data points were taken after allowing 10 min. of temperature equilibration at each voltage step. The dashed lines represent Equation 1 as fitted to the data using only one fitting parameter ( $h = 13 \pm 1 \text{ W m}^{-1} \text{ K}^{-1}$ ). (b) Set-up used to obtain static contact angle measurements of the responsive surface using pEDOT coating to provide resistive heating. Static contact angles for glass slides coated with pEDOT followed by pEGDMA and p(NIPAAm-co-DEGDVE) both (c) below the film's LCST ( $\sim 22^\circ \text{C}$ ) and (d) above the film's LCST ( $\sim 35^\circ \text{C}$ ) as achieved via application of 15 V AC across the substrate ( $R = 1,200 \Omega$ ).

Equation 1 shows good agreement with the experimental data, as does the value obtained for the fit parameter  $h$  for the four samples of different resistances spanning an order of magnitude. The convective heat transfer coefficient determined by these fits was  $13 \pm 1 \text{ W m}^{-1} \text{ K}^{-1}$ , which lies within the range expected for stagnant air.<sup>21</sup> Using this value, we were able to verify the validity of the assumption that the glass and pEDOT temperatures were approximately equivalent by calculating the dimensionless Biot number (Bi) for the system, which compares heat transfer resistances inside of a body to those at the surface. Using the fitted value for  $h$  and  $1.05 \text{ W m}^{-1} \text{ K}^{-1}$  as the thermal conductivity of glass,<sup>22</sup> Bi was calculated to be 0.006. Because Bi is significantly less than one, it implies the temperature profile within the glass slide is not significant and therefore our assumption is valid. Also, although generally good agreement is seen between the fitted Equation 1 and the data, there are some deviations at higher temperatures. This can be attributed to the fact that at higher temperatures other heat loss mechanisms other than convection, such as conduction, become significant. This would then cause greater total heat loss than estimated by Equation 1 and therefore temperatures below the model prediction as observed. Therefore, the model would need to be modified to include these factors if we wish to go to high temperature values, but because these temperatures are well past the responsive temperature for our system, it is unnecessary for this application.

After understanding the heating properties of pEDOT, the buffer and temperature responsive layers were added to the surface. The LCST of the temperature responsive polymer film, p(NIPAAm-co-DEGDVE) is estimated to be  $\sim 28 \text{ }^\circ\text{C}$ .<sup>17</sup> To test the

combination of voltage responsive heating and temperature responsive hydrophilicity changes, static contact angle measurements were performed (Figure 5-2(a) and (b)). At ambient temperatures of approximately 22 °C, below the LCST of the p(NIPAAm-co-DEGDVE) film, the static contact angle was 50 °C. Subsequently, an AC voltage of 15 V was applied across the silver electrodes on the substrate ( $R = 1,200 \Omega$ ) leading to a temperature increase to 35 °C, taking the temperature-responsive polymer layer well above its LCST. At these temperatures, a contact angle of 80° was observed, which illustrates the hydrophobic switch of the surface layer. The 30° contact angle swing is what we would expect for flat surfaces functionalized with a NIPAAm-based polymer.<sup>17, 23</sup>

## **5.4.2 Membrane Application**

### ***Material Characterization***

Several membrane samples were prepared via the deposition steps outlined previously to use for further characterization and analysis. The thickness of the different layers as measured on reference Si wafers using VASE are given in Table 5-1. The primary difference between the two samples is the difference in thickness of the p(NIPAAm-co-DEGDVE) responsive layer, where sample 2 had approximately half the thickness of this polymer film compared to sample 1.

Table 5-1. Details of deposition thickness as measured from profilometry for pEDOT and VASE for pEGDMA and p(NIPAAm-co-DEGDVE) on reference Si wafers for the two different 2  $\mu\text{m}$  track-etched PC membrane samples used in subsequent permeation studies.

Sample	Resistance [ $\Omega$ ]	Film Thickness*		
		[nm]		
		pEDOT	pEGDMA	p(NIPAAm-co-DEGDVE)
1	200	624	200	530
2	650	450	200	240

\*Thicknesses are as measured on a flat reference Si wafer.

After each deposition step, a piece of the membrane was removed for subsequent elemental analysis via XPS. Figure 5-3 confirms the elements we would expect to be present after each deposition step. After the pEDOT deposition, sulfur can be seen, which is not present in any of the other polymers or scans. After the pEGDMA deposition, peaks are only seen for carbon and oxygen and the sulfur is no longer present, indicating that the pEDOT layer has been fully covered by pEGDMA. In the final scan, nitrogen is present along with carbon and oxygen, indicating that NIPAAm is present at the surface. These scans are all taken from the top side of the membrane (top is defined as per Figure 5-1). Scans were also taken of the bottom of the membranes with qualitatively similar results, showing the functionalization steps occurred similarly on the bottom side of the membrane and that the monomers were able to pass through the membrane pores to polymerize on the bottom side of the membrane. This indicates that the pore structure of the membrane was retained because if the pores became blocked, we would not observe deposition on the bottom side of the membranes.



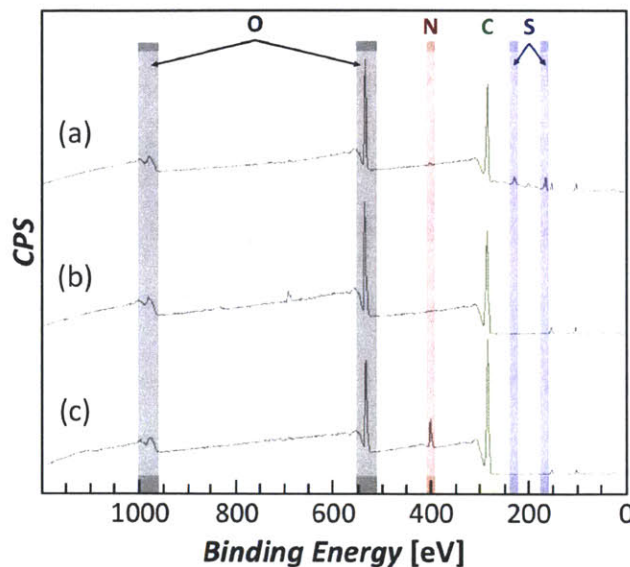


Figure 5-3. XPS survey scan taken of the top side (as in Figure 5-1) of a PC track etched membrane after (a) pEDOT deposition followed by (b) pEGDMA and (c) p(NIPAAm-co-DEGDVE). The important elemental peaks are highlighted where as expected S is present only after the pEDOT deposition, only C and O are present following the subsequent pEGDMA deposition and N is present only after the subsequent p(NIPAAm-co-DEGDVE) deposition.

An analysis of elemental percentages was used to further investigate the properties of the polymer films. For the pEDOT layer, the doping level is 25% as calculated by comparison of the elemental percentages of chlorine and sulfur. This is very close to the maximum doping, theoretically calculated to be 33%,<sup>24</sup> therefore we expect the resistances achieved are close to the lowest possible for the given polymer structure. Also, although 4.4% sulfur was observed on the top side of the membrane, only 1.1% was present on the back side, indicating that although the pEDOT did penetrate the membrane fully, less reached through to the back side of the membrane. The proportion of doped sulfur remained at approximately 25%, indicating that the polymer properties were consistent between the top and bottom side of the membrane.

Table 5-2. Expected and actual elemental compositions as calculated from XPS survey scans on the top side of 2  $\mu\text{m}$  pore size membranes after pEDOT, subsequent pEGDMA and subsequent p(NIPAAm-co-DEGDVE) depositions.

Deposition		Elemental Percentages				
		O	N	C	Cl	S
pEDOT	Expected	21.4	-	64.3	3.6	10.7
	Actual	26.1	-	68.4	1.1	4.4
pEGDMA	Expected	28.6	-	71.4	-	-
	Actual	28.5	-	71.5	-	-
p(NIPAAm- co-DEGDVE)	Expected*	15.7	9.8	74.5	-	-
	Actual	14.6	9.6	75.7	-	-

\* Expected percentage calculated using 83% NIPAAm 27% EGDMA composition for copolymer as determined from amount of N as compared to O and C in survey scan.

The pEGDMA expected ratio of carbon to oxygen is very similar to that observed experimentally, indicating pEGDMA is in fact what is present on the surface. From the elemental percentage obtained for the final p(NIPAAm-co-DEGDVE) surface layer, the nitrogen composition was used to estimate the percent NIPAAm and DEGDVE monomers present in the film. A calculated percentage of 83% NIPAAm to 17% DEGDVE gives very good agreement to the experimental data. This ratio of NIPAAm to DEGDVE is slightly higher than that observed previously,<sup>17</sup> and can be attributed to the higher flow rate of DEGDVE during the deposition, which allowed for more DEGDVE to be incorporated into the films.

### ***Permeation Study***

The responsive characteristics of the membrane systems were studied by monitoring the heating properties and water permeation rate through the membrane using a set-up as depicted in Figure 5-4(d), where volumetric flow rate of the permeate was measured

at various temperatures (applied AC voltages) around the LCST. The results of the permeation study are depicted in Figure 5-4(a).

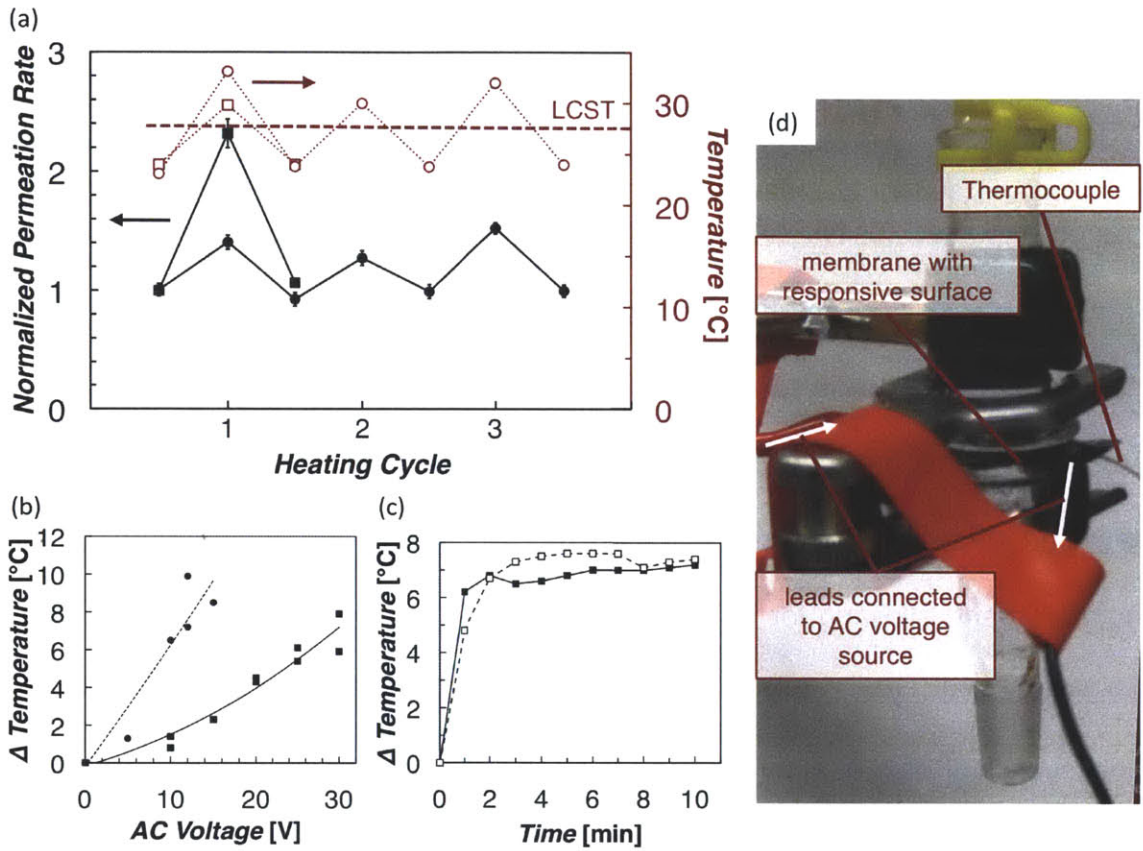


Figure 5-4. (a) Data representing the normalized (to the first low temperature measurement, Sample 1:  $4.3 \text{ mL hr}^{-1}$ , Sample 2:  $6.2 \text{ hr}^{-1}$ ) DI water permeation rate of membrane Sample 1 ( $\blacklozenge$ ) and 2 ( $\blacksquare$ ). The temperature at which the measurements were taken are given in red open points on the second axis and the LCST of the polymer film is represented by the dashed line at  $28 \text{ }^\circ\text{C}$ , illustrating that low temperature measurements were taken below this value and high temperature measurements above it. (b) Temperature changes as measured by a thermocouple affixed to the membrane in DI water from the base system temperature with applied AC voltage for the two different membrane samples. The dashed (sample 1) and solid (sample 2) lines are included merely as guides. (c) Transient temperature change profiles for a AC voltage jump of 0 to 12 V (open points) and 0 to 15 V (solid points) for sample 2. (d) Image of set-up for permeation study.

From these data, we see a distinctive trend that at high temperatures, the membrane flux is 50% - 150% higher than the flux at low temperatures, which is the general trend expected. At low temperatures, the p(NIPAAm-co-DEGDVE) film swells in the pores, effectively making them smaller, which decreases flow rates. When the temperature is increased above the LCST, the film collapses onto the pore walls, making the pores larger and allowing for higher flow rates. This percent change in permeability is within the range expected for NIPAAm-grafted membranes.<sup>25</sup> Also, it is pertinent to note that the base permeability of Sample 1 is significantly higher than that for Sample 2, which is contrary to what we would expect given that 1 has both thicker pEDOT and p(NIPAAm-co-DEGDVE) coating (thus we would expect a smaller pore size). Given this as well as a lower percentage change in membrane flux, we believe there may have been a defect in the membrane allowing for higher permeability and effecting the responsive behavior of the responsive layer in this area. With more care in the handling of the membranes, we believe this discrepancy can be rectified and more consistent and expected permeation rates would be achieved. It is important to note though that despite this possible issue we still see significant permeation rate changes indicating the temperature-responsive aspect of the membrane is functioning as expected.

Also, these data show the dual functionality of the membrane. We were successfully able to achieve membrane heating via application of an AC voltage across the functionalized membrane (Figure 5-4(a), (b), (c)). Temperature changes of up to 10 °C were observed. We believe greater changes could be induced based on the relatively small amount of voltage applied to achieve this heating, especially for Sample 1, which

had significantly lower resistance than Sample 2, allowing for more current to provide greater power generation. But, for this application, it was best to keep the temperature swing as low as possible to minimize work input into the system. This does show the versatility of our design, which could be applied to other systems with different temperature requirements.

The heating and permeability switching were both shown to be repeatable over multiple cycles. (Figure 5-4(a)). Sample 1 was subjected to three heating cycles, and repeatable permeability and heating was seen for all three. This indicates that both the temperature-responsive and conductive polymer were not degrading significantly throughout several swelling / deswelling cycles or after carrying a current. The only variation that was seen was a slight shift in baseline permeability, which was corrected in Figure 5-4(a), and is a feature that has been observed previously for other systems of functionalized track-etched membranes. This baseline did level off towards the end of the measurements, so we would expect repeatability of measurements would continue over more cycles as well as the measurements to be more repeatable without a baseline correction necessary.

From an application standpoint, it is also important to understand the response time of the system. We observed the transient temperature profile for a voltage jump of 0 to 12 V AC for Sample 1. The system response is relatively fast, with a time constant of approximately 1 min. This indicates the system has relatively fast temperature-switching characteristics, but due to the swelling constraints of the temperature-responsive layer, we would expect the time constant for this part of the system to be slower. Data points

in Figure 5-4(a) were taken after allowing for equilibration, and after 20 minutes the permeation had reached a steady value.

## 5.5 Conclusions

We successfully achieved functionalization of both flat and structured surfaces using the vapor-phase techniques of oCVD and iCVD. The heating of flat surfaces was successfully modeled using a basic energy balance and only one fit parameter through a voltage range of 0 – 20 V AC, achieving temperatures up to 70 °C and for surfaces with resistances spanning an order of magnitude. These fully-functionalized flat surfaces showed a static contact angle change of 50° to 80° as the temperature is increased via application of 15 V AC to temperatures above the responsive polymer, p(NIPAAm-co-DEGDVE)'s LCST. XPS data confirms functionalization of membranes with the same responsive polymer layers. Membranes were then successfully heated in water through application of an AC voltage with temperature changes of up to 10 °C were observed and was sufficient to achieve temperature switching above and below the LCST. Control over water permeation rate was achieved with fluxes that varied by 50% and 150% for the two different samples studied. These results exhibit the applicability of these functionalization technique to surfaces varying in composition and structure, thereby illustrating how this is a general procedure that can be used to provide dynamically switchable surface properties to a wide variety of substrates for a range of applications.

## 5.6 Acknowledgments

The authors thank Jonathan Shu at the Cornell Center for Materials research for performing XPS measurements. The authors thank Rachel Howden of the Gleason Group at MIT for performing the profilometry measurements to determine pEDOT thicknesses. This research was supported by, or supported in part by, the US Army through the Institute for Soldier Nanotechnologies, under Contract DAAD-19-02-0002 with the US Army Research Office.

## 5.7 References

1. Schild, H. G. *Progress In Polymer Science* 1992, 17, 163-249.
2. Gil, E.; Hudson, S. M. *Progress In Polymer Science* 2004, 29, 1173-1222.
3. Huber, D. L.; Manginell, R. P.; Samara, M. A.; Kim, B. I.; Bunker, B. C. *Science* 2003, 301, 352-354.
4. Stuart, M. A. C.; Huck, W. T. S.; Genzer, J.; Mueller, M.; Ober, C.; Stamm, M.; Sukhorukov, G. B.; Szleifer, I.; Tsukruk, V. V.; Urban, M.; Winnik, F.; Zauscher, S.; Luzinov, I.; Minko, S. *Nat Mater* 2010, 9, 101-113.
5. Chaterji, S.; Kwon, I. K.; Park, K. *Progress In Polymer Science* 2007, 32, 1083-1122.
6. Yavuz, M. S.; Cheng, Y.; Chen, J.; Cobley, C. M.; Zhang, Q.; Rycenga, M.; Xie, J.; Kim, C.; Song, K. H.; Schwartz, A. G.; Wang, L. V.; Xia, Y. *Nat Mater* 2009, advance online publication SP - EP -.
7. Richter, A.; Paschew, G. *Advanced Materials* 2009, 21, 979-+.

8. Takei, Y. G.; Aoki, T.; Sanui, K.; Ogata, N.; Sakurai, Y.; Okano, T. *Macromolecules* 1994, 27, 6163-6166.
9. Cunliffe, D.; Alarcon, C.; Peters, V.; Smith, J.; Alexander, C. *Langmuir* 2003, 19, 2888-2899.
10. Cho, E. C.; Kim, Y. D.; Cho, K. *Polymer* 2004, 45, 3195-3204.
11. Ishida, N.; Biggs, S. *Langmuir* 2007, 23, 11083-11088.
12. Fu, G. D.; Xu, L. Q.; Yao, F.; Zhang, K.; Wang, X. F.; Zhu, M. F.; Nie, S. Z. *Acs Applied Materials & Interfaces* 2009, 1, 239-243.
13. Teare, D. O. H.; Barwick, D. C.; Schofield, W. C. E.; Garrod, R. P.; Ward, L. J.; Badyal, J. P. S. *Langmuir* 2005, 21, 11425-11430.
14. Pan, Y. V.; Wesley, R. A.; Luginbuhl, R.; Denton, D. D.; Ratner, B. D. *Biomacromolecules* 2001, 2, 32-36.
15. Tamirisa, P. A.; Hess, D. W. *Macromolecules* 2006, 39, 7092-7097.
16. Cheng, X. H.; Canavan, H. E.; Stein, M. J.; Hull, J. R.; Kveskin, S. J.; Wagner, M. S.; Somorjai, G. A.; Castner, D. G.; Ratner, B. D. *Langmuir* 2005, 21, 7833-7841.
17. Alf, M. E.; Godfrin, P. D.; Hatton, T. A.; Gleason, K. K. *Macromolecular Rapid Communications* 2010, 31, 2166-2172.
18. Baxamusa, S. H.; Im, S. G.; Gleason, K. *Physical Chemistry Chemical Physics* 2009, 11, 5227-5240.
19. Im, S. G.; Kusters, D.; Choi, W.; Baxamusa, S. H.; de Sanden, M.; Gleason, K. *Acs Nano* 2008, 2, 1959-1967.



20. Chelawat, H.; Vaddiraju, S.; Gleason, K. K. *Chemistry of Materials* 2010, 22, 2864-2868.
21. Typical Heat-Transfer Coefficients. In *Perry's Chemical Engineers' Handbook*, 8th ed.; Green, D. W.; Perry, R. H., Eds. McGraw-Hill: 2008; pp 11-24.
22. Thermal Conductivity of Glasses. In *CRC Handbook of Chemistry and Physics*, 91st (Internet Version) ed.; Haynes, W. M., Ed. CRC Press/Taylor and Francis: Boca Raton, FL, 2011; pp 12-205.
23. Sun, T.; Wang, G.; Feng, L.; Liu, B.; Ma, Y.; Jiang, L.; Zhu, D. *Angewandte Chemie-International Edition* 2004, 43, 357-360.
24. Im, S. G.; Gleason, K.; Olivetti, E. A. *Applied Physics Letters* 2007, 90, 152112.
25. Yang, B.; Yang, W. T. *Journal Of Membrane Science* 2003, 218, 247-255.

# **6. CHAPTER SIX:**

*Conclusions*

We have shown iCVD to be a very useful surface modification technique for depositing thin films of temperature-responsive polymers. As shown in CHAPTER TWO, because iCVD follows a traditional free radical mechanism, complete functional retention is achieved. This assures a sharp LCST transition region, which is better than films deposited by the common vapor phase technique of PECVD and as good or better by the traditional solution-phase techniques of “grafting to” or “grafting from.” But, unlike the solution-phase grafting techniques, iCVD polymers can conformally coat structured surfaces with controlled thickness from the nano- to micro-scale, making it a process that can be used for a wide variety of applications.

Utilizing the bottom-up nature of iCVD, we were able to successfully fabricate the novel structure of a compositionally graded responsive film with a NIPAAm-rich surface as described in CHAPTER THREE. This structure was found to give rapid swelling and deswelling transition kinetics. The details of this response were investigated using QCM-D, which distinctly showed the differences between this novel structure and a comparable film of homogeneous composition. Because of the surprisingly strong results obtained by QCM-D, additional questions have arisen regarding what is happening during the transition.

It was difficult to determine the exact composition as a function of height in the graded films. For future work, it would be useful to get a better idea of how the composition varies, e.g. true gradient in composition vs. pNIPAAm layer on top of a homogeneous film. One thought is to try heavy metal staining of the films together with transmission electron microscopy (TEM) imaging to show how one of the monomer’s

presence changes throughout the film thickness. Research should be done as well to find other methods that would have the resolution needed to detect the compositional variations.

Also, it would be useful to investigate the kinetic response further to understand the mechanism by which the graded films' kinetic response is improved. I would like to look at different film thicknesses and variations in amount of grading throughout the films thickness. Doing this could help determine what conditions are necessary to achieve the improved kinetic response as well as better understand the transition behavior as observed via QCM-D.

CHAPTER FOUR showed how QCM-D can be used to elucidate the thermodynamic properties of surface-attached thin films, which is difficult using traditional experimental techniques. The van't Hoff enthalpy was seen to decrease when moving from a standard pNIPAAm to iCVD pNIPAAm to iCVD (pNIPAAm-co-DEGDVE), which is due both to decreases in cooperative unit size and reduced enthalpic contribution per NIPAAm monomer unit. Unfortunately due to the characteristics of the DSC instrument used, we were unable to calculate the van't Hoff enthalpy from DSC measurements. These would be useful to illustrate the differences in enthalpy between surface-attached and free thin films.

Also, we were able to observe the diffusion of BSA into swollen p(NIPAAm-co-DEGDVE) films below their LCST. This is especially useful considering the importance of NIPAAm-based polymers for drug delivery applications. To prove the utility of the technique and to better understand the diffusion properties of molecules into the thin

films, it would be useful to study a range of polymers with different cross-linking ratios as well as molecules with different sizes and hydrophobicities.

Finally, in CHAPTER FIVE, we show the applicability of complementary vapor phase deposition techniques to create a self-contained heating unit with temperature-responsive properties. Changes in contact angle on modified surfaces as well as permeability through modified membranes were observed. Moving forward, a technique for better temperature monitoring of the surface should be developed. One idea is to place a thermocouple on the surface before the depositions to assure thermal contact with the surface and thus responsive film. Also, there were significant differences seen for different thicknesses of p(NIPAAm-co-DEGVE). A series of depositions of varying thicknesses should be performed to determine how to tailor the deposition properties to best achieve the desired control.